CONSTRAINING INFILTRATION RATE THROUGH AN AQUITARD BY MODELING THE GENERATION OF METHANE GAS POCKETS

Eric B. Dieck

101 Pages May 2012

This study simulates the generation of methane gas pockets in order to constrain the recharge rate through an aquitard using a 2D multiphase model.

APPROVED:

_____

Date Eric W. Peterson, Chair

_____

Date Stephen J. Van der Hoven

_____

Date Steven F. Carle

CONSTRAINING INFILTRATION RATE THROUGH AN AQUITARD BY MODELING THE GENERATION OF METHANE GAS POCKETS

Eric B. Dieck

101 Pages May 2012

A 2D multiphase flow model was developed to simulate the production of biogenic CH_4 "drift gas" pockets in an aquitard to put a geochemical constraint on the amount of groundwater recharging the aquifer. The aquitard is a glacial till characterized by unsorted clay, silt, sand, and gravel matrix (diamicton) with sand and gravel lenses, where the "drift gas" accumulates. Noble gas concentrations from the underlying aquifer indicate the groundwater has been degassed at some point. It is believed that as total dissolved gas pressure increases, due to actively occurring methanogenesis within organic rich, buried paleosols, hydrostatic pressure is exceeded and CH_4 and other dissolved gases are exsolved from solution. It was hypothesized by using the NUFT code the model will be able to constrain the amount of groundwater infiltrating through the aquitard by simulating the production of these "drift gas" pockets. Components included in the model were, CH_4, CO_2, N_2, ^{40}Ar, ^{84}Kr, and ^{20}Ne. Model validity was assessed by comparing the model output to known drift gas composition and dissolved noble gas ratios in the groundwater. Parameters varied included recharge rate, CH_4 production rate, CO_2 production rate and hydraulic conductivities of the diamicton matrix. The models successfully produced drift gas concentrations within the observed range of

compositions. As a gas pocket would form and degassing would occur dissolved noble gas concentrations became depleted. The modeled dissolved noble gas ratios in the aquitard overlapped well with the observed groundwater data. The model was not capable of capturing the full extent of groundwater with depleted noble gases that is transported to the aquifer. A recharge rate between 1 to 2.5 percent annual precipitation (3.31×10^{-10} to 8.26×10^{-10} m/s) through the aquitard provided the best representation of the observed data.

APPROVED:

_____

Date Eric W. Peterson, Chair

_____

Date Stephen J. Van der Hoven

_____

Date Steven F. Carle

CONSTRAINING INFILTRATION RATE THROUGH AN AQUITARD BY MODELING THE GENERATION OF METHANE GAS POCKETS

ERIC B. DIECK

A Thesis Submitted in Partial
Fulfillment of the Requirements
for the Degree of

MASTER OF SCIENCE

Department of Geography-Geology

ILLINOIS STATE UNIVERSITY

2012

CONSTRAINING INFILTRATION RATE THROUGH AN AQUITARD BY MODELING THE GENERATION OF METHANE GAS POCKETS

ERIC B. DIECK

THESIS APPROVED:

_____

Date Eric W. Peterson, Chair

_____

Date Stephen J. Van der Hoven

_____

Date Steven F. Carle

ACKNOWLEDGEMENT

I would like to thank the entire Geography-Geology Department at Illinois State University. I truly value the great experience I had in Normal, IL from the knowledge I have gained to the friendships I have made in the department. I especially thank Dr. Stephen J. Van der Hoven and Dr. Eric W. Peterson for their continued help throughout the entire completion of my degree and thesis. Dr. Stephen J. Van der Hoven's expert advice and knowledge on the subject was vital to the development and completion of my thesis. Dr. Eric W. Peterson provided me with a solid background in groundwater modeling and has been extremely helpful with the thesis submittal process.

I would also like to thank Lawrence Livermore National Laboratory (LLNL) for awarding me with a Student Summer Intern position. This intern position provided me the opportunity to work with one of the world's experts in multiphase modeling, Dr. Steven F. Carle, and learn the NUFT code. In particular, I would like to thank Steven F. Carle for all his advice and unparalleled knowledge of the NUFT code and multiphase modeling.

Finally, I would like to thank both my family and the Sileo family for their unwavering moral support. I very much appreciate all you have done for me and your continued aid in all my endeavors. Above all, I would like to thank my girlfriend Jennifer L. Sileo. She has provided me with steadfast support and has been the basis for all I have achieved.

E. B. D.

CONTENTS

TABLES

FIGURES

CHAPTER I

INTRODUCTION

The generation of a gas phase beneath the water table occurs as total dissolved gas pressure exceeds hydrostatic pressure. Degassing can be caused by a decrease in hydrostatic pressure as a result of groundwater pumping (Fortuin and Willemsen, 2005), water level decline (Yager and Fountain, 2001), or hydraulic testing (Jarsjo and Destouni, 2000); or an increase of the total dissolved gas pressure by the subsurface production of gases such as nitrogen (N_2), carbon dioxide (CO_2), hydrogen sulfide (H_2S) or methane (CH_4) by biogeochemical processes. Degassing has been observed as a result of N_2 production by denitrification from agricultural pollution (Blicher-Mathiesen et al., 1998; Visser et al., 2007) and as a result of CH_4 production under landfills (Solomon et al., 1992), in lake sediments (Brennwald et al., 2005; Holzner et al., 2008), from the biodegradation of coal beds (Zhou et al., 2005) and the natural attenuation of petroleum hydrocarbons (Amos et al, 2005; Amos and Mayer, 2006).

Noble gases have been widely used to investigate subsurface gas and water interaction. The atmospheric noble gases are particularly powerful tools to trace and study gas partitioning and environmental conditions during groundwater recharge because of their conservative behavior and wide range of solubilities (Aeschbach-Hertig et al., 2008). Because noble gases repartition between the water and gas phase after gas formation, onward flowing groundwater can have noble gas concentrations below atmospheric equilibrium (Visser et al. 2007). The extent of this “stripping” of noble gases and other inert gases has been used to quantify the amount of degassing in subsurface processes. Ar and N_2 stripping has been used to assess the amount of degassing due to denitrification in a Danish riparian wetland (Blicher-Mathiesen et al.,

1998), microbial CH_4 production at a petroleum-hydrocarbon contaminated site (Amos et al., 2005) and in an organic rich Dutch aquifer (Fortuin and Willemsen, 2005).

The objective of this study is to develop a multiphase flow model to simulate the generation of biogenic CH_4 "drift gas" pockets in an aquitard to put a geochemical constraint on the amount of groundwater recharging the aquifer underlying the confining unit. The aquitard is a glacial till characterized by unsorted clay, silt, sand, and gravel matrix (diamicton) with sand and gravel lenses, where the "drift gas" accumulates. These "drift gas" pockets form as CH_4 is produced as a microbial byproduct during the decomposition of an organic rich, buried paleosol within the aquitard. Noble gas concentrations from the underlying aquifer indicate the groundwater has been degassed at some point. Total dissolved gas pressure (TDGP) increases and approaches dissolved gas saturation as groundwater moves vertically through the aquitard and CH_4 is accumulated in the degrading paleosol. It is believed the more permeable sand and gravel lenses drive lateral groundwater flow through these features causing a drop in hydrostatic pressure below TDGP. As hydrostatic pressure is exceeded by TDGP, CH_4 and other dissolved gases are exsolved from solution, forming a drift gas pocket. It is hypothesized that modeling the generation of drift gas will provide constraint on the amount of groundwater infiltrating through the aquitard and recharging the aquifer.

Significance of the Problem

Groundwater is an important source of freshwater for much of the population in the United States. Approximately 21% of the population in Illinois relies on groundwater as their primary source of drinking water (USGS, 1999). With increasing population groundwater resources and maintenance of water quality in potable aquifers becomes a

crucial issue. Glacial aquifers throughout Illinois have been contaminated by improperly contained or disposed chemicals, routine application of agricultural chemicals, and de-icing chemicals (USGS, 1999). In the case of a major freshwater resource like the Mahomet Aquifer it is critical to be able to constrain the amount of water recharging the aquifer and the locations recharge is occurring. In many parts of the world, vertical leakage through regionally extensive aquitards is an important source of recharge to underlying aquifers (Gerber and Howard, 2000). Depleted noble gas concentrations within the Mahomet Aquifer suggest that significant vertical recharge is occurring through the glacial till aquitards that confine it. Quantifying vertical leakage through an aquitard has proven to be a difficult task and poorly understood (Gerber and Howard, 2000, Neuzil, 1986). Response of large scale tests of flow through aquitards takes too long to observe and is severely limited by constraints of time. Thus, the best estimates for flow through aquitards are normally obtained by integrating values obtained from a wide range of tests small in scale relative to the volume of interest (Neuzil, 1986). The uncertainty involved with these small scale tests is further amplified with heterogeneity of aquitards containing features such as sand lenses, as the case of the glacial tills confining the Mahomet Aquifer (Gerber and Howard, 2000). The aim of this study is to provide insight to the ability to quantify infiltration through an aquitard by modeling the evolution of groundwater geochemistry.

Geology/Hydrogeology

The Mahomet Bedrock Valley is a preglacial drainage system that eroded into bedrock across Illinois (Figure 1). During successive periods of Pleistocene glaciations this paloevalley has been filled with up to 100 meters of a complex sequence of glacial

sediments (Kempton et al., 1991). These glacial deposits are divided into Wedron, Glasford, and Banner Formations. These three major till deposits are typically separated by weathered zones, which in some cases coincide with substantial soil development during interglacial periods. These paleosols can be enriched with organic matter, and in some areas contain peat deposits (Hackley et al., 2010).

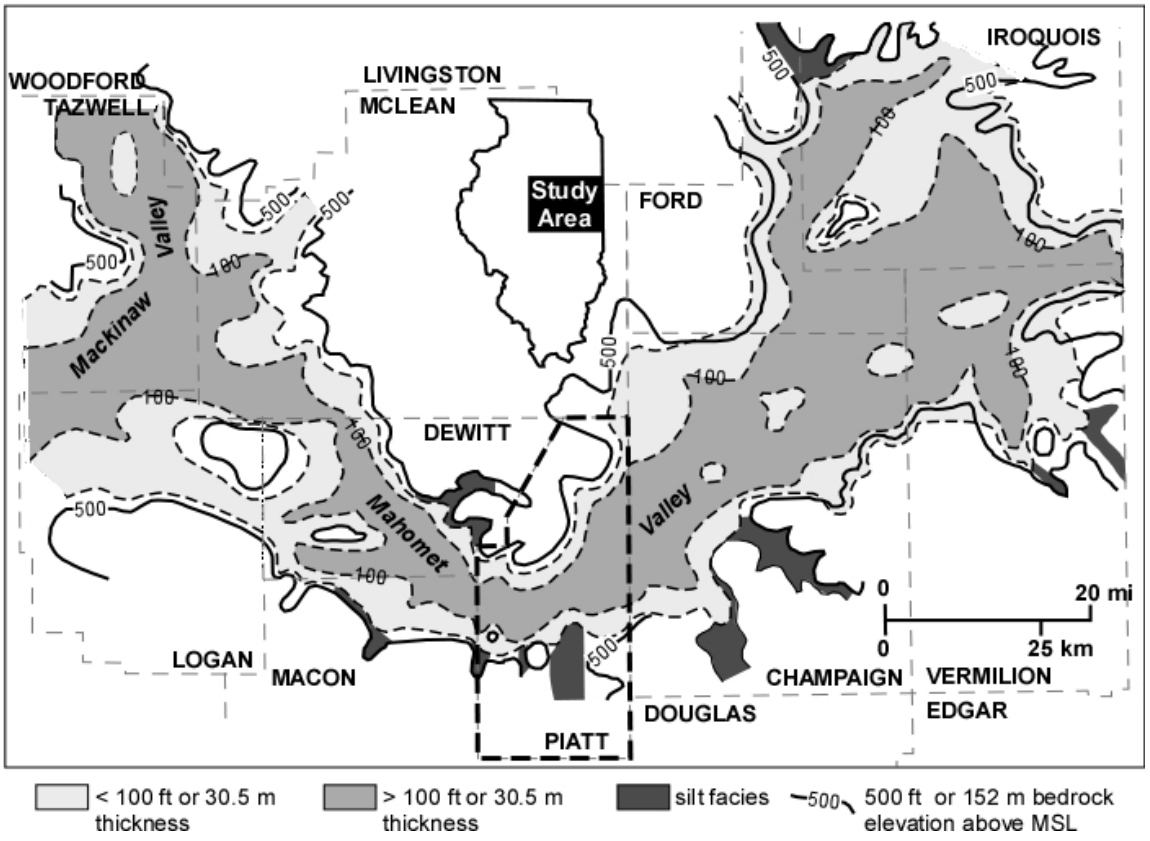

Figure 1. Distribution and thickness of the Mahomet Sand Member (Mahomet Aquifer) and location of related silt facies. The Mahomet Bedrock Valley defined by 500 ft contours (modified from Hackley et al., 2010). Study site is outlined in thick black dashed line (Piatt County).

Banner Formation

The Banner Formation is pre-Illinoisan in age and was deposited more than 400,000 ka. It includes the glacial tills and underlying and intercalated sands, gravels, and silts. The Banner Formation can be as much as 300 feet thick and contains nine

different lithologic members (Willman et al., 1975). The Mahomet Sand Member of the Banner Formation consists of a sand facies that occurs in the main valley and a silt facies that occurs in tributary valleys (Kempton et al., 1991) (Figure 1). The sand facies of the Mahomet Sand Member is commonly referred to as the Mahomet Aquifer. The sand facies is restricted primarily to the main valley and is more than 30 meters thick, and is often more than 45 meters thick in the deepest part of the Mahomet Valley. This facies consists of coarse, gravelly sand that tends to fine upward. The origin of the Mahomet Aquifer is unclear but is interpreted to be glacial outwash deposited by braided glacial rivers during multiple glaciations (Kempton et al., 1991). The Mahomet Aquifer is a major aquifer in east-central Illinois. Kempton et al. (1991) report an average hydraulic conductivity of ~1.3×10^{-3} m/s. The Mahomet Aquifer is overlain by tills of the Banner, Glasford, and Wedron Formations (Hackley et al., 2010).

Glasford Formation

The Glasford Formation was deposited during the Illinoisan Episode between 180 and 125 ka. The formation includes glacial tills, intercalated outwash deposits of gravel, sand, and silt, and the overlying accretion-gley deposits. The Glasford Formation is almost continuous throughout Illinois and ranges from a meter to more than 45 meters thick (Willman et al., 1975). The central and eastern part of the Glasford Formation contains significant sand and gravel deposits within the low permeability till. These sand and gravel layers or lenses can be a significant aquifer within the Mahomet Bedrock Valley and are referred to as the Glasford Sand (Hackley et al., 2010). These sand and gravel lenses are also important to the focus of this study as this is where “drift gas” has been found to accumulate. These sand and gravel units are thought to have functioned as

a drainage way for glacial melt water during the Illinoian Episode. Hydraulic conductivities in the Glasford aquifer range to as much 2×10^{-3} m/s and have a median of 4×10^{-4} m/s throughout east-central Illinois (Kempton et al., 1991). The western portion of the Glasford contains little or no sand and gravel, and is composed of thick tills. The Glasford Formation is overlain by the Wisconsinan age tills.

Robein Silt

The Robein Silt occurs within a substage of the Wisconsinan glaciations and has been radiocarbon dated at 28,000 to 22,000 years B.P (Coleman et al., 1979). The Robein is brown, gray, dark gray to black, leached silt and contains abundant organic material. The Robein ranges from centimeters to more than 1.5 meters thick. It is discontinuous but widely distributed in Illinois (Willman et al., 1975). Glessner and Roy (2009) described the occurrence of the Robein in Piatt County as having a silt, sandy loam, or peaty silt texture and being grayish brown, dark grayish brown, or black in color. Reported organic carbon content of the Robein Silt ranged from 0.52% to 17.2% with a mean of 3.9% ± 4.2% (Glessner and Roy, 2009). The decomposition of this organic material is the source of methane in the drift gas pockets (Coleman et al., 1979). The Robein Silt is overlain by the Wedron Formation.

Wedron Formation

The Wisconsinan age Wedron Formation overlies all the older glacial materials and forms the present day land surface for much of Piatt County (Anliker and Sanderson, 1995). The formation consists of glacial till and outwash. Although largely till, the Wedron contains numerous intercalated beds of outwash gravel, sand, and silt. The Wedron Formation contains fewer sand and gravel deposits than the Banner and

Glasford. The Wedron sand and gravel deposits are relatively small and much thinner (Hackley et al., 2010).

Hydrogeology

Recharge to the Mahomet aquifer is thought to occur primarily as vertical leakage of precipitation through the overlying glacial sediments and by upward leakage through the bedrock (Kempton et al., 1991; Panno et al., 1994). Kempton et al. (1991) determined hydraulic conductivities of the confining beds to range from 1×10^{-9} to 2×10^{-7} m/s, and assumed an average annual recharge rate of 1.81×10^{-9} m/s for the entire Mahomet Valley Bedrock Lowland (Kempton et al., 1991). The main recharge to the central and eastern part of the aquifer appears to occur at a potentiometric high point near the town of Paxton, IL (Wilson et al., 1998). The overlying Glasford Formation in this region contains relatively thick and well connected sand and gravel units that allow for significant recharge to the Mahomet Aquifer. From this potentiometric high point ground water flows to the north, east, and southwest (Wilson et al., 1998). The hydraulic gradient for most of the Mahomet Aquifer is ~0.00019, except near the major cone of depression that has developed near the cities of Champaign-Urbana (Hackley et al., 2010).

Previous Research

Drift Gas

CH_4 is most commonly formed in the subsurface by thermal (thermogenic) or by microbial decomposition (biogenic) of buried organic materials. Drift gas is a term that refers to CH_4 (with varying amounts of N_2 and CO_2) that accumulates in glacial deposits

throughout Illinois. The CH_4 in the drift gas pockets is produced by methanogenesis during the decomposition of an organic rich paleosol.

Methanogenesis is the process in which microbes produce CH_4 as a by-product as they degrade organic material. When all other terminal electron acceptors have been utilized methanogenesis begins to take place. The two dominant pathways for methanogenesis are the reduction of CO_2 and acetate fermentation. The stoichiometries of these reactions are shown respectively:

$$4H_2 + CO_2 \longrightarrow CH_4 + 2H_2O$$

$$CH_3COOH \longrightarrow CH_4 + CO_2$$

Molecular hydrogen is an essential component for CO_2 pathway. The methanogenic bacteria rely on a symbiotic relationship with fermentative bacteria that produce hydrogen. The hydrogen produced is used by methanogens as an electron donor. These anaerobic bacteria use the energy from the reduction of CO_2 to degrade organic material. In the acetate fermentation process, acetate produced as a by-product by fermentive bacteria, is degraded to methane by the reaction above (Kehew, 2000).

The specific microbial pathway in which methane is produced can be defined by the isotopic composition of CH_4 produced and the associated groundwater and CO_2. It has been demonstrated that the relationship between the isotopic compositions of microbial methane and the associated CO_2 is dependent on methanogenic pathway (Whiticar et al., 1986). This relationship is a result of the fractionation that occurs with respect to C, as microbes preferentially use the lighter $_{12}C$ isotope as these bonds require less energy to break. During CO_2 reduction isotopically light CH_4 is produced and the associated CO_2 becomes relatively enriched. Coleman et al. (1988) provided substantial

isotopic data indicating that the drift gas in Illinois is of microbial origin, specifically through CO_2 reduction. Hackley et al. (2010) showed that the $\delta^{13}C$ and δD values for the dissolved CH_4 in the Glasford formation and the Mahomet Aquifer also indicate a microbial origin by CO_2 reduction.

Coleman et al. (1979) used radiocarbon (^{14}C) dating to determine that the majority of drift gas is formed from the degradation of the organic rich Robein Silt, which generally dates from 22,000 to 28,000 years old. The sand and gravel lenses directly above and below this buried soil horizon provide a reservoir for the drift gas, and the overlying till serves as a cap (Coleman et al., 1979). ^{14}C ages of all drift gas samples presented in Coleman et al. (1979) were equal to or younger than the reservoir material in which gas has accumulated. This indicates that upward migration of CH_4 produced in sediments older than the sand and gravel lenses has not been a major factor in the formation of drift gas deposits. The downward transport CH_4 into sand and gravel lenses below the Robein silt seems to be a more likely occurrence.

Drift gas commonly exists some distance from the probable source material, and it appears that movement of CH_4 as a solute in groundwater is the most probable mechanism for drift gas migration (Coleman et al. 1979). In order for degassing to occur, and the formation of a drift gas pocket, groundwater must encounter a zone in which the hydrostatic pressure is less than the sum of the partial pressures of the dissolved gases. As the total dissolved gas pressure (TDGP) exceeds the threshold pressure, the dissolved gases will partition into the gas phase. Nested well data shows that groundwater flow is primarily vertical downward through the aquitard overlying the Mahomet Aquifer. It is believed that where larger sand and gravel lenses are present, horizontal groundwater

movement occurs as water moves through the higher hydarulic conductivity (K) material. It is hypothesized that the mechanism for drift gas generation is a result of the vertical flow through the low K diamicton, and the subsequent horizontal flow through the sand and gravel lenses, shown in Figure 2. As water moves vertically through the diamicton and passes through the Robein Silt, dissolved CH_4 is acquired and transported downward. As CH_4 accumulates, the TDGP may increase to where it equals the hydrostatic pressure (point 1 shown in Figure 2). As the water moves horizontally through the sand and gravel lens a drop in hydrostatic pressure occurs and TDGP exceeds hydrostatic pressure causing the exsolution of gas (point 2 in Figure 2 and the degassing point shown in Figure 2.

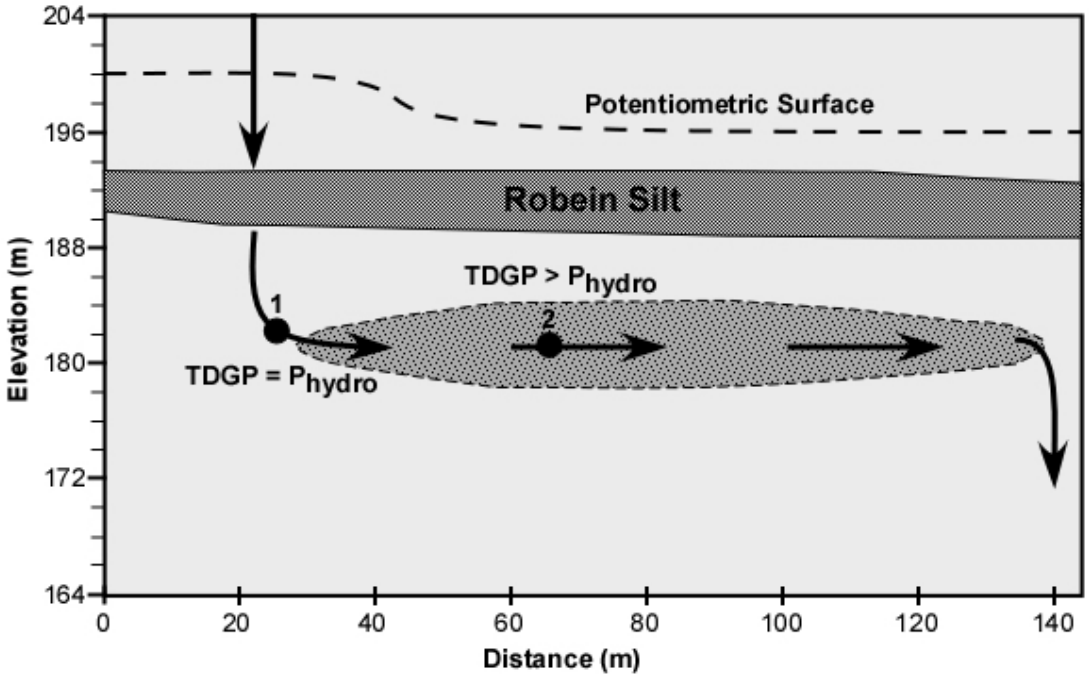

Figure 2. Conceptual model of the suspected mechanism causing a decrease in hydrostatic pressure and the ensuing degassing (after Coleman et al., 1979). Notice the drop of the potentiometric surface above the sand and gravel lens causing the decrease in hydrostatic pressure from point 1 to point 2.

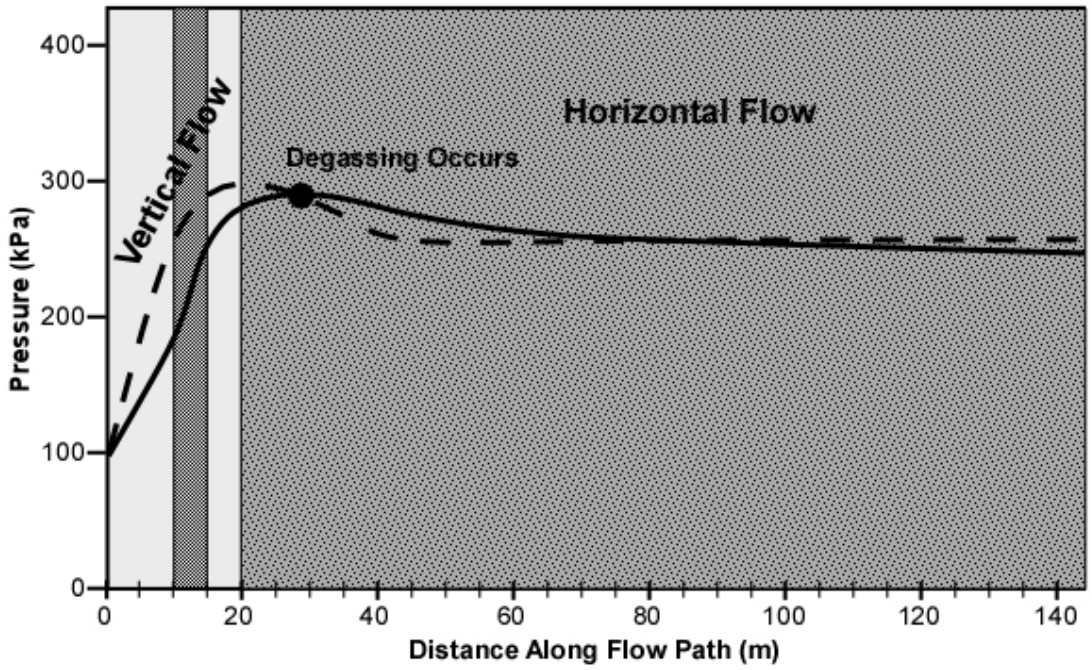

Figure 3. Graphical display of TDGP exceeding hydrostatic pressure along groundwater flow path shown in Figure 2. The shading of the graph plot area is representative of the geologic materials groundwater encounters along flow path shown in Figure 3.

Figure 3 shows a graphical display of TDGP exceeding hydrostatic pressure along groundwater flow path shown in Figure 2. The dashed line represents hydrostatic pressure and the solid line represents TDGP. Hydrostatic pressure increases as groundwater flows vertically downward from the surface, then decreases during lateral flow through the sand and gravel lens. TDGP increases along flow path from CO_2 and CH_4 production, exceeding hydrostatic pressure at the threshold point.

Ebullition is the process in which gas bubbles are transported upward. Ebullition is a common phenomenon and has been documented to occur in lake sediments (Brennwald et al. 2003), marine sediments (Holzner et al., 2008), peats (Kellner et al., 2006, Laing et al., 2008), and contaminated aquifers (Amos et al., 2005). As gas bubbles are formed ebullition will take place when buoyancy forces overcome capillary forces. Ebullition of CH_4 is suspected to occur in a nearly identical geologic situation in central

Iowa in which Wisconsinan age loess is decomposing (Simpkins and Parkin, 1993). It is possible that ebullition does occur as the Robein Silt decomposes and some CH_4 escapes to the surface but at the present there are no data to suggest that ebullition is occurring.

Groundwater Interaction with Drift Gas

Atmospheric noble gases enter the groundwater by gas partitioning during air/water exchange with the atmosphere. Most noble gases have negligible sources and sinks in the subsurface so the concentrations of dissolved noble gases below the water table will be in equilibrium with the atmosphere at the pressure and temperature during recharge. Due to the dissolution of trapped atmospheric bubbles during groundwater table fluctuations, a slight excess of dissolved noble gases is commonly observed (Kipfer et al., 2002). It is suspected that groundwater becomes stripped of noble gases during the generation and/or interaction with the drift gas pockets. As drift gas is generated, CH_4 along with all other dissolved gases in the groundwater will partition into the gas phase, causing the onflowing groundwater to have noble gas concentrations less than atmospheric equilibrium. Groundwater that interacts with a previously formed drift gas pocket will also experience gas partioning as the groundwater equilibrates with the free gas phase. Extensive dissolved gas data from both the Mahomet Aquifer and the Glasford Formation, along with drift gas composition data have been collected throughout the Mahomet Bedrock Valley that suggests the depleted noble gas concentrations in the groundwater are a result of interaction with drift gas (Van der Hoven et al., 2005).

Coleman (1979) collected several gas samples of drift gas pockets throughout Illinois. These samples were archived in stainless steel containers, and were reanalyzed

by gas chromatography and mass spectrometry. As seen in Table 1 drift gas composition is variable, consisting of mostly CH_4 and N_2. Drift gas concentrations of CH_4 and N_2 range from 0.369 to 0.961 and 0.0177 to 0.595 mole fractions, respectively.

Table 1. Drift gas compositions from 8 different drift gas pockets. Gas chromatography and mass spectrometry analysis were performed on each of the samples.

	Isotech Lab Gas Chromatoraphy Analysis mole fractions				University of Utah mass spectrometry analysis mole fractions				
Sample ID	CH_4	CO_2	N_2	Ar (Total)	CH_4	N_2	^{40}Ar	^{84}Kr	^{20}Ne
N. Goloff	3.69×10^{-1}	2.73×10^{-2}	5.95×10^{-1}	8.21×10^{-3}	3.84×10^{-1}	5.80×10^{-1}	7.94×10-3	1.30×10^{-6}	8.64×10^{-6}
D.Gooch	7.89×10^{-1}	9.90×10^{-3}	1.98×10^{-1}	2.89×10^{-3}	8.14×10^{-1}	2.07×10^{-1}	2.85×10-3	2.29×10^{-7}	3.21×10^{-6}
Seaton	8.55×10^{-1}	2.36×10^{-2}	1.18×10^{-1}	2.16×10^{-3}	9.32×10^{-1}	1.21×10^{-1}	2.33×10-3	2.25×10^{-7}	1.47×10^{-6}
G.Shimp	9.61×10^{-1}	2.03×10^{-2}	1.77×10^{-2}	5.54×10^{-4}	9.55×10^{-1}	2.33×10^{-2}	5.35×10-4	1.12×10^{-6}	2.57×10^{-7}
D. Turner	4.80×10^{-1}	3.90×10^{-3}	5.09×10^{-1}	6.30×10^{-3}	4.86×10^{-1}	5.12×10^{-1}	6.08×10-3	3.86×10^{-7}	9.67×10^{-6}
Old Holt Tavern	9.13×10^{-1}	1.90×10^{-3}	8.42×10^{-2}	1.23×10^{-3}	9.08×10^{-1}	8.52×10^{-2}	1.29×10-3	1.07×10^{-7}	1.51×10^{-6}
Daly	9.24×10^{-1}	7.80×10^{-3}	6.69×10^{-2}	1.30×10^{-3}	9.20×10^{-1}	7.37×10^{-2}	1.37×10-3	1.40×10^{-7}	9.46×10^{-7}
M. Walters	5.39×10^{-1}	2.10×10^{-4}	4.55×10^{-1}	6.03×10^{-3}	5.36×10^{-1}	4.62×10^{-1}	5.84×10-3	4.56×10^{-7}	7.59×10^{-6}

Van der Hoven et al. (2005) found dissolved noble gas concentrations less than atmospheric in the Mahomet aquifer southwest of the main recharge area near Paxton, IL. The loss of inert noble gases indicates the groundwater has experienced degassing. Van der Hoven et al. (2005) showed ^{20}Ne concentrations in the Mahomet aquifer became progressively less than atmospheric equilibrium as it moves along its flow path southwest from the main recharge area. This progressively decreasing ^{20}Ne concentration trend suggests groundwater that has experienced gas loss becomes a significant component of the total aquifer reservoir with distance southwest from the main recharge area.

Use of Noble Gases for Analysis of Subsurface Gas and Water Interaction

Dissolved noble gases in groundwater provide valuable tools for assessing subsurface gas and water interaction. Atmospheric noble gases enter the groundwater by gas partitioning during air/water exchange with the atmosphere. Most noble gases have negligible sources and sinks in the subsurface so the concentrations of dissolved noble

gases below the water table will be in equilibrium with the atmosphere at the pressure and temperature during recharge (Kipfer et al., 2002). An excess of dissolved noble gases is commonly seen and is a result of excess air during recharge and/or terrigenic/radiogenic sources. Since noble gases are inert, a decrease in dissolved noble gases from in equilibrium with atmosphere can only be explained by the interaction with a gas phase below the water table and the subsequent partitioning of the dissolved noble gases into the gas phase. The extent of dissolved noble gas depletion and/or fractionation of noble gas ratios can give insight to the amount of degassing (Amos et al., 2005, Visser et al., 2007, Zhou et al., 2005), depth degassing occurs (Fortuin and Willemsen, 2005), production rates of biogenic gases (Amos et al., 2005), gas transport (Amos and Mayer, 2006a), and physical processes involved with bubble formation (Amos et al., 2005, Amos and Mayer, 2006b).

Visser et al. (2007) observed degassing caused by the production of nitrogen gas by denitrification of agricultural pollution. Using ^{4}He depletion along with TDGP a single-step degassing model was developed to correct for ^{3}He loss to degassing and $^{3}H/^{3}He$ groundwater ages. Once a gas phase is formed, the gas pressure within that gas phase will equilibrate with the sum of atmospheric pressure, hydrostatic pressure, and capillary pressure. Neglecting capillary pressure and assuming a constant atmospheric pressure, the hydrostatic pressure, or depth below the water table, controls the gas pressure within a gas bubble (Visser et al., 2007). The partial pressures of the gases within the bubble are related to the dissolved gas concentrations before bubble formation and their respective solubilities. Therefore, the dissolved gas concentrations of the groundwater around the bubble and TDGP after bubble formation are also controlled by

the depth below the water table (Visser et al., 2007). Using the depletion of dissolved ^{4}He from in equilibrium with the atmosphere and a Henry's law partitioning coefficient, Visser et al. (2007) were also able to calculate the volume of the gas phase, or amount of degassing. Using the depth below the water table that degassing occurred to constrain the time of degassing, and the amount of degassing to calculate the loss of 3He to degassing, Visser et al. (2007) were able to correct $^{3}H/^{3}He$ ages for degassed groundwater.

Fortuin and Willemsen (2004) found depleted N_2 and Ar concentrations due to the formation of bubbles as a result of methanogenesis in a Dutch aquifer. The production of CH_4 and the subsequent exsolution of Ar and N_2 was modeled using the hydrogeochemical transport model PHREEQC. CH_4 and CO_2 partial pressures were increased simulating the decomposition of organic material. A gas phase was allowed to form if the sum of partial pressures exceeded a fixed total pressure. Six simulations were run with total pressures of 1.05, 1.1, 1.5, 2.0, 2.5 and 3.0 atm (Fortuin and Willemsen, 2004). To compare the validity of the PHREEQC model runs with the sampling data, plots were constructed of Ar and N_2 partial pressures versus CH_4 partial pressure. Comparing the modeled partial pressures to the sampling data indicated that the maximum total pressure under which gas bubbles have formed is 3.0 atm. The modeled maximum total pressure for gas bubble formation corresponded well to the maximum TDGP sampled (2.93 atm) (Fortuin and Willemsen, 2004).

Zhou et al. (2005) developed a simple physical model using noble gases to describe the gas-water interaction in a coalbed natural gas field. Noble gas concentrations in the natural gas field are depleted and a greater decrease of noble gases is seen in the areas of increased gas production. Zhou et al. (2005) also found that noble

gas ratios in all samples showed a clear fractionation trend consistent with a gas/groundwater phase partitioning process. However, absolute noble gas concentrations are much less than the simple model could predict and required the addition of "dilution" gas, which is thought to be gas desorbed from coalbeds (Zhou et al., 2005).

Amos et al. (2005) used dissolved Ar and N_2 concentrations to gain a better understanding of the physical and chemical processes within the saturated and unsaturated zones at a petroleum-hydrocarbon contaminated site. Degassing of groundwater has occurred at this site as a result of biodegradation through methanogenesis. In areas of the unsaturated zone data suggests that microbial oxidation of the methane is occurring (Amos et al., 2005). The stoichiometry of this reaction results in gas consumption and a decrease in total pressure. The occurrence of microbial oxidation is further supported by the enrichment of dissolved Ar and N_2 in these areas as CH_4 and O_2 are consumed (Amos et al., 2005). Amos et al. (2005) assumed that areas of Ar enrichment represented areas of maximum gas consumption and lowest total pressure, and the areas of greatest depletion indicated the largest source areas for gas and highest total pressure. Ar concentrations in the unsaturated zone were contoured and used as proxies for total pressure. Using these contours advective gas flow was inferred. Amos et al. (2005) assumed the system was in steady state, and that Ar and N_2 advective fluxes were of equal and opposite direction to the calculated diffusive fluxes. Using this assumption linear velocity was calculated using both Ar and N_2 concentrations. The velocities calculated for Ar and N_2 were similar and differed less than 10 percent. Using the average of the calculated velocities, advective mass flux of CH_4 was able to be calculated at given points (Amos et al., 2005). By using Ar and N_2 Amos et al. (2005)

showed that reaction-induced gas advection is a significant process in the unsaturated zone at a petroleum-hydrocarbon contaminated site.

In the saturated zone Amos et al. (2005) found a significant relationship between increased CH_4 concentrations and greater depletion of Ar and N_2, indicating that the depletion is due to degassing caused by methane production. Amos et al. (2005) used a simple batch model to simulate the production of CH_4 and CO_2 caused by methanogenesis and the subsequent degassing. The production of CH_4 and CO_2 by methanogenesis was simulated by incremental additions of CH_4 and CO_2 as reaction steps. In this study they did not attempt to correlate reaction progress to time (Amos et al., 2005). The modeled dissolved gas concentrations were compared to the observed concentrations by matching the sampled dissolved CH_4 concentration to the predicted CH_4 concentration, and comparing the N_2, CO_2, and Ar concentrations associated with that reaction step to the observed concentrations. The measured N_2, CO_2, Ar, and total pressure data for the source zone and downgradient wells were close to the predicted pressures from the model (Amos et al., 2005). The data from each well were correlated to CH_4 and CO_2 production and amount of degassing. As an example, one well was found to have been exposed to the production of 9.6×10^{-4} mol of CH_4 (16 steps$\times6\times10^{-5}$ mol CH_4 per step) and 3.84×10^{-3} mol of CO_2 (16 steps$\times2.4\times10^{-4}$ mol CO_2 per step) and has degassed, depleting N_2 and Ar to ~70 percent of their background concentrations (Amos et al., 2005). The model presented by Amos et al. (2005) showed that Ar and N_2 concentrations can be used to quantify degassing processes, better constrain total gas loss from the water phase, and therefore provide a better estimate of methanogenic biodegradation rates and gas-phase saturation in the saturated zone (Amos et al., 2005).

As shown, several studies have used dissolved noble gases to assess subsurface gas and water interaction. Fewer studies have used numerical models to simulate the generation of a gas phase by the production of biogenic gases and the depletion of dissolved noble gases. These models can give better understanding to the physical and chemical processes involved in subsurface gas generation (Amos and Mayer, 2006a, Amos and Mayer, 2006b, Visser et al., 2009).

Amos and Mayer (2006b) used the reactive transport code MIN3P to simulate the production of CH_4 and degassing occurring at a petroleum hydrocarbon contaminated aquifer. The simulations were constrained by comparing observed and modeled dissolved gas concentrations. In a previous study, Amos et al. (2005), a simple batch model was unable to provide insight on the sharp decrease of CH_4 concentrations and attenuation of depleted N_2 and Ar concentrations downgradient from the methanogenic source. Degassing alone was unable to explain the observed trend, and physical processes not unable to be modeled were suspected (Amos et al., 2005). The numerical model suggests that the observed decrease in CH_4 concentration and Ar and N_2 depletion is a result of permeability reduction due to gas bubble formation and dissolution of entrapped atmospheric bubbles near the water table (Amos and Mayer, 2006b). As gas bubbles formed, permeability was reduced, resulting in groundwater deflection around the methanogenic source zone. The deflected groundwater attenuates the downgradient plume, returning the Ar and N_2 concentrations back to atmospheric and decreasing CH_4 concentration. Groundwater deflection around the source zone along with entrapped atmospheric bubbles due to water table fluctuations provided the best representation of the data at the crude oil spill site (Amos and Mayer 2006b).

Amos and Mayer (2006a) also used the reactive transport code MIN3P to simulate the ebullition in a methanogenic sand column. The numerical model along with dissolved gas analysis provided insight to the main factors controlling rate of ebullition and gas composition. The objective of the model was to find a formulation that could describe gas bubble movement on the macro-scale, constrained by dissolved gas data observed in a column experiment. The model was calibrated to ebullition volume and dissolved gas concentrations along the column. The model could not reproduce the erratic bubble movement typically observed in real systems. However, the model provided a good match of the simulated dissolved gas concentrations, gas phase saturation, and ebullition volume to the experimental observations. The study provided evidence that dissolved gas analysis and reactive transport modeling can an effective means of investigating ebullition and quantifying gas transport.

Degassing has occurred due to the generation of a gas phase produced by denitrification under agricultural land in the south of the Netherlands (Visser et al., 2007, Visser et. al. 2009). Visser et al. (2009) used a two-phase groundwater flow and transport model to study simulate the generation of gas phase and fate of dissolved gases. The goal of the study was to assess the usefulness of tracers in situations where degassing occurs and the capability of a two-phase flow and transport model to assist in the interpretation of degassed groundwater age tracer measurements. The components included in the model were the groundwater age tracers ^{3}H, ^{3}He, ^{4}He, Ne, CFCs and SF_6. The 2D model was calibrated to head, TDGP, ^{4}He and Ne concentrations (indicating degassing), ^{3}H and tritiogenic ^{3}He ($^{3}He^{*}$) concentrations and calculated $^{3}H/^{3}He$ ages from a downgradient dual screened monitoring well (Visser et al., 2009). The model was not

only capable of simulating the process of degassing but also the amount of degassing. Modeled amount of degassing, observed as depletion of ^{4}He and Ne, was close to the measured values. The shallow screen underestimated the amount of degassing; therefore modeled age $^{3}H/^{3}He$ range is less than observed. The modeled $^{3}H/^{3}He$ age range matched the observed age range at the deep screen because the amount of degassing was modeled accurately (Visser et al., 2009). Visser et al. (2009) also successfully constrained recharge rate by calibrating to ^{3}H and $^{3}He^{*}$ measurements.

Statement of Problem

The primary goal of this research is to develop a geochemical flow model in order to better constrain recharge through the low permeability glacial till formations overlying the Mahomet Aquifer. This research may also be able to provide insights on time scales of the generation of microbial CH_4 gas pockets and in situ CH_4 production rates. In situ CH_4 production rates have also been difficult to constrain, especially CH_4 production as the result of the biodegradation of a natural feature such as a buried paleosol. The proposed model could quantitatively asses a possible range of CH_4 production rates.

I hypothesized that there is a significant amount of groundwater recharging the Mahomet Aquifer through the confining glacial till units southwest of the main recharge area. The increasing percentage of groundwater that has experienced gas loss along the southwest flow path in the Mahomet aquifer was believed to support this. As there is no known mechanism capable of causing degassing within the Mahomet Aquifer itself, it was theorized that a significant amount of water is infiltrating through the Glasford/Wedron Formations, interacting with the drift gas pockets, and contributing "stripped" groundwater to the underlying aquifer. This is contrary to the belief that all

significant recharge to the Mahomet along this flow path is through the main recharge area near Paxton, IL. It was proposed by simulating the generation of the drift gas pockets within the glacial till units confining the aquifer using a 2D multiphase flow model, we would be able to constrain the amount of groundwater infiltrating through the Glasford/Wedron till into the Mahomet Aquifer.

Objectives

To test this hypothesis, the following objectives are to be accomplished.

1. Construct a 2D multiphase flow model that simulates the generation of drift gas pockets within the glacial till confining units using the NUFT code.
2. Adjust methane production rates and infiltration rates in order to generate drift gas pockets similar in size and location to what is seen in the field.
3. Calibrate the model to known drift gas composition and the dissolved gas concentrations of the associated groundwater in both the Glasford and Mahomet Aquifer.
4. Check if infiltration and methanogenesis rates are plausible in this setting.

CHAPTER II

MANUSCRIPT FOR APPLIED GEOCHEMISTRY

Introduction

The generation of a gas phase beneath the water table occurs as total dissolved gas pressure exceeds hydrostatic pressure. Degassing can be caused by a decrease in hydrostatic pressure as a result of groundwater pumping (Fortuin and Willemsen, 2005), water level decline (Yager and Fountain, 2001), or hydraulic testing (Jarsjo and Destouni, 2000); or an increase of the total dissolved gas pressure by the subsurface production of gases such as nitrogen (N_2), carbon dioxide (CO_2), hydrogen sulfide (H_2S) or methane (CH_4) by biogeochemical processes. Degassing has been observed as a result of N_2 production by denitrification from agricultural pollution (Blicher-Mathiesen et al., 1998; Visser et al., 2007) and as a result of CH_4 production under landfills (Solomon et al., 1992), in lake sediments (Brennwald et al., 2005; Holzner et al., 2008), from the biodegradation of coal beds (Zhou et al., 2005) and the natural attenuation of petroleum hydrocarbons (Amos et al, 2005; Amos and Mayer, 2006b).

Noble gases have been widely used to investigate subsurface gas and water interaction. The atmospheric noble gases are particularly powerful tools to trace and study gas partitioning and environmental conditions during groundwater recharge because of their conservative behavior and wide range of solubilities (Aeschbach-Hertig et al., 2008). Because noble gases repartition between the water and gas phase after gas formation, onward flowing groundwater can have noble gas concentrations below

atmospheric equilibrium (Visser et al. 2007). The extent of this "stripping" of noble gases and other inert gases has been used to quantify the amount of degassing in subsurface processes. Ar and N_2 stripping has been used to assess the amount of degassing due to denitrification in a Danish riparian wetland (Blicher-Mathiesen et al., 1998), microbial CH_4 production at a petroleum-hydrocarbon contaminated site (Amos et al., 2005) and in an organic rich Dutch aquifer (Fortuin and Willemsen, 2005).

The objective of this study is to develop a multiphase flow model to simulate the generation of biogenic CH_4 "drift gas" pockets in an aquitard to put a geochemical constraint on the amount of groundwater recharging the aquifer underlying the confining unit. The aquitard is a glacial till characterized by unsorted clay, silt, sand, and gravel matrix (diamicton) with sand and gravel lenses, where the "drift gas" accumulates. These "drift gas" pockets form as CH_4 is produced as a microbial byproduct during the decomposition of an organic rich, buried paleosol within the aquitard. Noble gas concentrations from the underlying aquifer indicate the groundwater has been degassed at some point. Total dissolved gas pressure (TDGP) increases and approaches dissolved gas saturation as groundwater moves vertically through the aquitard and CH_4 is accumulated in the degrading paleosol. It is believed the more permeable sand and gravel lenses drive lateral groundwater flow through these features causing a drop in hydrostatic pressure below TDGP. As hydrostatic pressure is exceeded by TDGP, CH_4 and other dissolved gases are exsolved from solution, forming a drift gas pocket. It is hypothesized that modeling the generation of drift gas will provide constraint on the amount of groundwater infiltrating through the aquitard and recharging the aquifer.

Glacial aquifers throughout Illinois have been contaminated by improperly contained or disposed chemicals, routine application of agricultural chemicals, and de-icing chemicals (USGS, 1999). In the case of a major freshwater resource like the Mahomet Aquifer it is critical to be able to constrain the amount of water recharging the aquifer and the locations recharge is occurring. In many parts of the world, vertical leakage through regionally extensive aquitards is an important source of recharge to underlying aquifers (Gerber and Howard, 2000). Depleted noble gas concentrations within the Mahomet Aquifer suggest that significant vertical recharge is occurring through the glacial till aquitards that confine it. Quantifying vertical leakage through and aquitard has proven to be a difficult task and poorly understood (Gerber and Howard, 2000, Neuzil, 1986). Response of large scale tests of flow through aquitards takes too long to observe and is severely limited by constraints of time. Thus, the best estimates for flow through aquitards are normally obtained by integrating values obtained from a wide range of tests small in scale relative to the volume of interest (Neuzil, 1986). The uncertainty involved with these small scale tests is further amplified with heterogeneity of aquitards containing features such as sand lenses, as in the case of the glacial tills confining the Mahomet Aquifer (Gerber and Howard, 2000). The aim of this study is to provide insight to the ability to quantify infiltration through an aquitard by modeling the evolution of groundwater geochemistry.

Geology/Hydrogeology

The Mahomet Bedrock Valley is a preglacial drainage system that eroded into bedrock across Illinois (Figure 1). During successive periods of Pleistocene glaciations this paloevalley has been filled with up to 100 meters of a complex sequence of glacial

sediments (Kempton et al., 1991). These glacial deposits are divided into Wedron, Glasford, and Banner Formations. These three major till deposits are typically separated by weathered zones, which in some cases coincide with substantial soil development during interglacial periods. These paleosols can be enriched with organic matter, and in some areas contain peat deposits (Hackley et al., 2010).

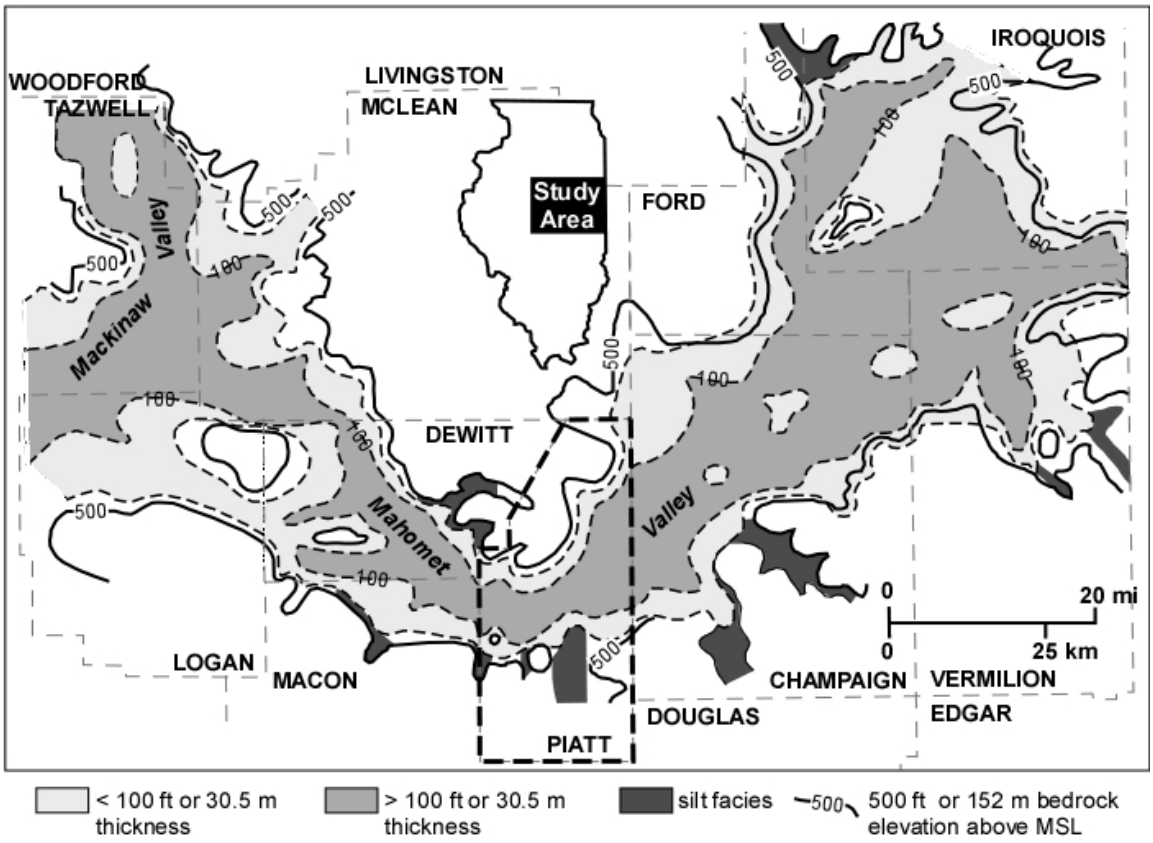

Figure 4. Distribution and thickness of the Mahomet Sand Member (Mahomet Aquifer) and location of related silt facies. The Mahomet Bedrock Valley defined by 500 ft contours (modified from Hackley et al., 2010). Study site is outlined in thick black dashed line (Piatt County).

Banner Formation

The Banner Formation is pre-Illinoisan in age and was deposited more than 400,000 ka. It includes the glacial tills and underlying and intercalated sands, gravels,

and silts. The Banner Formation can be as much as 300 feet thick and contains nine different lithologic members (Willman and Frye, 1975). The Mahomet Sand Member of the Banner Formation consists of a sand facies that occurs in the main valley and a silt facies that occurs in tributary valleys (Kempton et al., 1991) (Figure 1). The sand facies of the Mahomet Sand Member is commonly referred to as the Mahomet Aquifer. The sand facies is restricted primarily to the main valley and is more than 30 meters thick, and is often more than 45 meters thick in the deepest part of the Mahomet Valley. This facies consists of coarse, gravelly sand that tends to fine upward. The origin of the Mahomet Aquifer is unclear but is interpreted to be glacial outwash deposited by braided glacial rivers during multiple glaciations (Kempton et al., 1991). The Mahomet Aquifer is a major aquifer in east-central Illinois. Kempton et al. (1991) report an average hydraulic conductivity of ~1.3 x 10^{-3} m/s. The Mahomet Aquifer is overlain by tills of the Banner, Glasford and Wedron Formations (Hackley et al., 2010).

Glasford Formation

The Glasford Formation was deposited during the Illinoisan Episode between 180 and 125 ka. The formation includes glacial tills, intercalated outwash deposits of gravel, sand, and silt, and the overlying accretion-gley deposits. The Glasford Formation is almost continuous throughout Illinois and ranges from a meter to more than 45 meters thick (Willman et al., 1975). The central and eastern part of the Glasford Formation contains significant sand and gravel deposits within the low permeability till. These sand and gravel layers or lenses can be a significant aquifer within the Mahomet Bedrock Valley and are referred to as the Glasford Sand (Hackley et al., 2010). These sand and gravel lenses are also important to the focus of this study as this is where “drift gas” has

been found to accumulate. These sand and gravel units are thought to have functioned as a drainage way for glacial melt water during the Illinoian Episode. Hydraulic conductivities in the Glasford aquifer range to as much 2×10^{-3} m/s and have a median of 4×10^{-4} m/s throughout east-central Illinois (Kempton et al., 1991). The western portion of the Glasford contains little or no sand and gravel, and is composed of thick tills. The Glasford Formation is overlain by the Wisconsinan age tills.

Robein Silt

The Robein Silt occurs within a substage of the Wisconsinan glaciations and has been radiocarbon dated at 28,000 to 22,000 years B.P (Coleman et al., 1979). The Robein is brown, gray, dark gray to black, leached silt and contains abundant organic material. The Robein ranges from centimeters to more than 1.5 meters thick. It is discontinuous but widely distributed in Illinois (Willman et al., 1975). Glessner and Roy (2009) described the occurrence of the Robein in Piatt County as having a silt, sandy loam, or peaty silt texture and being grayish brown, dark grayish brown, or black in color. Reported organic carbon content of the Robein Silt ranged from 0.52% to 17.2% with a mean of 3.9% ± 4.2% (Glessner and Roy, 2009). The decomposition of this organic material is the source of methane in the drift gas pockets (Coleman et al., 1979). The Robein Silt is overlain by the Wedron Formation.

Wedron Formation

The Wisconsinan age Wedron Formation overlies all the older glacial materials and forms the present day land surface for much of Piatt County (Anliker and Sanderson, 1995). The formation consists of glacial till and outwash. Although largely till, the Wedron contains numerous intercalated beds of outwash gravel, sand, and silt. The

Wedron Formation contains fewer sand and gravel deposits than the Banner and Glasford. The Wedron sand and gravel deposits are relatively small and much thinner (Hackley et al., 2010).

Hydrogeology

Recharge to the Mahomet aquifer is thought to occur primarily as vertical leakage of precipitation through the overlying glacial sediments and by upward leakage through the bedrock (Kempton et al., 1991; Panno et al., 1994). Kempton et al. (1991) determined hydraulic conductivities of the confining beds to range from 1×10^{-9} to 2×10^{-7} m/s, and assumed an average annual recharge rate of 1.81×10^{-9} m/s for the entire Mahomet Valley Bedrock Lowland (Kempton et al., 1991). The main recharge to the central and eastern part of the aquifer appears to occur at a potentiometric high point near the town of Paxton, IL (Wilson et al., 1998). The overlying Glasford Formation in this region contains relatively thick and well connected sand and gravel units that allow for significant recharge to the Mahomet Aquifer. From this potentiometric high point groundwater flows to the north, east, and southwest (Wilson et al., 1998). The hydraulic gradient for most of the Mahomet Aquifer is ~0.00019, except near the major cone of depression that has developed near the cities of Champaign-Urbana (Hackley et al., 2010).

Geochemistry

Drift Gas

CH_4 is most commonly formed in the subsurface by thermal (thermogenic) or by microbial decomposition (biogenic) of buried organic materials. Drift gas is a term that refers to methane (with varying amounts of N_2 and CO_2) that accumulates in glacial

deposits throughout Illinois. The CH_4 in the drift gas pockets is produced by methanogenesis during the decomposition of an organic rich paleosol. Coleman et al. (1988) provided substantial isotopic data indicating that the drift gas in Illinois is of microbial origin, specifically through CO_2 reduction. Hackley et al. (2010) showed that the $\delta^{13}C$ and δD values for the dissolved CH_4 in the Glasford formation and the Mahomet Aquifer also indicate a microbial origin by CO_2 reduction.

Coleman et al. (1979) used radiocarbon (^{14}C) dating to determine that the majority of drift gas is formed from the degradation of the organic rich Robein Silt, which generally dates from 22,000 to 28,000 years old. The sand and gravel lenses directly above and below this buried soil horizon provide a reservoir for the drift gas, and the overlying till serves as a cap (Coleman et al., 1979). ^{14}C ages of all drift gas samples presented in Coleman et al. (1979) were equal to or younger than the reservoir material in which gas has accumulated. This indicates that upward migration of CH_4 produced in sediments older than the sand and gravel lenses has not been a major factor in the formation of drift gas deposits. The downward transport CH_4 into sand and gravel lenses below the Robein silt seems to be a more likely occurrence.

Drift gas commonly exists some distance from the probable source material, and it appears that movement of CH_4 as a solute in groundwater is the most probable mechanism for drift gas migration (Coleman et al. 1979). In order for degassing to occur, and the formation of a drift gas pocket, groundwater must encounter a zone in which the hydrostatic pressure is less than the sum of the partial pressures of the dissolved gases. As the total dissolved gas pressure (TDGP) exceeds the threshold pressure, the dissolved gases will partition into the gas phase. Nested well data shows that groundwater flow is

primarily vertical downward through the aquitard overlying the Mahomet Aquifer. It is believed that where larger sand and gravel lenses are present, horizontal groundwater movement occurs as water moves through the higher hydarulic conductivity (K) material. It is hypothesized that the mechanism for drift gas generation is a result of the vertical flow through the low K diamicton, and the subsequent horizontal flow through the sand and gravel lenses, shown in Figure 5. As water moves vertically through the diamicton and passes through the Robein Silt, dissolved CH_4 is acquired and transported downward. As CH_4 accumulates, the TDGP may increase to where it equals the hydrostatic pressure (point 1 shown in Figure 5). As the water moves horizontally through the sand and gravel lens a drop in hydrostatic pressure occurs and TDGP exceeds hydrostatic pressure causing the exsolution of gas (point 2 in Figure 5 and the degassing point shown in Figure 6).

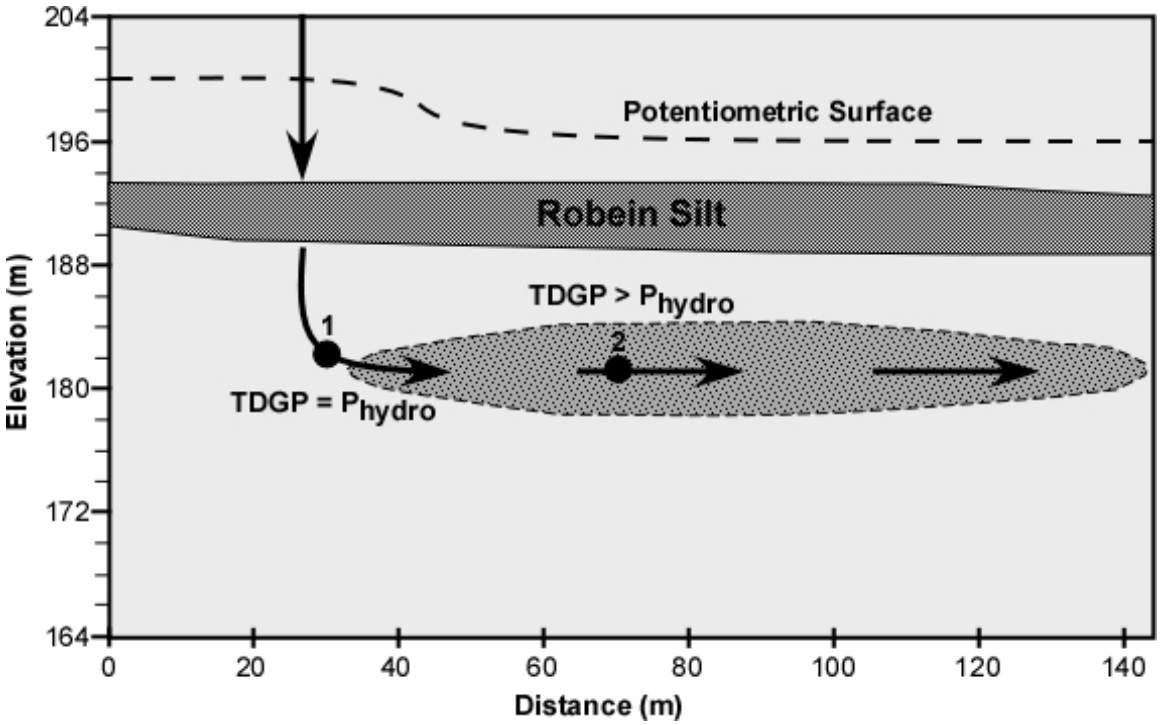

Figure 5. Conceptual model of the suspected mechanism causing a decrease in hydrostatic pressure and the ensuing degassing (after Coleman et al., 1979). Notice the

drop of the potentiometric surface above the sand and gravel lens causing the decrease in hydrostatic pressure from point 1 to point 2.

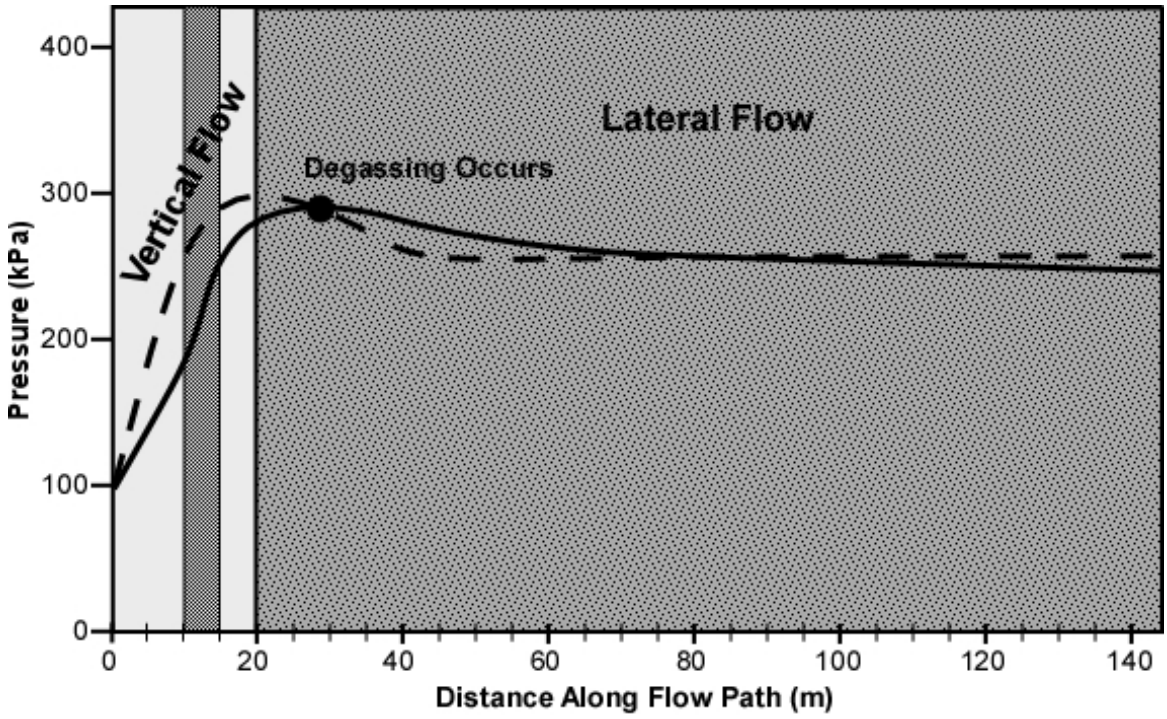

Figure 6. Graphical display of TDGP exceeding hydrostatic pressure along groundwater flow path shown in Figure 5. The shading of the graph plot area is representative of the geologic materials groundwater encounters along flow path shown in Figure 5.

Figure 6 shows a graphical display of TDGP exceeding hydrostatic pressure along groundwater flow path shown in Figure 5. The dashed line represents hydrostatic pressure and the solid line represents TDGP. Hydrostatic pressure increases as groundwater flows vertically downward from the surface, then decreases during lateral flow through the sand and gravel lens. TDGP increases along flow path from CO_2 and CH_4 production, exceeding hydrostatic pressure at the threshold point.

Ebullition is the process in which gas bubbles are transported upward. Ebullition is a common phenomenon and has been documented to occur in lake sediments (Brennwald et al. 2003), marine sediments (Holzner et al., 2008), peats (Kellner et al., 2006, Laing et al., 2008), and contaminated aquifers (Amos et al., 2005). As gas bubbles

are formed ebullition will take place when buoyancy forces overcome capillary forces. Ebullition of CH4 is suspected to occur in a nearly identical geologic situation in central Iowa in which Wisconsinan age loess is decomposing (Simpkins and Parkin, 1993). It is possible that ebullition does occur as the Robein Silt decomposes and some CH_4 escapes to the surface but at the present there are no data to suggest that ebullition is occurring.

Groundwater Interaction with Drift Gas

Atmospheric noble gases enter the groundwater by gas partitioning during air/water exchange with the atmosphere. Most noble gases have negligible sources and sinks in the subsurface so the concentrations of dissolved noble gases below the water table will be in equilibrium with the atmosphere at the pressure and temperature during recharge. Due to the dissolution of trapped atmospheric bubbles during groundwater table fluctuations, a slight excess of dissolved noble gases is commonly observed (Kipfer et al., 2002). It is suspected that groundwater becomes stripped of noble gases during the generation and/or interaction with the drift gas pockets. As drift gas is generated, CH_4 along with all other dissolved gases in the groundwater will partition into the gas phase, causing the onflowing groundwater to have noble gas concentrations less than atmospheric equilibrium. Groundwater that interacts with a previously formed drift gas pocket will also experience gas partioning as the groundwater equilibrates with the free gas phase. Extensive dissolved gas data from both the Mahomet Aquifer and the Glasford Formation, along with drift gas composition data have been collected throughout the Mahomet Bedrock Valley that suggests the depleted noble gas concentrations in the groundwater are a result of interaction with drift gas (Van der Hoven et al., 2005).

Coleman (1979) collected several gas samples of drift gas pockets throughout Illinois. These samples were archived in stainless steel containers, and were reanalyzed by gas chromatography and mass spectrometry. As seen in Table 2 drift gas composition is variable, consisting of mostly CH_4 and N_2. Drift gas concentrations of CH_4 and N_2 range from 0.369 to 0.961 and 0.0177 to 0.595 mole fractions, respectively.

Table 2. Drift gas compositions from 8 different drift gas pockets. Gas chromatography and mass spectrometry analysis were performed on each of the samples.

	Isotech Lab Gas Chromatoraphy Analysis mole fractions				University of Utah mass spectrometry analysis mole fractions				
Sample ID	CH_4	CO_2	N_2	Ar (Total)	CH_4	N_2	^{40}Ar	^{84}Kr	^{20}Ne
N. Goloff	3.69×10^{-1}	2.73×10^{-2}	5.95×10^{-1}	8.21×10^{-3}	3.84×10^{-1}	5.80×10^{-1}	7.94×10-3	1.30×10^{-6}	8.64×10^{-6}
D.Gooch	7.89×10^{-1}	9.90×10^{-3}	1.98×10^{-1}	2.89×10^{-3}	8.14×10^{-1}	2.07×10^{-1}	2.85×10-3	2.29×10^{-7}	3.21×10^{-6}
Seaton	8.55×10^{-1}	2.36×10^{-2}	1.18×10^{-1}	2.16×10^{-3}	9.32×10^{-1}	1.21×10^{-1}	2.33×10-3	2.25×10^{-7}	1.47×10^{-6}
G.Shimp	9.61×10^{-1}	2.03×10^{-2}	1.77×10^{-2}	5.54×10^{-4}	9.55×10^{-1}	2.33×10^{-2}	5.35×10-4	1.12×10^{-6}	2.57×10^{-7}
D. Turner	4.80×10^{-1}	3.90×10^{-3}	5.09×10^{-1}	6.30×10^{-3}	4.86×10^{-1}	5.12×10^{-1}	6.08×10-3	3.86×10^{-7}	9.67×10^{-6}
Old Holt Tavern	9.13×10^{-1}	1.90×10^{-3}	8.42×10^{-2}	1.23×10^{-3}	9.08×10^{-1}	8.52×10^{-2}	1.29×10-3	1.07×10^{-7}	1.51×10^{-6}
Daly	9.24×10^{-1}	7.80×10^{-3}	6.69×10^{-2}	1.30×10^{-3}	9.20×10^{-1}	7.37×10^{-2}	1.37×10-3	1.40×10^{-7}	9.46×10^{-7}
M. Walters	5.39×10^{-1}	2.10×10^{-4}	4.55×10^{-1}	6.03×10^{-3}	5.36×10^{-1}	4.62×10^{-1}	5.84×10-3	4.56×10^{-7}	7.59×10^{-6}

Van der Hoven et al. (2005) found dissolved noble gas concentrations less than atmospheric in the Mahomet aquifer southwest of the main recharge area near Paxton, IL. The loss of inert noble gases indicates the groundwater has experienced degassing. Van der Hoven et al. (2005) showed ^{20}Ne concentrations in the Mahomet aquifer became progressively less than atmospheric equilibrium as it moves along its flow path southwest from the main recharge area. This progressively decreasing ^{20}Ne concentration trend suggests groundwater that has experienced gas loss becomes a significant component of the total aquifer reservoir with distance southwest from the main recharge area.

Methods

Three cross-sections through Piatt County were produced from well logs obtained from the Illinois State Geological Survey (ISGS) (Figure 7). The cross-sections A, B,

and C show the overlying diamicton units and the Mahomet Aquifer (Figure 8, 9, and 10). The quality of these logs varies, consisting of three high quality lithologic logs that were also geophysically logged, and the remaining logs are driller's logs. For the purpose of this study the Wedron and Glasford Formations along with other successive diamicton deposits will be generalized into one unit overlying the Mahomet Aquifer. The Wedron and Glasford Formations were deposited during similar glaciation events, and both consist of unsorted clay, silt, sand, and gravel (diamicton) with pockets of sorted outwash sand and gravels. Due to the similar composition and hydraulic properties of the formations, the Wedron and Glasford are combined into single unit in the model (Kempton et al. 1991, Willman and Frye, 1975, Anliker and Sanderson 1995). The sand and gravel lenses within the glacial till units appear to be the most influential features in drift gas generation; therefore the proposed model will only differentiate between unsorted diamicton and sand and gravel lenses. Three cross-sections were produced in order to account for the variety of different geologic settings in the field. The cross-sections represent transects through Piatt County with one of the high quality lithologic logs included in each transect (Figure 7). The Piatt County portion of the Mahomet Valley was chosen because this is where groundwater that has experienced gas loss appears to become a more significant component of the Mahomet Aquifer, and it is suspected groundwater is interacting with drift gas (Van der Hoven et al. 2005).

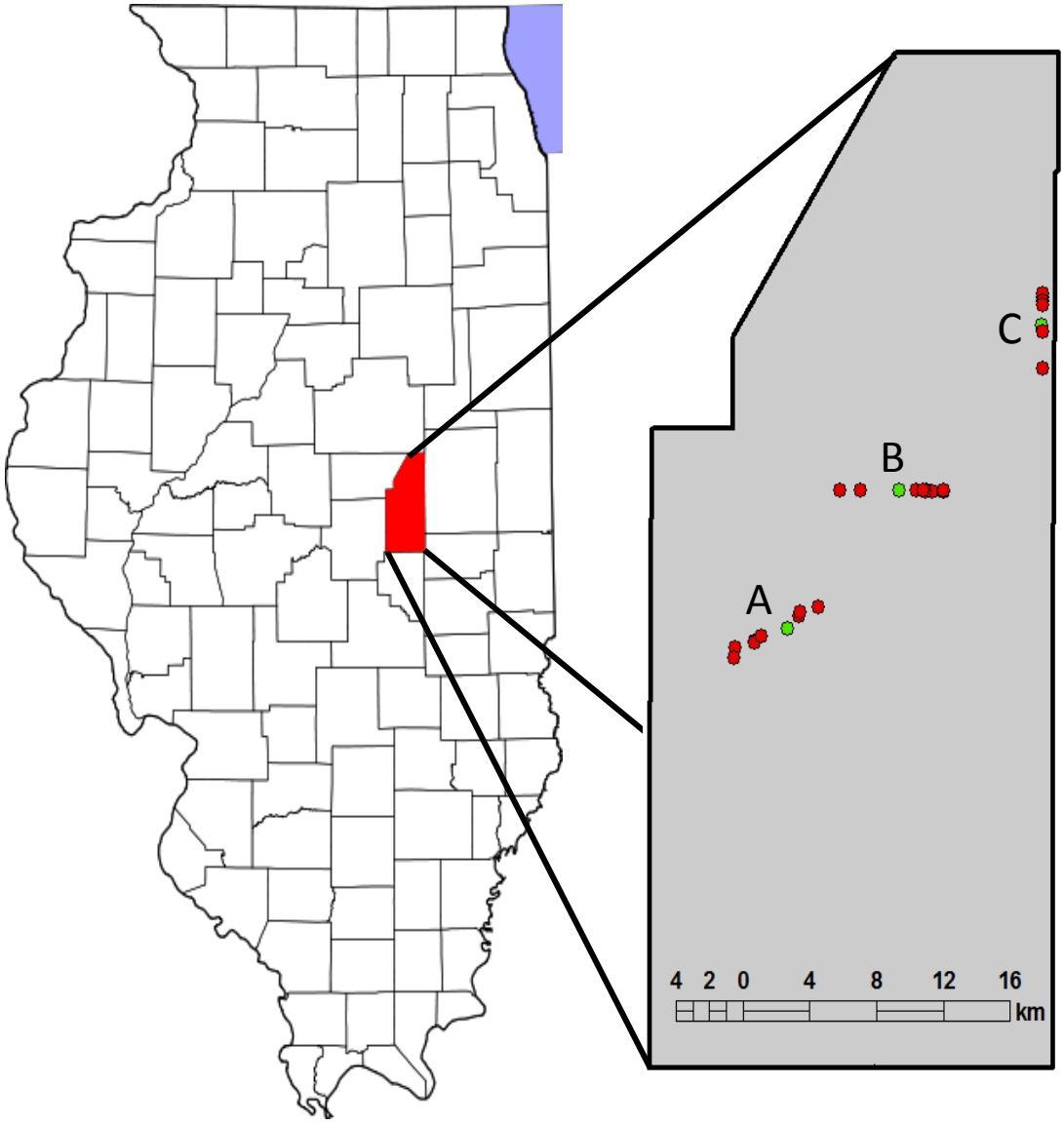

Figure 7. Site map with position of well logs used for cross-sections A, B, and C. Driller's logs are shown in red and high quality logs are shown in green.

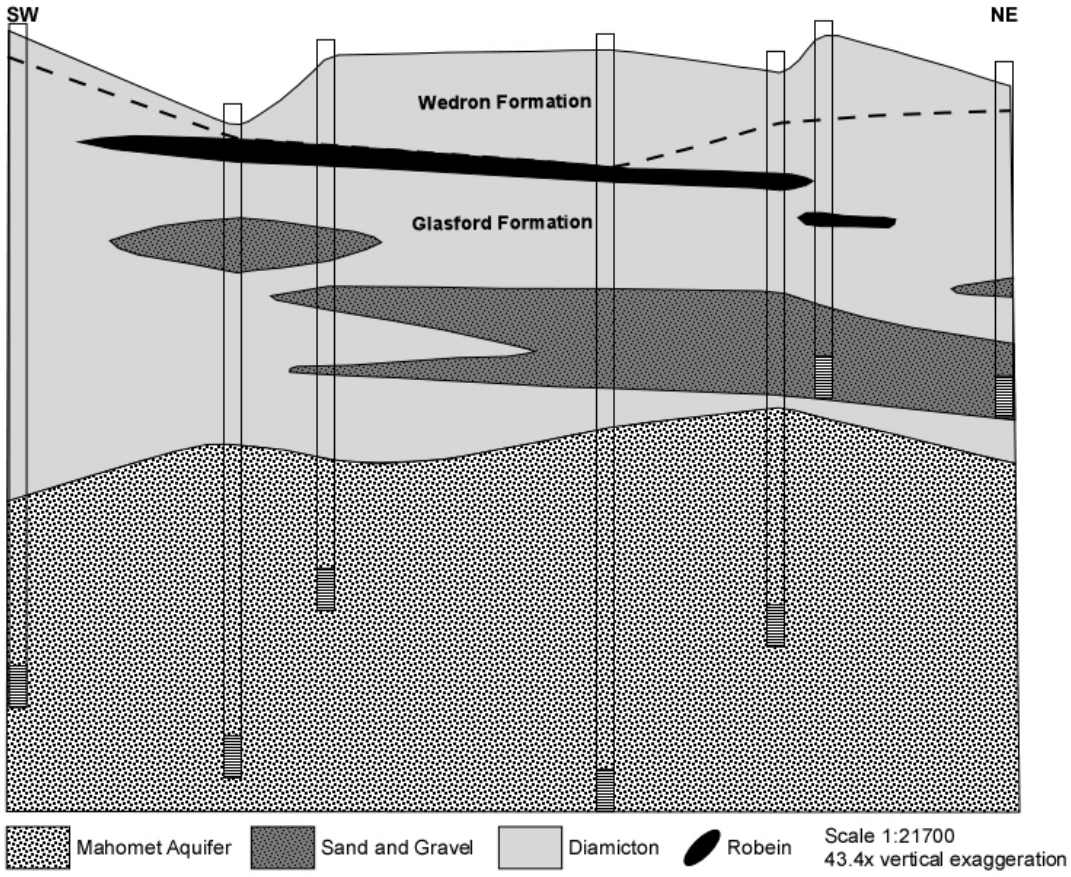

Figure 8. Cross-section A through Piatt County. Locations of wells are shown in Figure 7.

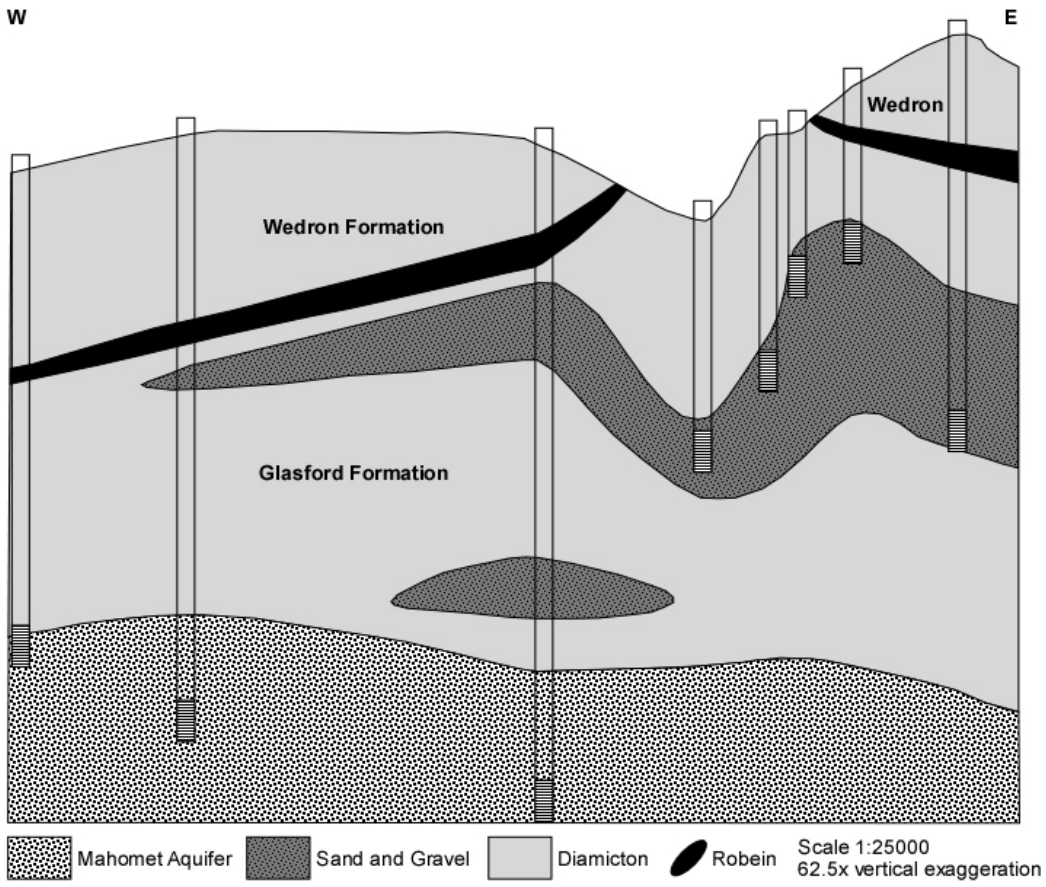

Figure 9. Cross-section B through Piatt County. Locations of wells are shown in Figure 7.

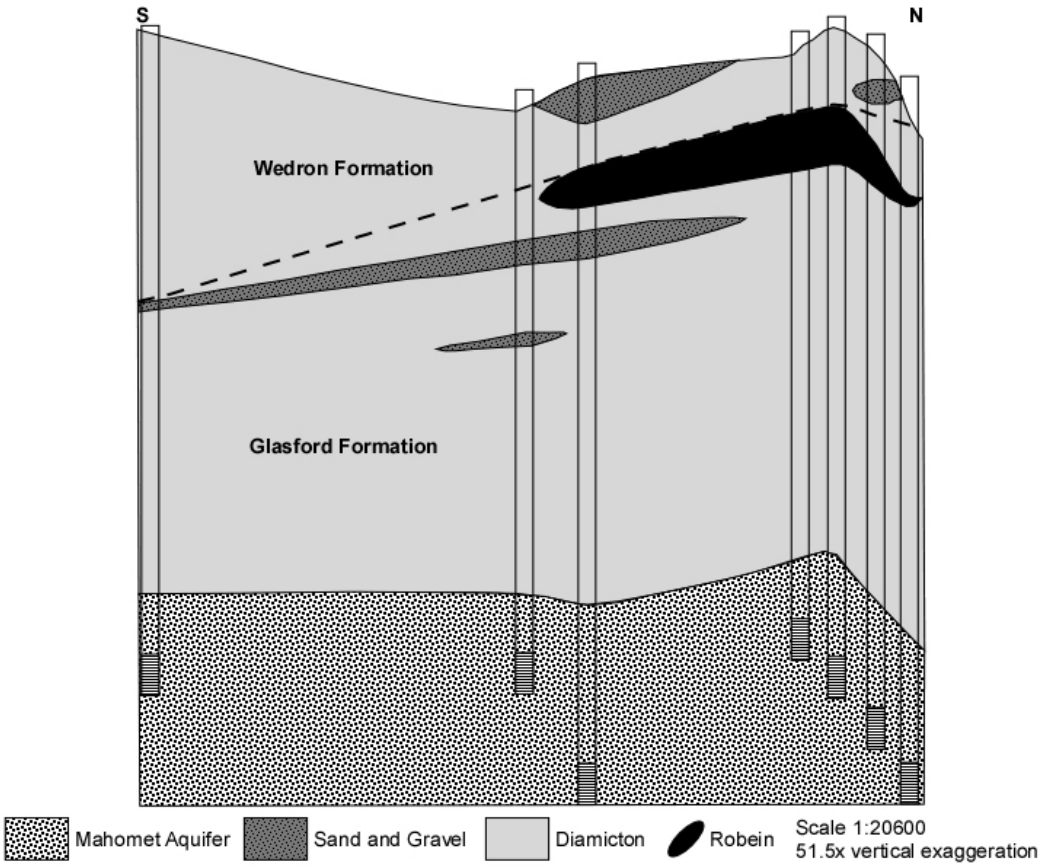

Figure 10. Cross-section C through Piatt County. Locations of wells are shown in Figure 7.

The multiphase 2D model simulating the generation of the drift gas pockets was run using the Nonisothermal Unsaturated-Saturated Flow and Transport (NUFT) code (Nitao, 2000). NUFT is a multiphase, multicomponent computer code for modeling fluid flow and transport in porous media under isothermal and non-isothermal conditions, with application to subsurface contaminant transport problems. An integrated finite-difference spatial discretization is used to solve the mass balance equations. The resulting non-linear equations are solved each time by the Newton-Raphson method (Nitao, 2000). NUFT allowed for the simulation of the transport and fate of several gases including, N_2, CO_2, CH_4, ^{20}Ne, ^{40}Ar, and ^{84}Kr in both the dissolved and gaseous phase. ^{3}He and ^{4}He

were removed from the components in order to decrease simulation time. Due to the anoxic conditions even in relatively shallow groundwater in this area, O_2 was also excluded from the model. The models were run for 10,000 years simulating the start of the Holocene epoch to present.

Model Construction

The three cross-sections of Piatt County were discretized and written in the NUFT code to distinguish cells represented as either diamicton or sand and gravel (sand/gravel). The geologic materials included in the model and their respective hydraulic parameters are shown in Table 3. Porosities within the ranges reported by Fetter (2001) for sand and till were used for the sand/gravel and diamicton, respectively. The hydraulic conductivities used for the sand/gravel and diamicton were obtained from the ranges reported for the Glasford Formation aquifers and till by Kempton (1991). The Van Genuchten parameters and residual water content reported by Schaap (1999) for sand and clay loam were used for the sand/gravel and the diamicton materials in the model, respectively.

Table 3. Geologic material hydraulic parameters.

Geologic Material	**ϕ**	**K_s (m/s)**	**α (cm^{-1})**	**m**	**n**	**Θ_{rwater}**	**Θ_{rgas}**
Diamicton	0.15	---	0.016	0.294	1.42	0.179	0.05
Sand and gravel	0.30	4.0×10^{-4}	0.035	0.685	3.18	0.141	0.05
Mahomet Aquifer	0.30	---	0.035	0.685	3.18	0.141	0.05

ϕ: porosity (Fetter 2001); K_s: saturated hydraulic conductivity (Kempton et al. 1991); α, n, and m ($m = 1 - 1/n$): van Genuchten parameters (Schaap 1999); Θ_{rwater}: residual water content (Schaap 1999); Θ_{rgas}: residual gas content.
* Hydraulic conductivity was varied for both the diamicton and aquifer material.

The hydraulic properties assigned to the sand/gravel were also used for the aquifer layer in the model, except for hydraulic conductivity. The hydraulic conductivity of the aquifer layer was adjusted for the various model runs in order to achieve the hydraulic gradient reported for the Mahomet Aquifer by Kempton et al. (1991). This is explained in more detail in the Sensitivity Analysis section.

The dimensions and cell sizes for each cross section are shown in Table 4. It should be noted that there is a y-dimension with a domain of 1 meter for all the models. Since one cell encompasses the entire domain in the y-dimension there is no change with respect y in the flow and transport equations, essentially making the model a 2D model with a thickness of 1 meter.

Table 4. Domains and cell sizes for model runs in units of meters.

Model	Domain Width (x)	Domain Depth (z)	Domain Thickness (y)	Cell Width	Cell Thickness	Cell Length
X-section A	5550	51	1	75	1.0	1.0
X-section B	6400	52	1	100	1.0	1.0
X-section C	4120	52	1	51.5	1.0	1.0

The conceptual model and the discretization of cross-section B are shown in Figure 11. The left and right extent of the model, from ground surface to the top of the Mahomet Aquifer, will be assigned no flow boundaries. These no flow boundaries can be implemented due to nested well data in this region showing flow is primarily vertical through the till (Panno et al., 1994). The second layer from the top of the model is where recharge is implemented as a specified flux boundary. The flux for this boundary was calculated by multiplying recharge times the surface area of the model (width×thickness). The top row of cells represents the atmosphere and is set to a constant pressure of 0.97 atm, zero saturation, and a porosity of one. All gas components, except N_2 and CH_4, in

this layer were set to atmospheric gas concentrations. N_2 was set 0.99 mole fraction accounting for both O_2 and N_2 in the atmosphere. In NUFT total mole fractions must be equal to 1. CH_4 concentration was set to zero as CH_4 entering the model from groundwater in equilibrium with the atmosphere will become negligible once CH_4 is produced from the degradation of the paleosol.

The bottom layer of the model is representative of the top of the Mahomet Aquifer. The bottom most right cell of the model is representative of the upgradient flow input of the Mahomet Aquifer and is set at a constant pressure and fully saturated. This cell will from now on be referred to as "Mahomet input" cell. The bottom most left cell of the model is where groundwater exits the model, and is set as a specified flux boundary. The flux boundary exiting the model was set equal to the flux of water recharging plus the water from the Mahomet Aquifer input. The Darcy's Law equation was used to calculate the flux (2.47×10^{-7} m^3/s) of water entering from the Mahomet input cell using the average hydraulic gradient and conductivity of the Mahomet Aquifer reported by Kempton et al. (1991). It was originally conceptualized that the bottom flux boundary would encompass the entire width of the model and be representative of the groundwater flowing vertically out through the bottom of the till.

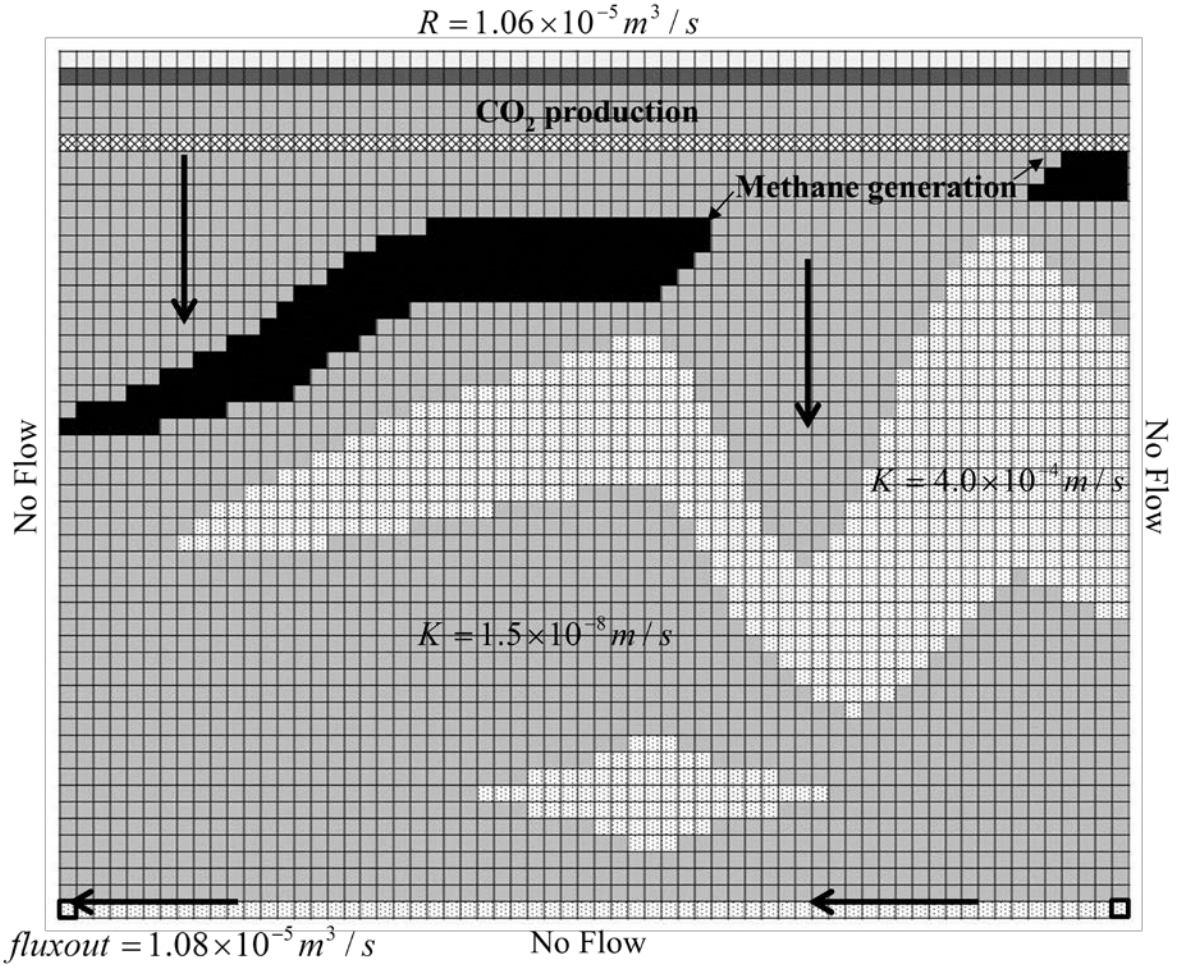

Figure 11. Conceptual model and discretization of cross-section B. The sand and gravel lenses are represented as textured white cells and the fine grained till as medium gray. The bottom row of textured white cells is representative of the top of the aquifer. The recharge flux boundary is shown in dark gray. The "Mahomet input" cell and the flux out cell are shown outlined in bold in the right and left bottom corners, respectively. The light gray row of cells is the atmosphere layer. The Robein Silt is represented by black cells and is the source of methane generation. The checkered cells show the layer of CO_2 production zone. Thick black arrows indicate groundwater flow direction.

This boundary was modified due to the inability to specify constant pressure and saturation at the bottom of the model, resulting in pressure loss and de-saturation at the bottom of the model as gas pockets were generated. As the boundaries are set now, groundwater flows vertically through the till recharging the top of the Mahomet Aquifer, then flows laterally out through the flux boundary at the bottom left corner of the model.

It is assumed the flow in the Mahomet Aquifer is primarily lateral, allowing for a no flow boundary to be implemented at the bottom of the model.

The recharge flux was initially set to 5 percent the annual precipitation in Piatt County (1.7×10^{-9} m/s) multiplied by surface area of the model and varied with model runs. The recharge flux boundary includes the following dissolved gases CO_2 ^{20}Ne, ^{40}Ar, ^{84}Kr in their respective concentrations in equilibrium with atmosphere at 12.5^{o}C (average annual temperature). Temperature was held constant at 12.5^{o}C throughout the model.

Dissolved N_2 concentration was set to groundwater in equilibrium with atmosphere consisting of 0.99 mole fraction N_2 gas, resulting in a greater than atmospheric concentration of N_2. Due to the agricultural activity and denitrification occurring in this area, dissolved N_2 concentrations are in excess of atmospheric and are generally even greater than the concentration used in the models. Dissolved noble gas and N_2 concentrations for recharge were calculated using empirical constants and equations from Solomon et al. (1998). CO_2 recharge concentration was calculated using a Henry's Law constant from Wilhelm et al. (1977).

A "setcomp-internal" command was implemented in the bottom phase flux boundary, to allow for NUFT to calculate the concentrations of all the dissolved gas components exiting the model. The dissolved gas concentrations in the "Mahomet input" cell (bottom right corner cell) were set to average values for N_2, CO_2, and CH_4 of the dissolved gas data from the Mahomet Aquifer upgradient from the study area (Van der Hoven et al., 2005). To better display the contribution of groundwater stripped of noble gases to the Mahomet Aquifer, dissolved noble gas concentrations in the Mahomet input cell were set to be in equilibrium with atmosphere.

Total pressure at the bottom of the model, applied at the Mahomet input cell, was held constant at 400 kPa. This total pressure at the boundary between the Glasford formation and Mahomet Aquifer is within the ranges calculated from head data from the driller's logs used in the cross-sections (Table 5) and was the best fit for drift gas generation in the models. Total pressure (Pa) was calculated by multiplying artesian head (m) × density of H_2O (1000kg/m^3) × gravity (9.8 m/s^2) + 98285.25 Pa (0.97 atm).

Table 5. Head data from driller's logs used in cross-sections to calculate total pressure at the boundary between the Glasford formation and Mahomet Aquifer (MA).

Well ID (County #)	Static water level below ground level (m)	Elevation (m)	Head (m)	Depth to MA (m)	Elevation of top of MA (m)	Artesian Head (m)	Total Pressure (kPa)
X-sect A							
21246	29.9	208.6	178.7	59.5	149.1	29.6	389
129	4.9	196.6	191.7	40.5	156.1	35.6	447
20944	14.6	206	191.4	51.5	154.5	36.9	460
20733	16.2	206.6	190.4	48.0	158.6	31.8	410
130	2.1	204	201.9	42.5	161.5	40.4	494
X-sect B							
21425	18.0	198.7	180.7	50.0	148.7	32.0	412
21117	23.8	203.3	179.5	51.6	151.7	27.8	371
X-sect C							
20957	23.8	213.6	189.8	57.6	156.0	33.8	430
21141	8.5	205.6	197.1	49.2	156.4	40.7	497
21424	23.5	210.1	186.6	53.2	156.9	29.7	390
21313	25.0	213.6	188.6	48.8	164.8	23.8	332
20909	23.8	210.3	186.5	53.2	157.1	29.4	387
21178	23.8	205.2	181.4	55.6	149.6	31.8	410
21291	24.4	205.2	180.8	52.4	152.8	28.0	373

CH_4 source zones are included in the model matrix where Robein Silt is present in well logs. The CH_4 production rate applied to the source cells was varied within ranges reported for microbial CH_4 production in coal (Luca Technologies, Jones et al., 2008), peats (Yavitt et al., 1990, Kellner et al., 2006), marine sediments (Schulz et al., 2009),

landfill plume (Ludvigsen et al., 1998), a shallow sandy anoxic aquifer (Hansen et al., 2001), and Wisconsinan age till and loess (Simpkins and Parkin, 1993). The microbial CH_4 production from the studies above were reported in both field and laboratory settings and is highly variable ranging from 1.0×10^{-4} to 1.5×10^{2} mole CH_4 m^{-3} yr^{-1}. A CO_2 source zone was included in the model to account for the increase in CO_2 along the groundwater flow path. The CO_2 source zone was implemented in the models as a continuous single layer above the position of the Robein (Figure 11). CO_2 production was adjusted to match the dissolved gas data. Hydraulic conductivities of the diamicton and the sand and gravel lenses were initially set to 1×10^{-8} m/s and 4×10^{-4} m/s respectively, as these values are within the ranges reported by Kempton et al. (1991).

The equilibrium partitioning coefficients were specified for each component gas (Table 6). The NUFT phase equilibrium model is formulated as;

$$K_{eq} = pg \cdot B + C/pg \quad (1)$$

Where *pg* is gas pressure in Pascals and *B* and *C* are the partitioning coefficients for the aqueous phase and gas phase respectively. NUFT allows for a reference phase to be chosen for each component. The coefficient for the reference phase is set to 1.0. The gas phase was chosen as the reference phase for all the components. Having chosen gas as the reference phase, parameter *C* in Equation 1 has a default value of zero. The aqueous phase coefficient *B* is equal to the mole fraction of the component in the aqueous phase divided by the mole fraction of the component in the gas phase. N_2, ^{20}Ne, ^{40}Ar, and ^{84}Kr partitioning coefficients were computed from the solubilities (cm^3/gH_20) calculated from Solomon et al. (1998). Under the assumption the components exhibit ideal gas law

behavior at 0.97atm and 12.5°C, the solubility concentrations (C_{aq}) can be converted to mole fraction (X_{aq}) by;

$$X_{aq} = \frac{C_{aq} \cdot P}{RT} \cdot \frac{18.0152g}{mole\ H_2O} \quad (2)$$

where

R = 0.08206 atm cm^3 $mole^{-1}$ K^{-1}

T = 285.15 K

P = 0.97 atm

Concentrations for the boundary conditions were converted to mole fractions in this same way. The calculated aqueous mole fractions are the divided by the mole fraction of that gas in the atmosphere (X_{aq}/ X_{gas}). The phase equilibrium model in NUFT calculates partitioning coefficients with respect to total gas pressure to account for pressure dependence, so the X_{aq}/Xg_{as} value is divided by the pressure at which the mole fraction ratio were calculated in this case 98285.25 Pascals (0.97atm). CH_4 and CO_2 partitioning coefficients were converted from Henry's Law constants (M/atm) to mole fraction and divided by 101325 Pa, the pressure at which they were calculated.

Table 6. Properties of solutes at 12.5°C.

	B ($\times 10^{-10}$)	**D ($\times 10^{-9}$ m^2/s)**	**C_{eq} (mole fraction)**
N_2	1.32[a]	2.0	$1.28\times10^{-5*}$
^{20}Ne	0.818[a]	2.93	1.32×10^{-10}
^{40}Ar	2.90[a]	2.5	2.66×10^{-7}
^{84}Kr	5.58[a]	1.20	3.56×10^{-11}
CH_4	1.94[b]	1.24	---
CO_2	42.5[b]	1.26	1.61×10^{-7}

B: Partioning coefficient.
D: Molecular diffusion coefficient.
C_{eq}: atmospheric equilibrium concentration. $^{*}N_2$ concentration is calculated with 0.99 mole fraction N_2 atmospheric composition (N_2+O_2).
[a] calculated from solubilities obtained from Solomon et al. (1999)
[b] converted from Henry's Law Constant Wilhelm et al. 1977.

Parameters that were varied include recharge rate, hydraulic conductivity of the diamicton, and CH_4 production rate. Each model run was preceded by an "initialization run" without CH_4 or CO_2 production. The objective of the initialization run was to set up the flow system and head conditions before the introduction of the gas production zones. During the initialization runs hydraulic conductivity of the diamicton was varied in order to set up similar head conditions for each cross section and the different recharge rates. With less recharge rate, a lower hydraulic conductivity was needed to achieve the same head condition as a higher recharge rate. Hydraulic conductivities of the sand and gravel lenses were not varied in order to simplify the model and kept constant at the median value reported (4.0×10^{-4} m/s) by Kempton et al. (1991). Similar head conditions were verified by visually comparing saturation profiles of the models. The desired saturation profile was characterized by 2-4 meters of a partially saturated vadose zone. This saturation profile is typical of what is observed in the field at this study site and also allows area for groundwater to be displaced as gas pockets are formed. During initialization runs the hydraulic conductivity of the aquifer material was also varied in order to achieve a pressure at the "flux out" cell (bottom left corner of model) that was close to the hydraulic gradient of the Mahomet Aquifer (0.00019) reported by Kempton et al (1991).

Once head conditions were achieved in the initialization runs, CH_4 and CO_2 production were added to the models. CO_2 production rates were held constant once the concentrations were within the range of the dissolved gas data. As with CH_4 production CO_2 production rates had to be increased with recharge rate in order to achieve similar dissolved CO_2 concentrations. To keep dissolved CO_2 concentrations uniform in all the

models CO_2 production was calculated by multiplying 0.324 mol/m^4 by the recharge rate (m/s) giving a production rates of 1.07×10^{-10} to 1.61×10^{-9} mol m^{-3} s^{-1} for recharge rates 1 to 15 percent annual precipitation, respectively. CH_4 production was adjusted within the ranges reported above to generate substantial drift gas pockets while preserving noble gas concentrations seen in the groundwater data. The recharge rates were varied from 3.3×10^{-10} m/s to 5.0×10^{-9} m/s, 1 percent to 15 percent annual precipitation in Piatt County.

Model Calibration

Since no monitoring wells were installed for this study, the models are not calibrated to any head data. The model was instead calibrated to dissolved gas data reported by Van der Hoven et al. (2005) and drift gas composition data. The model performance was assessed by the ability of the model to produce similar dissolved and drift gas concentrations to the available data. There were two particular areas of the model that were focused on for performance assessment; the cells with gas pocket formation and the "Mahomet out" cell from which groundwater is leaving the model. The gas phase concentrations in the cells with gas pocket formation are representative of drift gas, and were compared to drift gas mole fraction data seen in Table 2. The dissolved gas concentrations of the cells with gas pocket formation are representative of groundwater in equilibrium with drift gas. The "Mahomet out" cell is representative of the entire flux of water recharging through the till and mixing with groundwater from the Mahomet Aquifer. The amount of noble gas loss is expected to be diluted in this cell as recharging degassed water mixes with non-degassed groundwater concentrations from the "Mahomet input" cell. The dissolved gas concentrations produced by the model were

calibrated to dissolved gas ratios of groundwater in the Mahomet aquifer and the Glasford formation, seen in Figure 12.

Sensitivity Analysis

Numerous model runs were performed in order to assess the sensitivity of the model to certain parameters. As mentioned earlier there is a clear relationship between recharge rate, hydraulic conductivity, and water table elevation. During the initialization runs hydraulic conductivity of diamicton was varied with different recharge rates in order to create equivalent water table levels in each of the models. An increase in recharge rate would therefore also require an increase in the hydraulic conductivity of the diamicton, keeping in mind the sand and gravel hydraulic conductivity was held constant. It is apparent that the model is very sensitive to the hydraulic conductivity of the diamicton with respect to water table elevations produced, but as the model was calibrated to the ability to produce drift gas and dissolved gas concentrations, the sensitivity of the model to this parameter was noted but deemed not significant for drift gas generation. The aquifer hydraulic conductivity was also varied with increasing recharge rates in order to achieve the hydraulic gradient reported by Kempton et al. (1991) for the Mahomet Aquifer. With a greater recharge rate, a greater flux would move laterally through the aquifer layer and out the bottom left cell of the model. According to Darcy's Law in order to keep the hydraulic gradient the same in the aquifer an increase in flux also requires increase in hydraulic conductivity. Due to the small cross-sectional area (1 m^2) that the laterally moving water has to flow through (Table 4 and Figure 11) the aquifer material was varied into unrealistically high hydraulic conductivity values in order to maintain the hydraulic gradient of the Mahomet Aquifer.

For unsaturated flow conditions, the Darcy equations for mass flux can be written as

$$F_g = -\frac{k_g k_{r,g}}{\mu_g}\rho_g(\nabla P_g - \rho_g g) \quad (3)$$

$$F_l = -\frac{k_l k_{r,l}}{\mu_l}\rho_l(\nabla P_l - \rho_l g) \quad (4)$$

where F is mass flux, k is permeability, k_r is relative permeability, μ is viscosity, ρ is density, ∇P is pressure gradient, and g is the gravitational constant. Subscripts g and l are gas phase and liquid phase respectively (Ho and Webb, 2006). There are different pressures for the gas and liquid phases due to capillary forces and interfacial curvature. The difference between the gas (nonwetting) and liquid (wetting) pressures is referred to as the capillary pressure, or

$$P_c = P_g - P_l \quad (5)$$

For porous media where liquid is the wetting phase, the liquid phase pressure is less than the gas phase pressure, and the capillary pressure is a positive quantity. In order to close the equation set, relationships for the capillary pressure and relative permeability are needed. These relationships are often referred to as two-phase characteristic curves. In general, the two-phase characteristic curves are a function of the pore structure, phase saturation, surface tension, contact angle, and hysteresis (Ho and Webb, 2006). For this model NUFT uses the van Genuchten curves, in which the capillary pressure relationship is given by

$$S_e = \left[\frac{1}{1+(\alpha P_c)^n}\right]^m \quad (6)$$

which can be arranged as

$$P_c = \frac{1}{\alpha}\left[{S_e}^{-1/m} - 1\right]^{1/n} \quad (7)$$

S_e is the effective saturation, or

$$S_e = \frac{S_l - S_{l,r}}{1 - S_{l,r}} \quad (8)$$

Where α is the capillary pressure parameter, and *m* and *n* are fitting parameters, and $S_{l,r}$ is the residual liquid saturation (Ho and Webb, 2006). The relative permeability of the liquid phase can be predicted using Mualem's (1976) integral expression given by

$$k_{r,l} = {S_e}^{1/2}\left(1 - \left(1 - {S_e}^{1/m}\right)^m\right)^2 \qquad (m = 1 - 1/n) \quad (9)$$

Parker et al. (1987) extended the van Genuchten-Mualem characteristic curves to include the gas-phase relative permeability, or

$$k_{r,g} = (1 - S_e)^{1/2}\left(1 - {S_e}^{1/m}\right)^{2m} \quad (10)$$

As shown in equations 3 thru 10, numerical solutions of two-phase advection flow are a function of residual liquid saturation ($S_{l,r}$), and the van Genuchten parameters (α, *m*, *n*). The values for $S_{l,r}$, α, and *n* (or *m*) are usually determined from fitting experimental data for capillary pressure or head. No experimental data were available, therefore, USDA textural class average values used by Rosetta (Schaap, 1999), the Windows based program for estimating unsaturated hydraulic properties, where chosen for residual liquid saturation and van Genuchten parameters. Values for clay loam and sand were used for the diamicton and sand and gravel lenses in the model, respectively. The model was

sensitive to van Genuchten parameters and residual liquid values with respect to the size of drift gas pockets generated and the evolution of de-saturation in these cells. Different van Genuchten curve parameters and residual liquid values produced varying amounts of sand and gravel cells that were de-saturated and the degree of de-saturation within these cells. Since there is no experimental fitting data available for the capillary properties of the Glasford or Wedron formations, the sensitivity of the model to these parameters was noted but not looked into any further.

Model Limitations

Due to the numerous parameters involved in simulating the process of drift gas formation, this model was simplified and invariably contains an amount of uncertainty as a result. The temperature in the model was held constant at 12.5^{o}C. During dissolved gas sampling groundwater temperature was recorded and had an average value around 12.5^{o}C. NUFT has the capability for non-isothermal modeling, and the temperature dependence of the noble gases could affect the output of dissolved gases in a non-isothermal model. A constant temperature was assumed in the model due to the fairly static groundwater temperature in Illinois throughout the year.

The hydraulic conductivity of the sand and gravel lenses was also held constant in the models. The hydraulic conductivity of the sand and gravel lenses could possibly have an effect on drift gas formation as this is where the gas pockets form. Longer residence times of groundwater saturated with dissolved gases in the lower hydrostatic zones (sand and gravel lenses) could result in greater degassing. It is believed the large difference in the hydraulic conductivities of the sand and gravel compared to the diamicton has more of an effect on the extent of degassing. The much higher hydraulic

conductivity of the sand and gravel lens drives the horizontal flow through the sand and gravel lenses, which is the mechanism for the decrease in hydrostatic pressure causing degassing.

The 3-dimensionality of the process of drift gas formation has not been accounted for in the 2D model. A 3D model could better replicate the physical processes and groundwater mixing that occurs in reality. It is assumed that a 2D model can sufficiently capture the processes involved in order to constrain recharge rate through the aquitard.

It should also be noted that only the top of the Mahomet Aquifer was included in the model. It was originally conceptualized to only model the glacial tills confining the Mahomet Aquifer and not include the top of the aquifer (bottom layer in Figure 11). This layer was included in order to more accurately simulate drift gas formation in the glacial tills. It is not anticipated that this small 2D portion of the aquifer will be able to fully capture the dynamics of the Mahomet Aquifer.

Results and Discussion

Degassed Groundwater Chemistry

The noble gas concentrations in the Mahomet Aquifer and the Glasford Formation west of the main recharge areas, from Piatt County on are less than atmospheric equilibrium. Ne, Ar, and Kr concentrations are the best for indicating gas loss as they are not only inert but do not have any significant sources or sinks in the subsurface. Since there are no data on the total gas pressure of the drift gas pockets prior to exploitation as an energy resource, initial partial pressures and corresponding equilibrium dissolved gas pressures can't be calculated. However, the ratios of ^{20}Ne, ^{40}Ar, and ^{84}Kr can be used to assess gas loss. As degassing occurs, ^{20}Ne will become more depleted with respect to in

equilibrium with atmosphere compared to ^{40}Ar and ^{84}Kr isotopes. This is due to the preferential partitioning to the vapor phase of the lighter, less soluble isotope ^{20}Ne compared to the heavier, more soluble ^{40}Ar and ^{84}Kr isotopes. It is anticipated that there will be an inverse relationship with the amount of degassing and dissolved gas ratios as they are represented in Figure 12. As more degassing occurs it is expected that groundwater samples will plot further down the trend seen in Figure 8, due to a greater fractionation of $^{20}Ne/^{84}Kr$ and $^{20}Ne/^{40}Ar$.

Figure 12 shows dissolved gas ratios for groundwater samples in both the Mahomet Aquifer and the Glasford, the theoretical dissolved gas ratios of groundwater in equilibrium with drift gas pockets (Table 2) and air saturated water with and without excess air. Theoretical dissolved gas ratios in equilibrium with the drift gas pockets were calculated by dividing the measured $^{20}Ne/^{84}Kr$ and $^{20}Ne/^{40}Ar$ ratios of the drift gas pockets by the fractionation coefficients for the respective gas relationships. The fractionation coefficients were determined by the ratio of Henry's Law constants of ^{20}Ne, ^{40}Ar, and ^{84}Kr at 12.5^{o}C (Solomon et al., 1998). The air saturated water (ASW) with excess air point in Figure 8 was calculated using Solomon et al. (1998) gas solubility equation and the closed system equilibration (CE) model for excess air (Kipfer et al., 2002).

The actual groundwater ratios plot within the calculated ratios from drift gas composition, showing a similar $^{20}Ne/^{84}Kr$ and $^{20}Ne/^{40}Ar$ fractionation, indicating the gas loss observed in these samples is a result of groundwater interacting with drift gas. In Figure 12 groundwater samples that have experienced degassing (negative ΔNe values) are shown as open circles and the calculated groundwater in equilibrium with drift gas are

shown as asterisks. As suspected the majority of the calculated dissolved gas ratios fall within the groundwater samples that have experienced degassing.

The groundwater samples that have positive ΔNe values plot on either side of the air saturated water point and follow a similar fractionation trend as the rest of the data. The positive ΔNe values that plot below the air saturated water point could be groundwater that was equilibrated with excess air then experienced degassing. The extent of degassing in these samples would not have been enough to deplete noble gas concentrations to less than atmospheric but would still cause fractionation between ^{20}Ne and the heavier ^{40}Ar and ^{84}Kr resulting in noble gas ratios less than atmospheric.

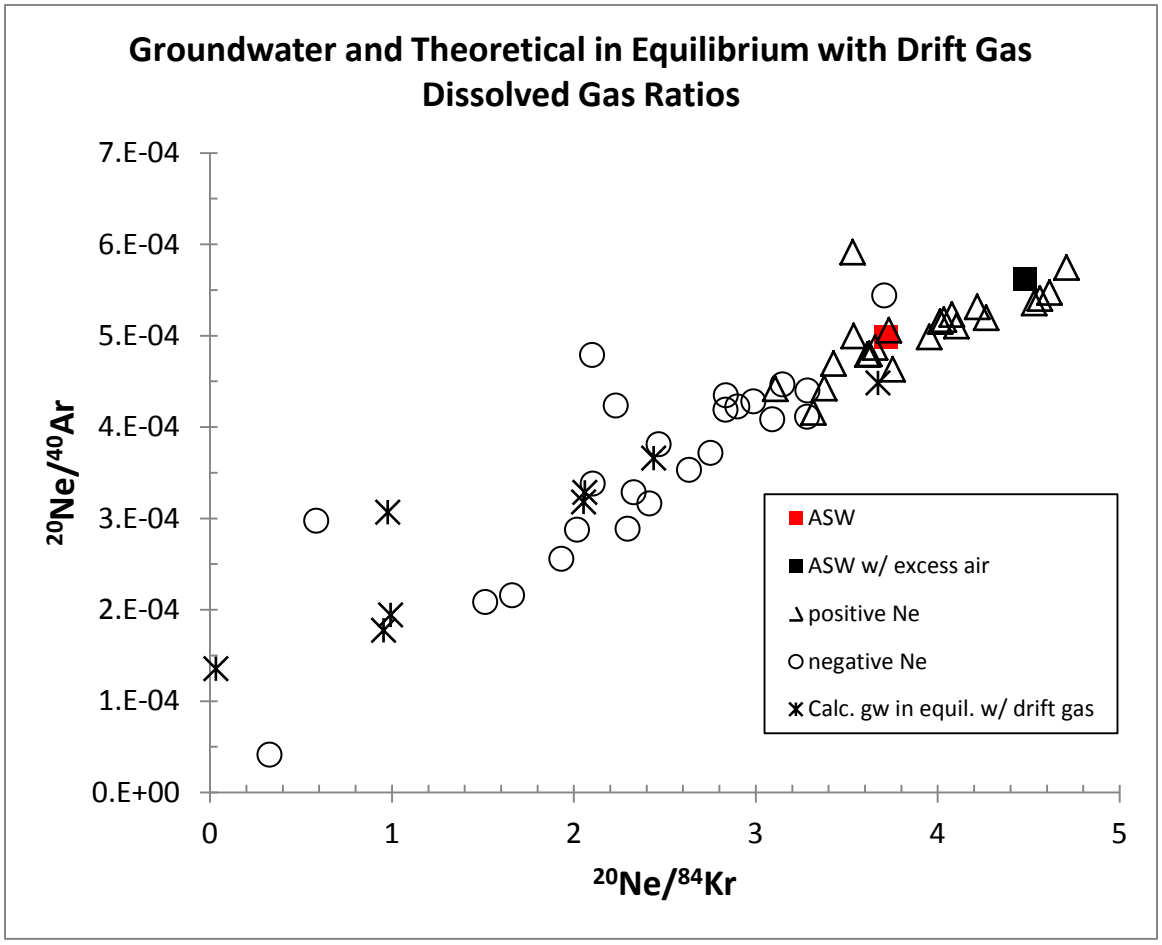

Figure 12. Dissolved noble gas ratios of groundwater from the Mahomet Aquifer and the Glasford Formation. Theoretical dissolved noble gas ratios in equilibrium with drift gas samples are also plotted.

General Patterns of Gas Pocket Formation

Some general desaturation patterns are seen in the models that produced drift gas pockets. Before gas pockets form in the sand and gravel lenses slight desaturation occurs in the overlying Robein and diamicton cells (Figure 13). Gas saturations reach ~5 percent in the Robein (CH_4 source zone) cells as CH_4 accumulates and TDGP exceeds hydrostatic pressure. Cells within the model that have low gas saturations, less than 10 percent, will be referred to as containing drift gas "bubbles". Gas saturations also reach ~5 percent in the diamicton cells between the Robein and sand and gravel lenses. Gas saturations remain at ~5 percent in these cells as the equilibrium saturation between the recharge rate and CH_4 production is reached (Figure 13).

More degassing occurs as TDGP exceeds hydrostatic pressure again in the sand and gravel lenses. The hydrostatic pressure decrease in the sand and gravel lenses is a caused by the lateral flow mechanism mentioned earlier. A greater decrease in hydrostatic pressure and the lower capillary pressures in these coarse grained sediments allow for bubble expansion, which in turn also lowers total pressure as groundwater is displaced. As bubble growth along with depressurizing of these cells continues, greater degassing occurs and gas saturations reach a maximum of ~85 percent. The high gas saturations and correlative low liquid saturations are representative of drift gas "pockets". These drift gas pockets form in the top of the sand and gravel lenses and grow within the lenses as more degassing occurs.

Where gas pockets form, the resulting saturation profile is fully saturated conditions from the top of the model down to the top of the Robein, partially saturated

conditions through the Robein and diamicton below CH_4 source zone with gas saturations at ~5 percent, and near complete de-saturated conditions in the top of the sand and gravel lenses where gas pockets have been generated (Figure 14). Conditions remain completely saturated below the gas pockets.

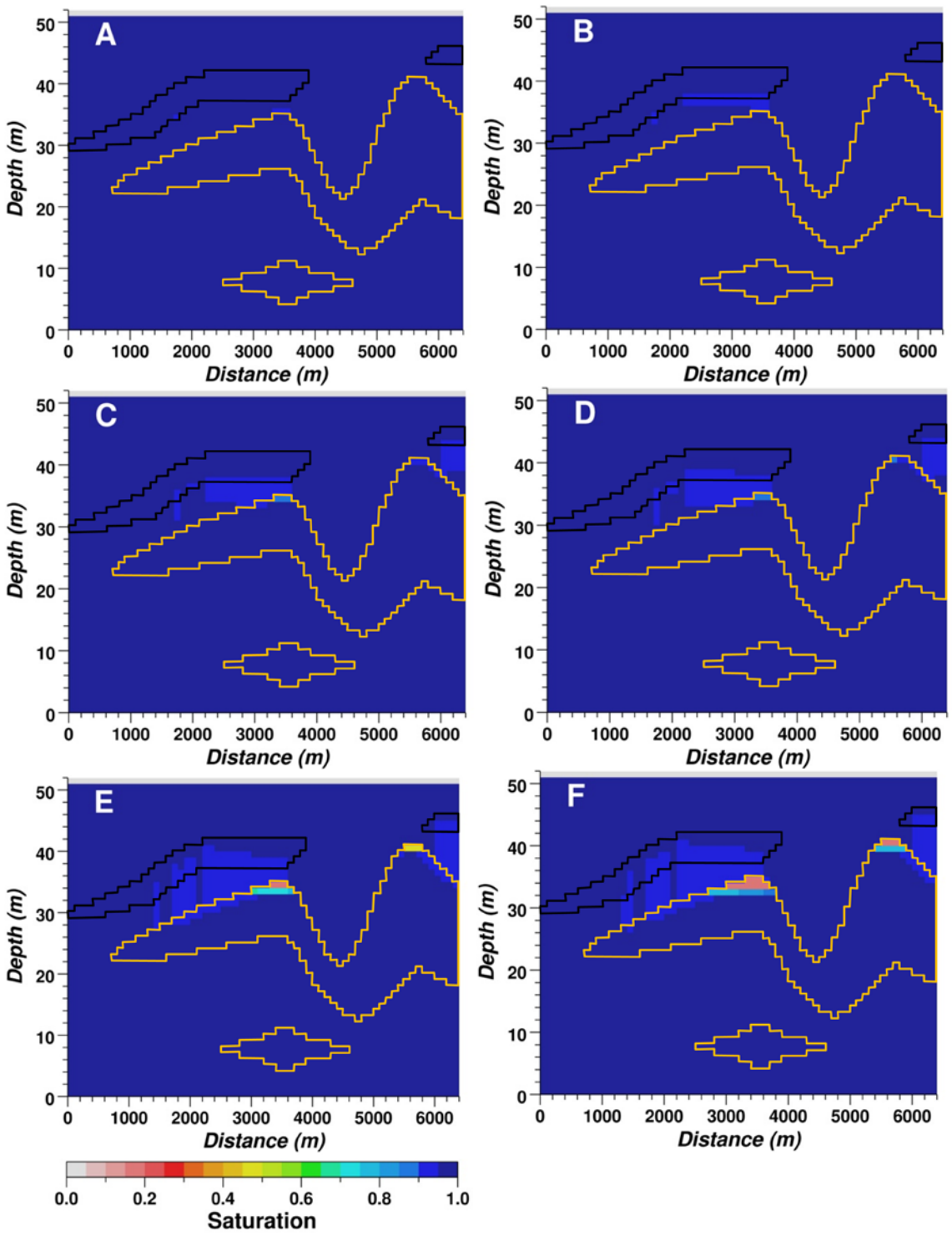

Figure 13. A thru F show the evolution of the liquid saturation profile of cross-section B (recharge rate of 2.5 percent annual precipitation) as gas pockets begin to form. A, B, C, D, E, and F show 600 yr, 700 yr, 900 yr, 1000yr, 2000 yr, and 3000 yr, respectively. The positions of the Robein and sand and gravel lenses are outlined in black and gold, respectively.

In the models ebullition occurs as the drift gas pockets grow larger and the buoyancy forces of the gas pockets overcome the capillary forces in the fully saturated diamicton above the Robein. Once the capillary forces of these cells were overcome, a vertical bubble channel forms, connecting the top of the gas pocket to the surface (Figure 15). The bubble channels through the diamicton have a gas saturation of ~5 percent. These bubble channels allow for the gas to escape from the gas pockets and rise to the surface. The gas concentrations in the bubble channels range from ~0.93 to greater than 0.99 mole fraction of CH_4 due to the abundance and lower solubility of CH_4 compared to the more soluble CO_2. Continued gas flow will severely strip the groundwater in the gas bubble channels, depleting noble gas concentrations several orders of magnitude more than what the groundwater data shows. The extremely depleted noble gas concentrations could be an artifact of decreased hydraulic conductivity in the bubble channel. This would result in the deflection of groundwater flow around the bubble channels (Amos and Mayer, 2006). This diversion of groundwater limits both the transport and replenishment of noble gases into the bubble channel and transport of CH_4 from the bubble channel, resulting in very depleted dissolved noble gas concentrations and very high CH_4 concentrations.

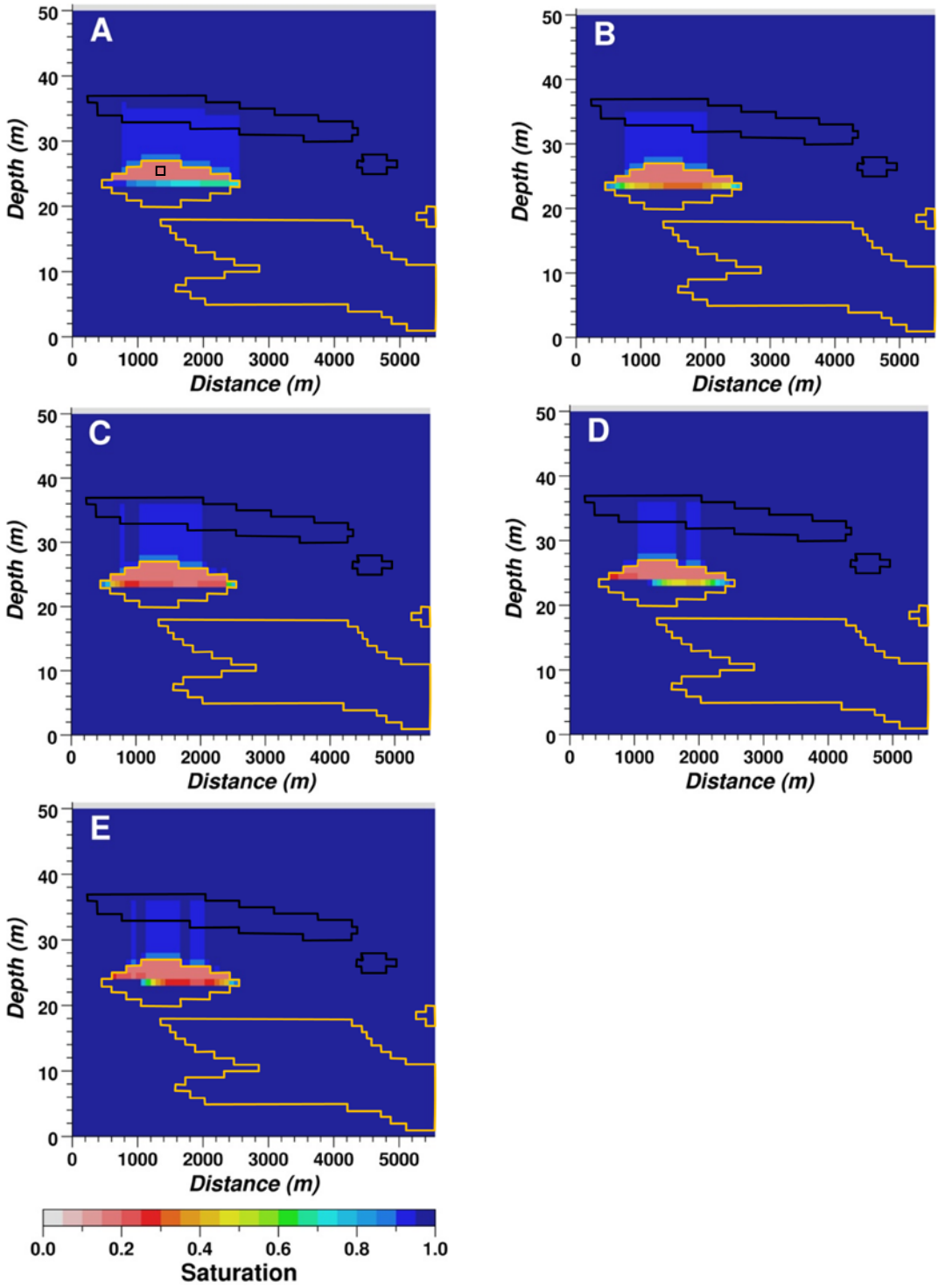

Figure 14. Liquid saturation profiles at 10 kyr of cross-section A. A, B, C, D, and E show recharge rates of 1, 2.5, 5, 10, and 15 percent annual precipitation, respectively. The approximate location of the cell used to analyze dissolved and gas concentrations within the gas pockets is shown outlined in black in Figure 14A. The positions of the Robein and sand and gravel lenses are outlined in black and gold, respectively.

In a model simulating methanogenic processes in a petroleum hydrocarbon contaminated aquifer Amos and Mayer (2006b) reported a more than 75 percent decrease in hydraulic conductivity where bubbles have formed below the water table. The subsequent diversion of water flow around the bubble zone resulted in the highest observed CH_4 concentrations and lowest observed N_2 concentrations (Amos and Mayer, 2006b). Even without the deflection of groundwater, noble gases would be continuously depleted in the bubble channel over time due to the fast upward ebullitive gas bubble transport relative to the downward avdective transport of the groundwater. Since there are no data to suggest that ebullition is occurring and continued ebullition in the models produces much lower noble gas concentrations than the data shows, CH_4 production rates were adjusted to achieve substantial drift gas pocket formation with little to no ebullition when possible.

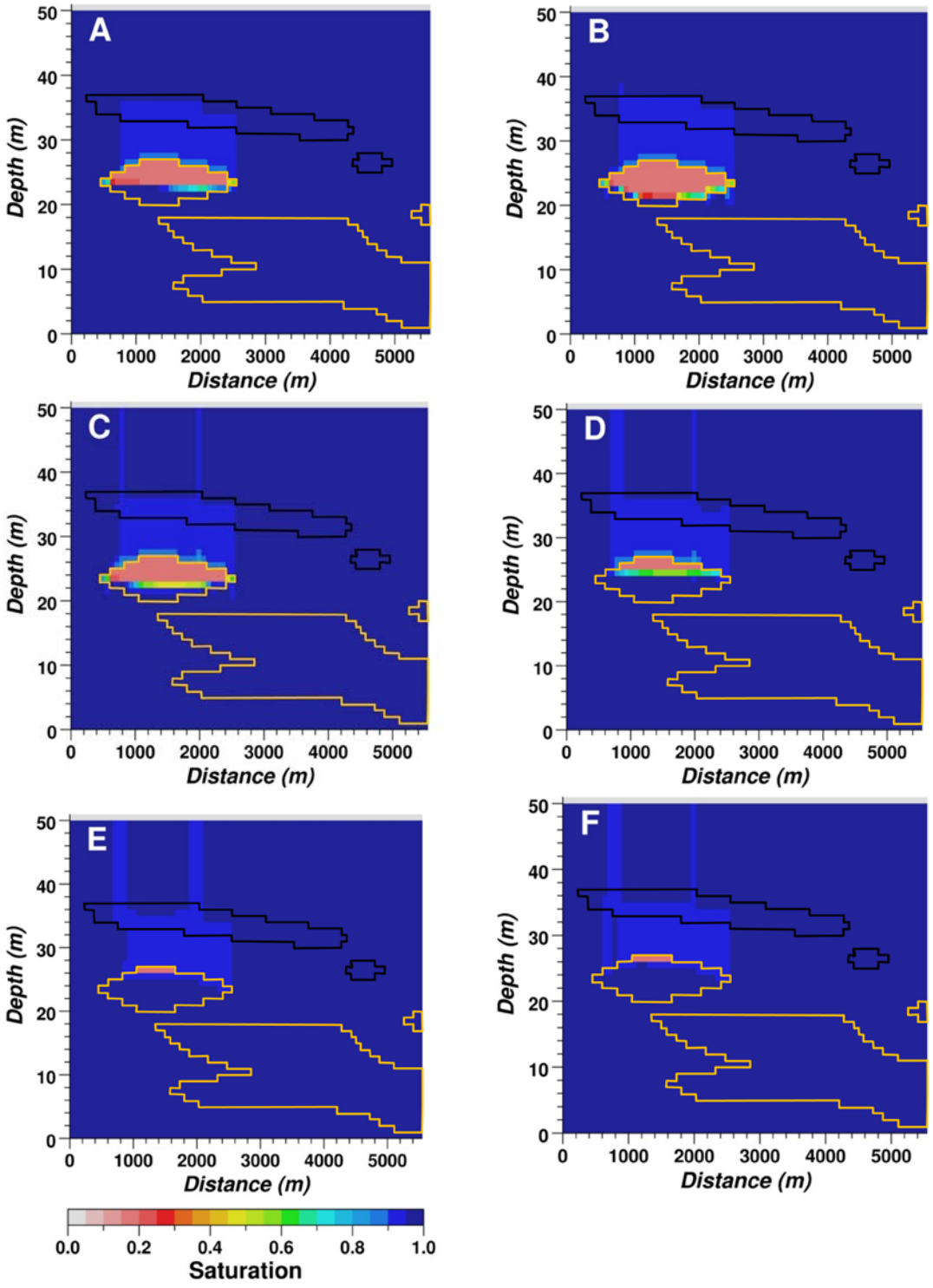

Figure 15. Cross-section A with a recharge rate of 5 percent annual precipitation showing ebullition and shrinking gas pocket. A, B, C, D, E, and F show 3 kyr, 4.4 kyr, 4.45 kyr, 4.5 kyr, 4.6 kyr, and 10 kyr, respectively. The positions of the Robein and sand and gravel lenses are outlined in black and gold, respectively.

Time scales of drift gas generation varied in the models with recharge and CH_4 production rates. When varying recharge rates, an increase in CH_4 production rate, approximately the same magnitude as the increase in recharge rate, was required in order to generate drift gas pockets of similar size. For example, a recharge rate of 5 percent annual precipitation required approximately 2X the CH_4 production rate used for 2.5 percent annual precipitation.

This linear increase in CH_4 production with recharge rate was kept constant for all model runs except for the 1 percent annual precipitation recharge rate for cross-section B. The higher CH_4 production rate used in the 1 percent annual precipitation recharge was applied in order to produce a gas pocket of similar size to the other cross-section B simulations. This resulted in the 1 percent annual precipitation recharge data points for cross-section B to plot off the trend in Figures 16 and 17.

For all recharge rates, except 1 percent annual precipitation, CH_4 production was about 2X greater in cross-section A compared to cross-section B in order to achieve drift gas generation at the same recharge rate. This was due to the greater depth of the Robein and the sand and gravel lens where drift gas accumulated in cross-section A. The higher pressure at this depth required greater CH_4 production to cause degassing. The higher CH_4 production rate caused degassing to occur early in cross-section A than B at the same recharge rates (Figure 16).

As shown in Figure 13 degassing begins in the Robein and continues downward into the sand and gravel lenses. The time elapsed before initial degassing occurred in the Robein ranged from 40 to 600 years (Figure 16). There is a clear relationship between

recharge rate and the time it takes for drift gas generation (Figures 16 and 17). Time scales for drift gas generation get exponentially smaller with increased recharge and CH_4 production rates. The higher CH_4 production rates caused initial degassing in the Robein to occur earlier with higher recharge rates. Along with the higher CH_4 production, the faster transport of CH_4 from the Robein to the sand and gravel lenses resulted in earlier drift gas pocket generation with higher recharge rates (Figure 17). It took less time between initial degassing in the Robein and the start of degassing in the sand and gravel lenses for cross-section B than A (Figure 17). This is due to the Robein being in closer proximity to the sand and gravel lenses in cross-section B and requiring less transport time.

Once initial degassing occurred in the sand and gravel lenses drift gas pockets would continue to grow as more cells desaturated. Gas pockets eventually stop growing in the highest recharge rates (15 and 10 percent annual precipitation) around 6,000 to 7,000 years, and appear to reach equilibrium. The 5 percent annual precipitation recharge rate appears to be very close to reaching equilibrium after 10,000 years. The slower recharge rates (1 and 2.5 annual precipitation) do not appear to reach equilibrium over 10,000 years, as gas pocket growth is still occurring and there is still some variation in the dissolved noble gas concentrations exiting the model.

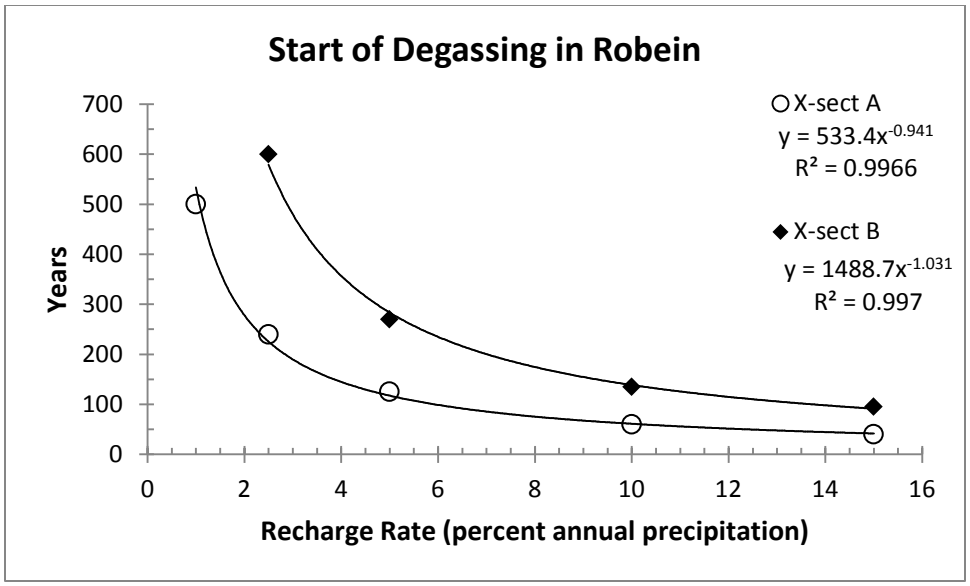

Figure 16. Time it took for initial degassing to occur in the Robein for varying recharge rates. The 1 percent annual precipitation recharge for X-section B plots at the same point as the 1 percent annual precipitation point for X-section A.

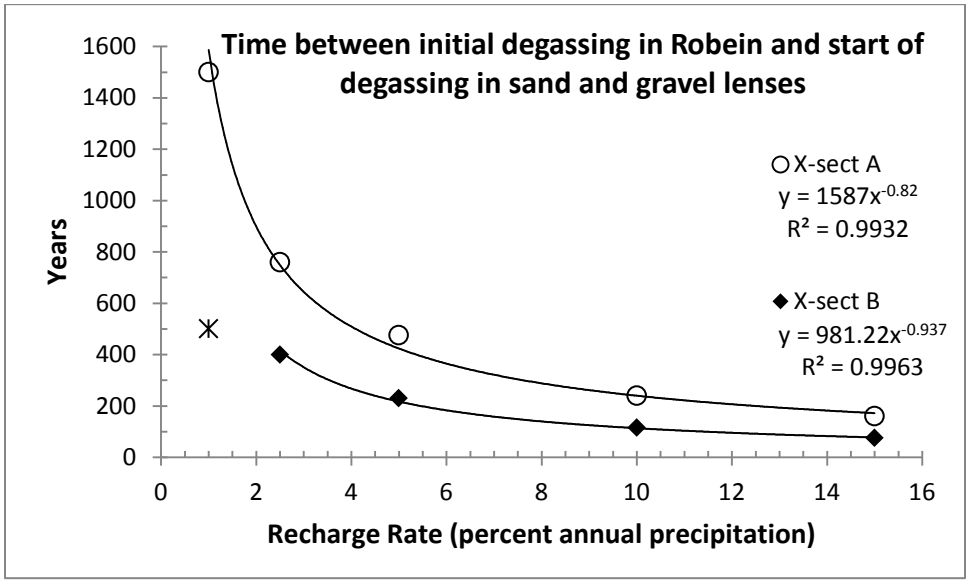

Figure 17. Elapsed time between initial degassing in the Robein and the start of degassing in the sand and gravel lenses. Once again the 1 percent annual precipitation recharge point for X-section B plots off the trend and is shown as an asterisk.

Cross-section A

A drift gas pocket was generated in the smaller sand and gravel lens in the southwest side of cross-section A (Figure 8). The saturation profiles of cross-section A

after 10,000 years for the varying recharge rates are shown in Figure 14. As expected higher recharge rates required higher CH_4 production rates to achieve similar degassing patterns (Figure 14).

It was difficult to generate drift gas pockets in this model, most likely due to the depth and small size of the sand and gravel lens in which the drift gas accumulated. CH_4 production rates had to be varied within a very small range in order to produce a drift gas pocket without ebullition occurring. When ebullition did occur and bubble channels formed, gas from the drift gas pocket along with any CH_4 gas that was produced in the Robein was transported upward through the bubble channels to the surface. If substantial gas flow persisted through these channels, the drift gas pockets would shrink as the sand and gravel lenses began to re-saturate with groundwater (Figure 15).

As expected depletion of the noble gases occurred as the drift gas pockets were generated. Figure 18A-F shows the dissolved noble gas concentrations after 10,000 years for the recharge rates 1 and 10 percent annual precipitation. When reading the noble gas concentration figures, the background color is equal to that noble gas in equilibrium with the atmosphere and varying colors represent depletion or enrichment.

With all recharge rates the greatest depletion of noble gases occurs in the Robein and in the diamicton between the Robein and the gas pocket (Figure 18). As described earlier this area is partially saturated with trapped gas bubbles and gas saturation of ~5 percent. This area also contains the highest concentration of CH_4 gas. Dissolved noble gas concentrations are depleted during bubble formation as gases partition into the vapor phase. The formation of the gas bubbles causes a decrease in hydraulic conductivity resulting in the deflection of groundwater. The diversion of groundwater around this area

limits the replenishment of noble gases and transport of CH_4 away from this area, just as seen in the ebullition bubble channels.

There is substantial noble gas enrichment around the drift gas pockets in the models with recharge rates greater than 2.5 percent annual precipitation (Figure 18D-F). This is thought to occur due to the high pressures around the gas pockets that result from the high CH_4 production rates needed to generate drift gas pockets at these recharge rates (Figure 19). More gas is dissolved at these high pressures due to the pressure dependent solubilities of the gases. This enrichment is seen more in the heavier noble gases, especially ^{84}Kr, as these gases are more soluble.

This enrichment seen in the models with recharge rates greater than 2.5 percent annual precipitation may be occurring in the field but there are no data to support this process. All dissolved gas data in this region of the Mahomet Bedrock Valley have less than atmospheric noble gas concentrations. For cross-section A we can constrain the recharge rate to less than 5 percent annual precipitation, as these higher recharge rates produce unrealistic noble gas enrichment in the models.

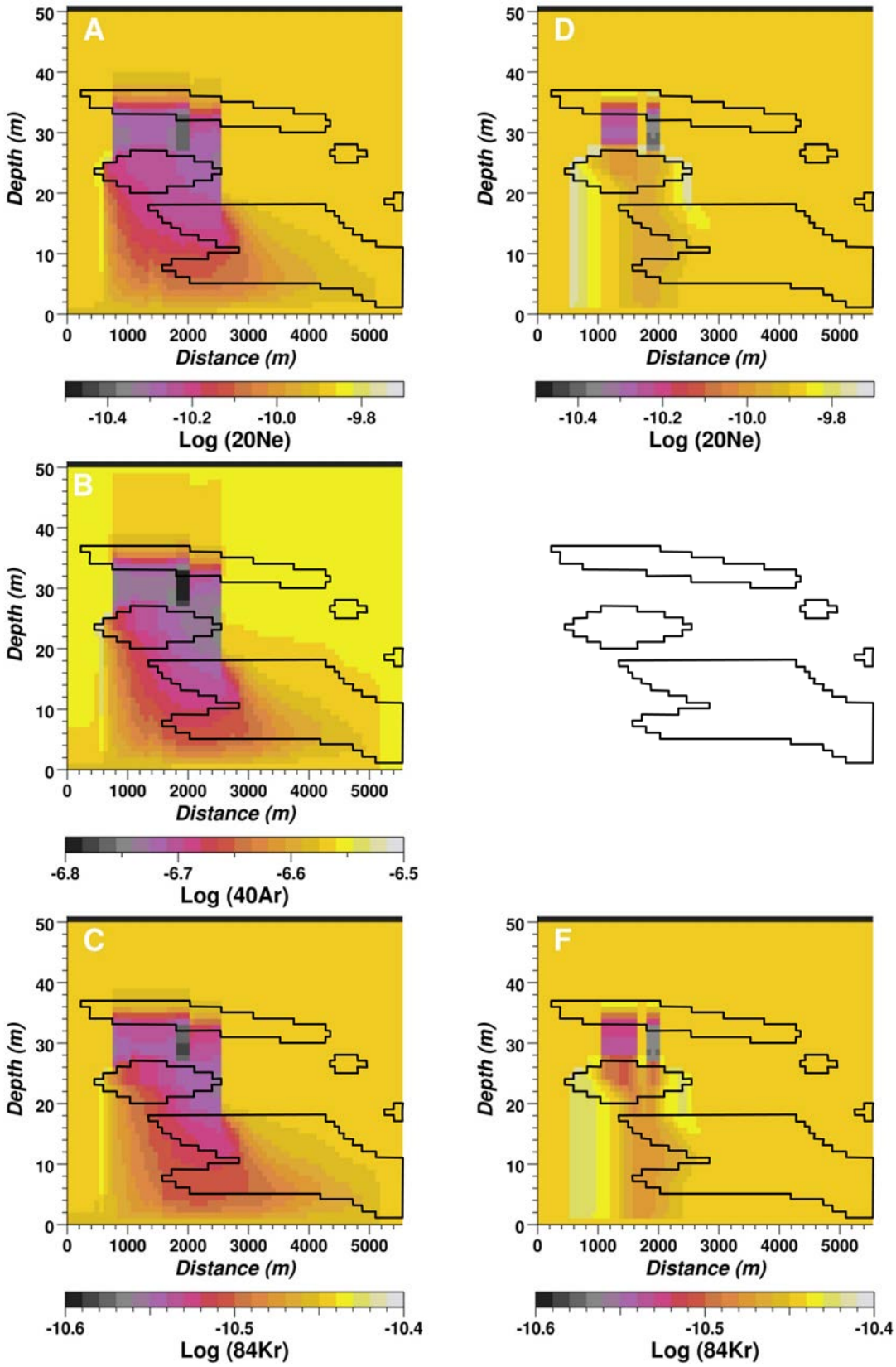
A
D
B
C
F
Depth (m)
Distance (m)
0
10
20
30
40
50
0
1000
2000
3000
4000
5000
-10.4
-10.2
-10.0
-9.8
Log (20Ne)
-6.8
-6.7
-6.6
-6.5
Log (40Ar)
-10.6
-10.5
-10.4
Log (84Kr)

Figure 18. Dissolved noble gas concentrations (Log mole fraction) after 10kyr. A, B, and C show recharge rates of 1pecent annual precipitation. D, E, and F show recharge rates of 10 percent annual precipitation.

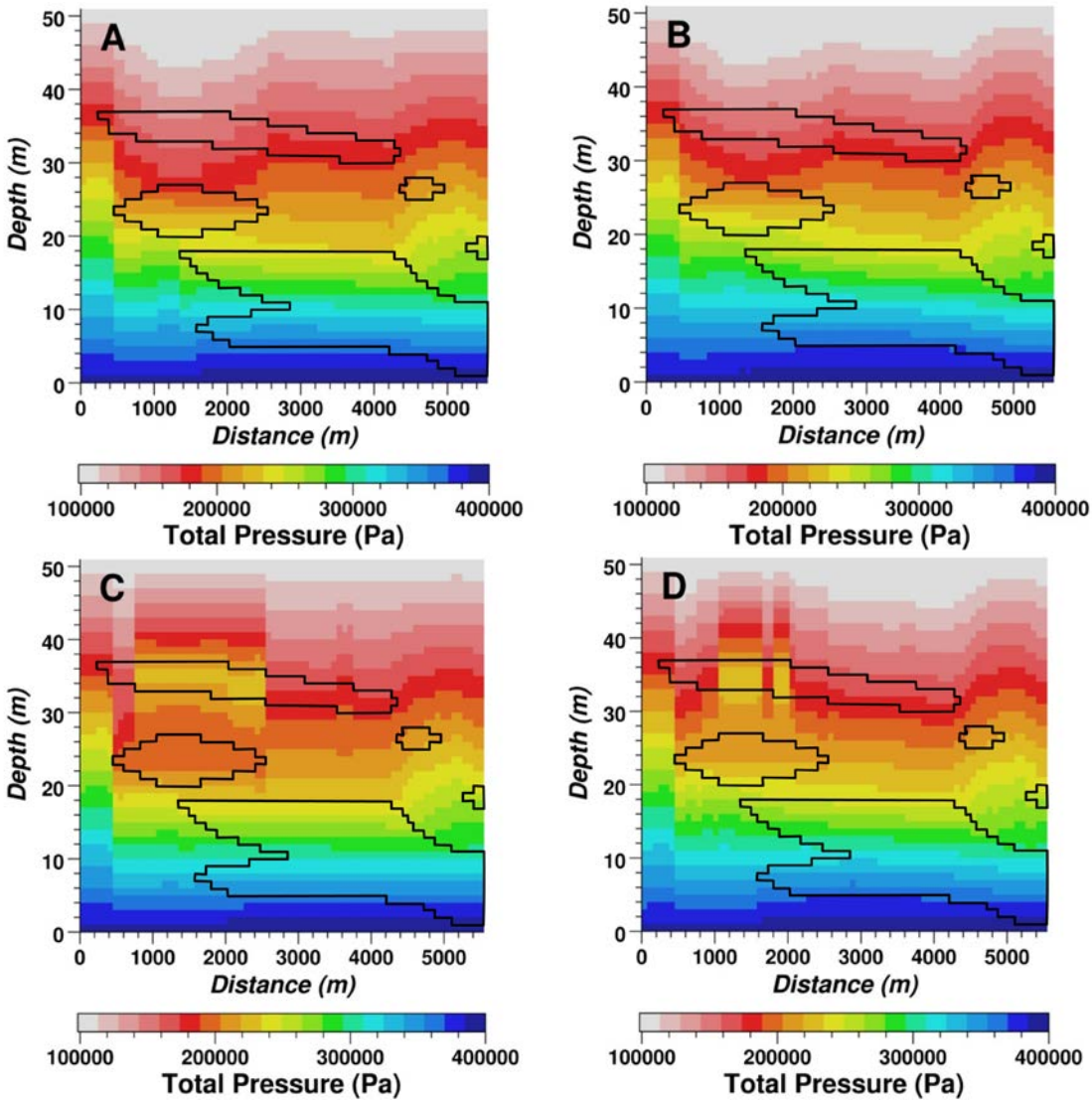

Figure 19. Pressure fields for cross-section A. A and B show the pressure fields after the initialization runs with no CH_4 or CO_2 production for recharge rates 1 and 10 percent annual precipitation, respectively. C and D show the pressure fields after 10,000 years of CH_4 and CO_2 production and drift gas generation for recharge rates of 1 and 10 percent annual precipitation, respectively.

Cross-section B

Cross-section B generated two separate gas pockets in each of the peaks of the long undulating sand and gravel lens (Figure 9). Saturation profiles after 10,000 years and drift gas generation for recharge rates of 1 to 15 percent annual precipitation are

shown in Figure 20. From left to right the gas pockets in this model will be referred to as "gas pocket 1" and "gas pocket 2" (Figure 20).

Ebullition occurred in recharge rates greater than 2.5 percent annual precipitation. Ebullition was tolerated in this model as it did not result in erroneously low dissolved noble gas concentrations or the shrinking of drift gas pockets. Although the dissolved noble gas concentrations within the bubble channels were within the groundwater data, they were also the lowest concentrations represented in those models (Figure 21). Once again this is most likely due to a deflection of groundwater around the bubble channels.

There is also significant enrichment in dissolved ^{84}Kr with all recharge rates greater than 1 percent annual precipitation (Figures 20 and 21). The majority of the enrichment is confined to the area underneath gas pocket 2. With the higher recharge rates, 5 to 15 percent annual precipitation, this enrichment is seen in all three noble gases.

The cause for the dissolved noble gas enrichment in this area is due to the Robein not extending over this part of the sand and gravel lens when this cross-section was discretized (Figure 11). As a result of the CH_4 source zone not overlying gas pocket 2 it contains much lower CH_4 gas concentrations than gas pocket 1 and noble gas concentrations close to equilibrium with the atmosphere. As the groundwater interacted with gas pocket 2, which contained noble gas concentrations close to atmospheric, more noble gases were able to be dissolved into the water due to the slightly higher pressure in the subsurface causing the enrichment (Figure 22). Once again, there are no field data that supports the enrichment of noble gases seen in the models with the recharge rates greater than 2.5 percent annual precipitation.

Two different alterations were made in order to eliminate the noble gas enrichment seen in the higher recharge rates. These alterations did not show much affect on the dissolved noble gas concentrations mixing with the Mahomet Aquifer and exiting the model. Therefore, it appears the noble gas enrichment seen in gas pocket 2 for the higher recharge rates is not a significant factor in how much depleted groundwater is being transported into the Mahomet Aquifer layer and exiting the model. Since the alterations did not significantly change the output calibration data (dissolved gas ratios exiting the model), the enrichment patterns seen in the higher recharge rates were deemed insignificant in the ultimate goal of constraining recharge rate through the aquitard.

The first alteration to eliminate the noble gas enrichment beneath gas pocket 2 was done by extending a thin continuous Robein layer across the entire width of the model. This did eliminate the noble gas enrichment underneath gas pocket 2 and also resulted in gas pocket 2 having gas concentrations more similar to gas pocket 1. Although this scenario did eliminate the enrichment of dissolved noble gases around gas pocket 2, new enrichment patterns developed around the outside of gas pocket 1 in the recharge rates greater than 2.5 percent annual precipitation recharge.

Another attempt was made to eliminate the noble gas enrichment seen in the higher recharge rates by adjusting the hydraulic conductivities of the sand/gravel lenses and the diamicton, so that the ratios of the conductivities in the higher recharge rates were similar to the 1 percent annual precipitation recharge rate. Since the hydraulic conductivity of the sand and gravel lenses were held constant in the models it is possible that the higher recharge rates, which required a higher hydraulic conductivity in the

diamicton, did not have as much lateral groundwater flow through the sand and gravel lenses.

It is hypothesized that a greater difference in the hydraulic conductivities of the sand and gravel and diamicton would drive more lateral flow through the sand and gravel lenses. This would explain why the enrichment underneath gas pocket 2 is more pronounced with higher recharge rates. Less lateral flow through the sand and gravel lens would transport less dissolved CH_4 from the portion of the Robein to right of gas pocket 2, resulting in lower CH_4 concentrations and noble gas concentrations closer to in equilibrium with the atmosphere.

The hydraulic conductivity of the sand and gravel lens was set at the maximum value reported by Kempton et al. (1991), and the hydraulic conductivity of the diamicton was adjusted so that the ratio of these values were equal to that of the 1 percent annual precipitation recharge model run. This model was run with a recharge rate of 10 percent the annual precipitation in order to assess if this would promote more lateral flow through the sand and gravel lens and reduce the enrichment of noble gases. This second alteration eliminated the enrichment of ^{20}Ne and ^{40}Ar underneath gas pocket 2, but ^{84}Kr was still enriched.

As seen in cross-section A, recharge rates greater than 2.5 percent annual precipitation also produced areas unrealistic noble gas enrichment in cross-section B. It is possible that noble gas enrichment could be occurring in the field and is not represented in the groundwater samples. However, since there are no data to support the noble gas enrichment, the models for cross-section B also constrain recharge rate to less than 5 percent annual precipitation.

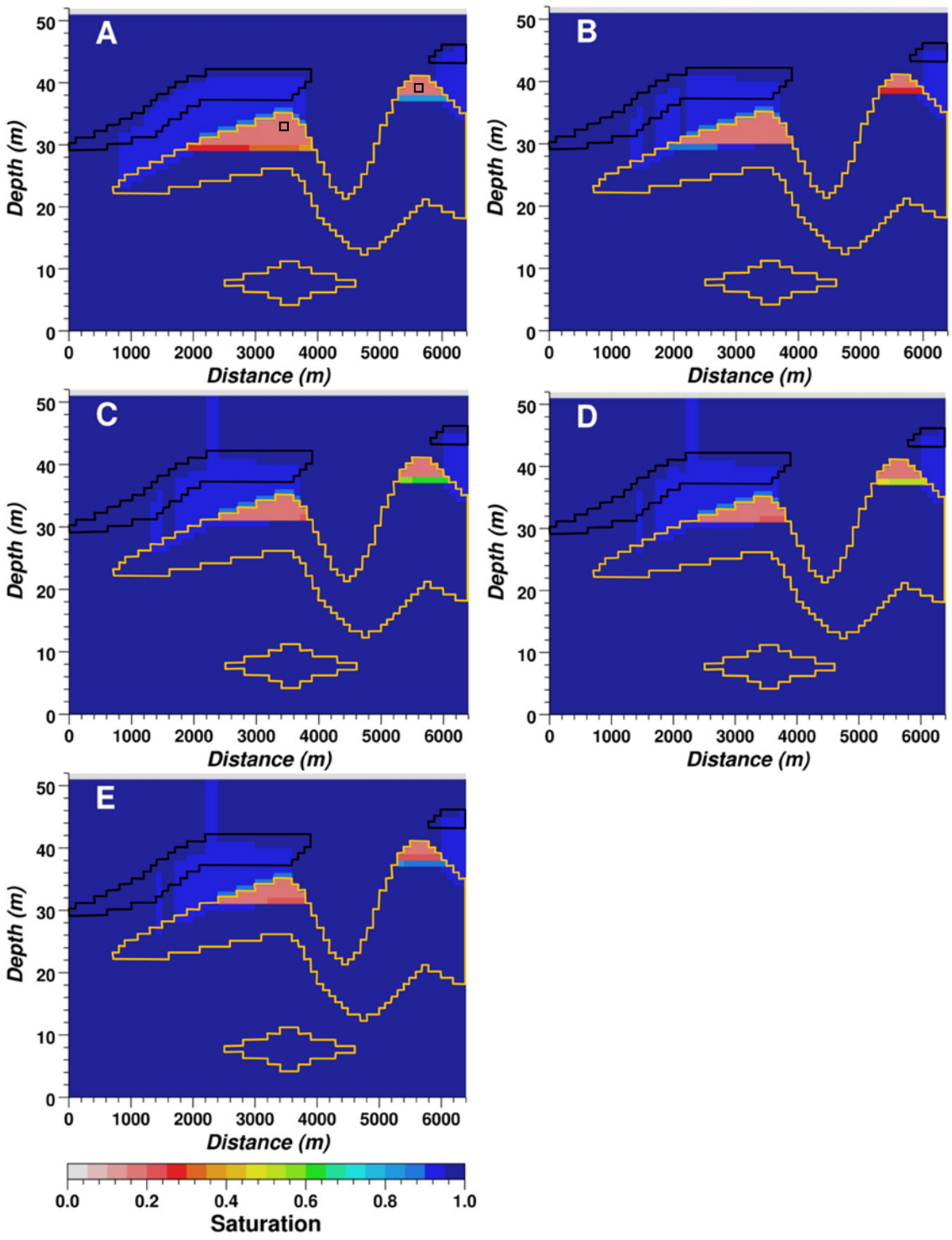

Figure 20. Liquid saturation profiles at 10 kyr of cross-section B. A, B, C, D, and E show recharge rates of 1, 2.5, 5, 10, and 15 percent annual precipitation, respectively. The approximate locations of the cells used to analyze dissolved and gas concentrations within the gas pockets are outlined in black in Figure 20A. The positions of the Robein and sand and gravel lenses are outlined in black and gold, respectively.

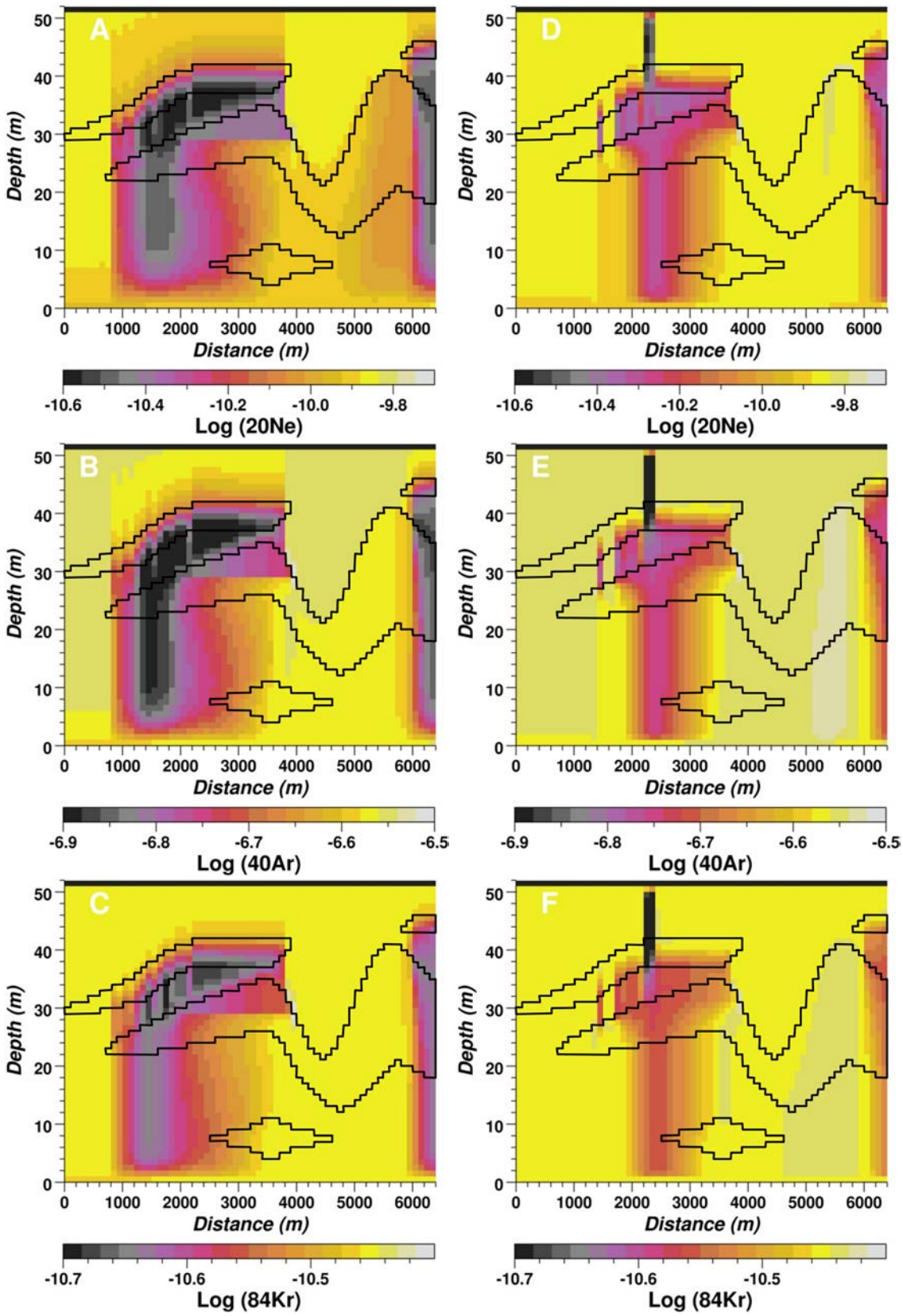
A
D
B
E
C
F
Depth (m)
Distance (m)
0
10
20
30
40
50
0
1000
2000
3000
4000
5000
6000
-10.6
-10.4
-10.2
-10.0
-9.8
Log (20Ne)
-6.9
-6.8
-6.7
-6.6
-6.5
Log (40Ar)
-10.7
-10.6
-10.5
Log (84Kr)

Figure 21. Dissolved noble gas concentrations (Log mole fraction) after 10kyr. A, B, and C show recharge rates of 1 percent annual precipitation. D, E, and F show recharge rates of 10 percent annual precipitation.

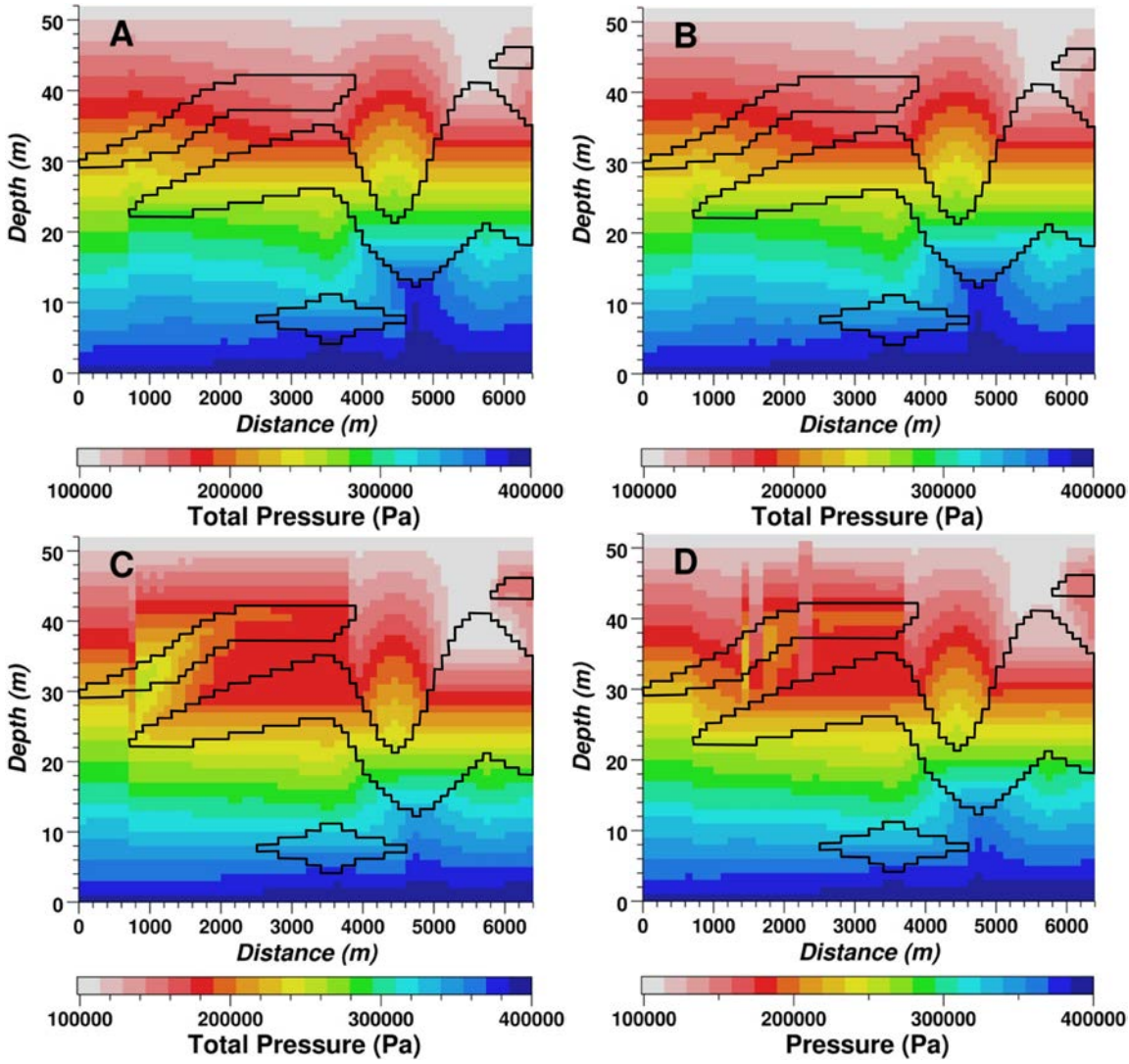

Figure 22. Pressure fields for cross-section B. A and B show the pressure fields after the initialization runs with no CH_4 or CO_2 production for recharge rates of 1 and 10 percent annual precipitation, respectively. C and D show the pressure fields after 10,000 years of CH_4 and CO_2 production and drift gas generation for recharge rates of 1 and 10 percent annual precipitation, respectively.

Cross-section C

No gas pockets could be generated in cross-section C. It appears the sand and gravel lens in this cross-section are too thin to produce the drop in hydrostatic pressure needed for drift gas generation.

Comparison of Gas Ratios in Drift Gas and Groundwater

Models for cross-section A and B successfully simulated the generation of drift gas pockets and produced dissolved gas concentrations and drift gas compositions similar to the field data. Dissolved noble gas concentrations and ratios were analyzed in cells that were encompassed in the gas pockets (Figure 14A and 20A) and also the output cell. The cells within the gas pockets are representative of groundwater in equilibrium with the drift gas pockets. The output cell is representative of the mixing of groundwater that has recharged through the aquitard and groundwater from the Mahomet Aquifer.

Table 7 shows the noble gas concentrations and ΔNe for the two models and the various recharge rates. Also shown is the CH_4 production rate applied for each recharge rate. ΔNe is calculated by

$$\Delta\text{Ne} = \left(\frac{\text{dissolved Ne concentration}}{\text{dissolved Ne concentration in equilibrium with atm}} - 1\right) \times 100.$$

Positive values show enrichment and negative values show depletion. The dissolved noble gas ratios from the gas pocket cells are plotted on Figure 23 along with dissolved gas concentrations from the Wedron, Glasford, and Mahomet Aquifer and theoretical dissolved gas concentrations in equilibrium with drift gas. The dissolved gas ratios exiting the model were not plotted, as they all cluster near the air-saturated water point (Table 8).

The modeled gas ratios plot nicely within the actual groundwater gas ratios and the calculated ratios in equilibrium with drift gas. Generally, the slower recharge rates plot lower down the trend of the graph, showing greater depletion and more degassing. The cells within gas pocket 2 of cross-section B with recharge rates greater than 2.5

percent annual precipitation plot above the air saturated water point showing enrichment of noble gases.

Table 8 shows the dissolved noble gas concentrations and ratios exiting the model through the output cell. The noble gases in this cell are much less depleted as the stripped groundwater is attenuated by mixing with groundwater that has recharged through the aquitard that did not interact with the drift gas pockets and groundwater from the Mahomet Aquifer layer. Slower recharge rates contribute more of the stripped groundwater signature to the Mahomet Aquifer.

Table 7. Dissolved noble gas concentrations (mole fraction) in the cells within the gas pockets. Dissolved noble gas concentrations for air saturated water with and without excess air at 12.5°C are also shown as a reference. The percent variation from equilibrium of ^{20}N e is shown to give an idea of the amount of depletion.

	CH_4 Prod. (kg/s)	^{20}Ne	^{40}Ar	^{84}Kr	ΔNe (%)
ASW w/ EA @ 12.5°C	--	1.86×10^{-10}	3.31×10^{-7}	4.15×10^{-11}	40
ASW w/o EA @ 12.5°C	--	1.32×10^{-10}	2.66×10^{-7}	3.56×10^{-11}	0
X-section A					
1% annual prec.	1.75×10^{-8}	5.74×10^{-11}	1.95×10^{-7}	2.99×10^{-11}	-57
2.5% annual prec.	4.00×10^{-8}	8.31×10^{-11}	2.16×10^{-7}	3.08×10^{-11}	-37
5% annual prec.	8.20×10^{-8}	1.00×10^{-10}	2.22×10^{-7}	3.13×10^{-11}	-24
10% annual prec.	1.7125×10^{-7}	1.01×10^{-10}	2.24×10^{-7}	3.17×10^{-11}	-24
15% annual prec.	2.615×10^{-7}	9.66×10^{-11}	2.18×10^{-7}	3.09×10^{-11}	-27
X-section B					
Gas Pocket 1					
1% annual prec.	1.50×10^{-8}	4.15×10^{-11}	1.71×10^{-7}	2.72×10^{-11}	-69
2.5% annual prec.	2.25×10^{-8}	5.18×10^{-11}	1.84×10^{-7}	2.85×10^{-11}	-61
5% annual prec.	4.50×10^{-8}	6.03×10^{-11}	1.97×10^{-7}	3.00×10^{-11}	-54
10% annual prec.	9.00×10^{-8}	6.11×10^{-11}	1.98×10^{-7}	2.99×10^{-11}	-54
15% annual prec.	1.35×10^{-7}	7.26×10^{-11}	2.09×10^{-7}	3.06×10^{-11}	-45
Gas Pocket 2					
1% annual prec.	1.50×10^{-8}	9.64×10^{-11}	2.54×10^{-7}	3.52×10^{-11}	-27
2.5% annual prec.	2.25×10^{-8}	1.29×10^{-10}	2.70×10^{-7}	3.61×10^{-11}	-3
5% annual prec.	4.50×10^{-8}	1.37×10^{-10}	2.75×10^{-7}	3.65×10^{-11}	4
10% annual prec.	9.00×10^{-8}	1.43×10^{-10}	2.79×10^{-7}	3.67×10^{-11}	8
15% annual prec.	1.35×10^{-7}	1.47×10^{-10}	2.81×10^{-7}	3.68×10^{-11}	11

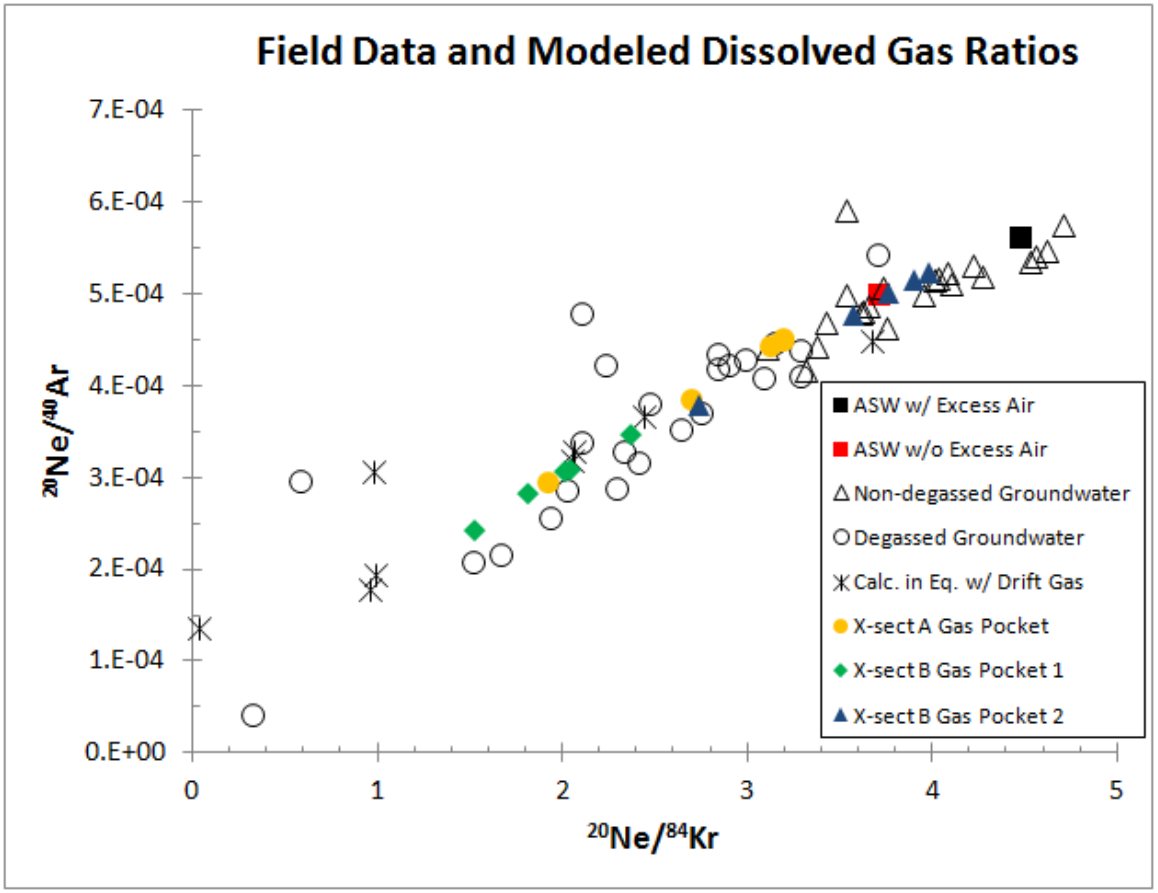

Figure 23. Dissolved noble gas ratios from the cells where gas pockets have formed are plotted with actual groundwater (degassed and non-degassed) and theoretical in equilibrium with drift gas ratios. Also plotted are the air saturated water with and without excess air 12.5°C ratios for reference.

Table 8. Dissolved noble gas concentrations (mole fraction) and ratios exiting the models from the output cell. Generally noble gas concentrations become more depleted with less recharge.

	CH_4 Prod. (kg/s)	^{20}Ne	^{40}Ar	^{84}Kr	ΔNe (%)	$^{20}Ne/^{84}Kr$	$^{20}Ne/^{40}Ar$
ASW w/ EA @ 12.5°C	--	1.86×10^{-10}	3.31×10^{-7}	4.15×10^{-11}	40	4.48	5.61×10^{-4}
ASW w/o EA @ 12.5°C	--	1.32×10^{-10}	2.66×10^{-7}	3.56×10^{-11}	0	3.72	4.99×10^{-4}
X-section A							
1% annual prec.	1.75×10^{-8}	1.23×10^{-10}	2.57×10^{-7}	3.49×10^{-11}	-7	3.52	4.79×10^{-4}
2.5% annual prec.	4.00×10^{-8}	1.25×10^{-10}	2.62×10^{-7}	3.54×10^{-11}	-5	3.54	4.79×10^{-4}
5% annual prec.	8.20×10^{-8}	1.30×10^{-10}	2.64×10^{-7}	3.55×10^{-11}	-2	3.64	4.90×10^{-4}
10% annual prec.	1.7125×10^{-7}	1.32×10^{-10}	2.65×10^{-7}	3.56×10^{-11}	0	3.71	4.98×10^{-4}
15% annual prec.	2.615×10^{-7}	1.32×10^{-10}	2.65×10^{-7}	3.56×10^{-11}	0	3.71	4.98×10^{-4}
X-section B							
1% annual prec.	1.50×10^{-8}	1.18×10^{-10}	2.51×10^{-7}	3.45×10^{-11}	-11	3.42	4.69×10^{-4}
2.5% annual prec.	2.25×10^{-8}	1.25×10^{-10}	2.60×10^{-7}	3.52×10^{-11}	-5	3.56	4.81×10^{-4}
5% annual prec.	4.50×10^{-8}	1.27×10^{-10}	2.61×10^{-7}	3.52×10^{-11}	-4	3.61	4.88×10^{-4}
10% annual prec.	9.00×10^{-8}	1.28×10^{-10}	2.61×10^{-7}	3.53×10^{-11}	-3	3.62	4.89×10^{-4}
15% annual prec.	1.35×10^{-7}	1.28×10^{-10}	2.62×10^{-7}	3.53×10^{-11}	-3	3.63	4.90×10^{-4}

Drift gas composition has been shown to be quite variable (Table 2). The modeled drift gas pockets have produced gas concentrations within the ranges seen in the field data. Table 9 shows the modeled drift gas composition of the gas pocket in cross-section A and the two gas pockets in cross-section B. Figure 24 shows a bar graph of the main constituents (CH_4, CO_2, and N_2) of drift gas from both cross-sections A and B next to reported drift gas concentrations. Gas pocket 2 from cross-section B is not shown as the CH_4 concentrations in this gas pocket are lower than any reported drift gas concentrations.

The two pockets shown in Figure 24 appear to do have successfully replicated the gas concentrations of a possible drift gas seen in the field. Both the cross-section A and B gas pockets have produced CH_4 and N_2 concentrations within the range of the observed data. It is also important to note that the modeled range of CH_4 to N_2 ratios of drift gas is much smaller than the range observed in the field. So, the models have only simulated a few of the possible scenarios of drift gas production and composition that exist. CO_2

concentrations appear to be a little high, especially in the cross-section B gas pocket. The CO_2 production applied in the models may have been a slightly more than what is occurring in the field.

Other than the three drift gas pockets with low CH_4 concentrations (N. Goloff, D. Turner, and M. Walters) it appears the models have under predicted CH_4 concentrations and over predicted N_2 concentrations (Figure 24). This could be a result of the high N_2 concentration implemented in the model through the recharge boundary. The concentration of dissolved N_2 was adjusted to match the groundwater data. This recent groundwater has data has high N_2 concentrations due to denitrification occurring form agricultural use in the area. Thousands of years ago at the time of possible drift gas pocket generation, N_2 concentrations would have been much less than what was used in the models. This could explain the discrepancy with the modeled and the actual drift gas compositions. Variation in groundwater chemistry during the time of drift gas generation such as this, most likely explains the variability seen in actual drift gas compositions.

Table 9. Modeled drift gas concentrations in mole fraction.

Modeled Drift Gas Compostion						
	CH_4	CO_2	N_2	^{40}Ar	^{84}Kr	^{20}Ne
X-section A						
1% annual prec.	7.02×10^{-1}	1.76×10^{-2}	2.77×10^{-1}	3.51×10-3	2.80×10^{-7}	3.66×10^{-6}
2.5% annual prec.	6.40×10^{-1}	2.00×10^{-2}	3.36×10^{-1}	3.66×10-3	2.73×10^{-7}	5.01×10^{-6}
5% annual prec.	6.23×10^{-1}	1.94×10^{-2}	3.54×10^{-1}	3.60×10-3	2.64×10^{-7}	5.75×10^{-6}
10% annual prec.	6.28×10^{-1}	1.64×10^{-2}	3.52×10^{-1}	3.61×10-3	2.66×10^{-7}	5.79×10^{-6}
15% annual prec.	6.45×10^{-1}	1.93×10^{-2}	3.32×10^{-1}	3.45×10-3	2.55×10^{-7}	5.43×10^{-6}
X-section B						
Gas Pocket 1						
1% annual prec.	7.47×10^{-1}	2.79×10^{-2}	2.22×10^{-1}	3.24×10-3	2.69×10^{-7}	2.80×10^{-6}
2.5% annual prec.	6.24×10^{-1}	3.33×10^{-2}	3.39×10^{-1}	3.98×10-3	3.04×10^{-7}	4.64×10^{-6}
5% annual prec.	6.42×10^{-1}	3.46×10^{-2}	3.20×10^{-1}	3.88×10-3	3.08×10^{-7}	4.21×10^{-6}
10% annual prec.	6.36×10^{-1}	3.53×10^{-2}	3.25×10^{-1}	3.92×10-3	3.07×10^{-7}	4.29×10^{-6}
15% annual prec.	5.97×10^{-1}	3.33×10^{-2}	3.66×10^{-1}	4.14×10-3	3.15×10^{-7}	5.09×10^{-6}
Gas Pocket 2						
1% annual prec.	1.63×10^{-1}	1.51×10^{-2}	8.14×10^{-1}	8.69×10-3	6.27×10^{-7}	1.17×10^{-5}
2.5% annual prec.	5.18×10^{-2}	1.34×10^{-2}	9.26×10^{-1}	8.80×10-3	6.13×10^{-7}	1.49×10^{-5}
5% annual prec.	7.28×10^{-2}	1.28×10^{-2}	9.06×10^{-1}	8.44×10-3	5.83×10^{-7}	1.50×10^{-5}
10% annual prec.	6.79×10^{-2}	1.28×10^{-2}	9.11×10^{-1}	8.36×10-3	5.75×10^{-7}	1.53×10^{-5}
15% annual prec.	5.61×10^{-2}	1.27×10^{-2}	9.23×10^{-1}	8.39×10-3	5.73×10^{-7}	1.56×10^{-5}

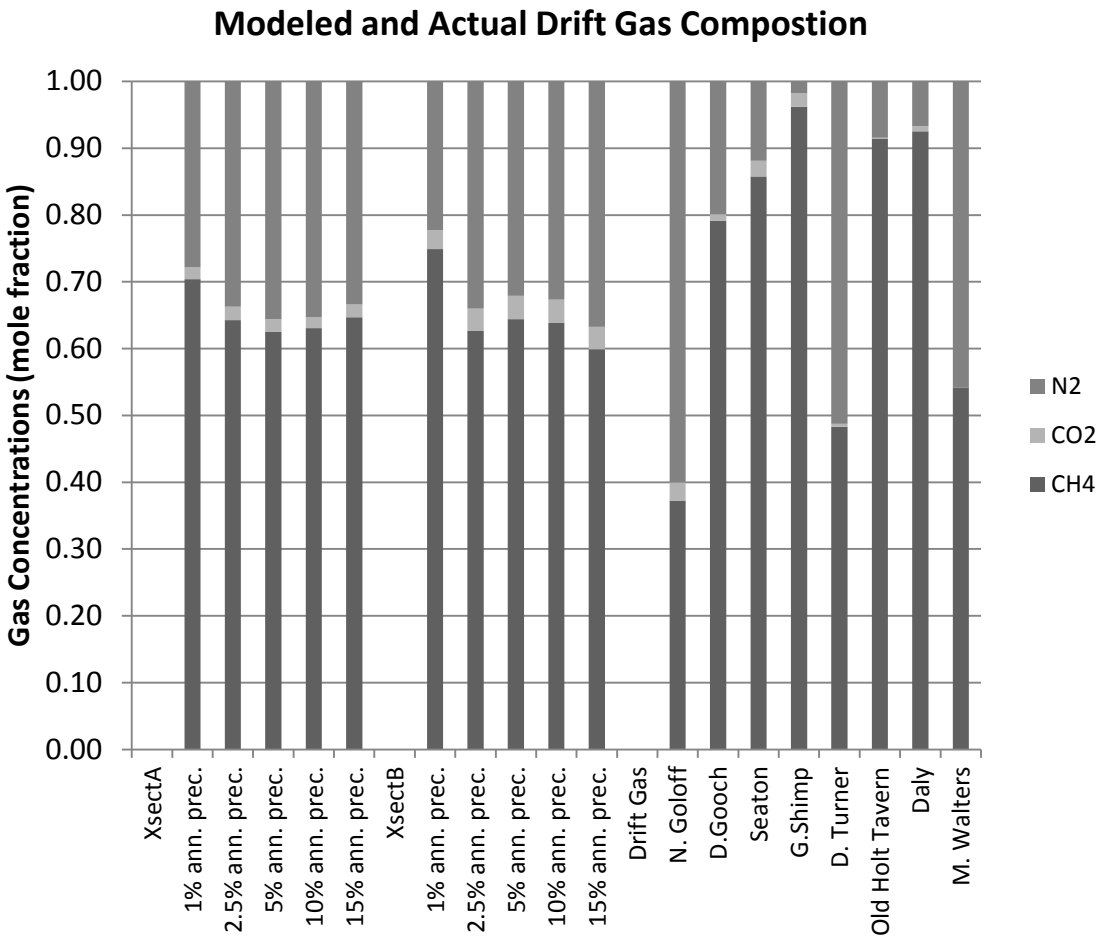

Figure 24. Modeled and field drift gas concentrations of CH_4, CO_2, and N_2 in mole fractions. Only gas pocket 1 from cross-section B is shown.

Recharge Rates Through Aquitard

Recharge rates were varied in the models from 1 to 15 percent annual precipitation, 3.31×10^{-10} to 4.96×10^{-9} m/s. Table 10 shows the recharge rates modeled, the respective hydraulic conductivities for the diamicton, and CH_4 and CO_2 production rates applied. The hydraulic conductivity of the sand and gravel lenses was held constant at 4×10^{-4} m/s.

Figure 25 shows the dissolved noble gas concentrations exiting the model over time for the different recharge rates. Slower recharge rates resulted in more depleted groundwater exiting model. This seems somewhat counter-intuitive as you would expect

higher recharge rates to be contributing more stripped groundwater into the Mahomet Aquifer layer resulting in more depleted groundwater exiting the model.

There appears there are two mechanisms causing the contribution of more depleted groundwater to the Mahomet aquifer layer with less recharge. First, groundwater at slower recharge rates experiences greater degassing (Table 7 and Figure 23), most likely due the greater residence times in the Robein and the low pressure areas of the sand and gravel lenses. A longer residence time through the Robein will acquire more CH_4 and a longer residence time in the low pressure sand and gravel lenses will allow for more degassing to occur.

Secondly, the higher recharge rates require higher CH_4 production rates in order to generate drift gas pockets (Table 10). The higher CH_4 production rates cause initial degassing and drift gas generation to occur very quickly. This can be seen as the low points on the line graphs in Figure 25. After drift gas generation (low point) noble gas concentrations begin to increase as groundwater is deflected around the gas pocket. In cross-section A, noble gas concentrations return to in equilibrium with the atmosphere with recharge rates greater than 5 percent annual precipitation (Figure 25). This is caused by the total deflection of groundwater around the gas pockets and no more degassing occurring after a gas pocket was generated. The higher CH_4 production rates also create a greater pressure build up around the Robein and gas pockets (Figures 19 and 22), which would also cause the diversion of groundwater around these areas.

A recharge rate of 1 percent of the annual precipitation (3.31×10^{-10} m/s) produced the best representation of groundwater that is suspected to have interacted with drift gas pockets. In both cross-section A and B the hydraulic conductivity of the diamicton was

adjusted lower than the range reported by Kempton et al. (1991) for this recharge rate (Table 10). So a recharge rate of 1 percent annual precipitation may be too low. But keep in mind that the sand and gravel hydraulic conductivity was held constant at the median value reported by Kempton et al. (1991). So, a lower *K* value for the sand and gravel with a higher *K* value for diamicton could produce similar results for a 1 percent annual precipitation. The uncertainty involved with hydraulic properties of aquitards should also be noted (Gerber and Howard, 2000, Neuzil, 1986).

The data from the models suggest that a recharge rate between 1 to 2.5 percent annual precipitation (3.31×10^{-10} to 8.26×10^{-10} m/s) through the aquitard provides the best representation of what is occurring in the field. The CH_4 production rates required for drift gas generation at these recharge rates are similar to what Simpkins and Parkin (1993) reported for a Wisconsinan loess (2.28×10^{-3} to 3.03×10^{-3} mol m^{-3} yr^{-1}). The CH_4 production rates reported by Simpkins and Parkin, (1993) were acquired from core samples from a very similar geologic feature and setting as the Robein. Because the core samples were amended with nutrients in the lab and CH_4 was produced under ideal conditions, these rates may be higher than what is occurring in situ. CH_4 production rates used for 1 percent annual precipitation recharge rate were less than the range reported by Simpkins and Parkin (1993) in both cross-section A and B (Table 10).

These production rates are also within the CH_4 production rates reported for methanogenesis in a landfill leachate plume (Ludvigsen et al., 1998), 2.90×10^{-3} to 5.36×10^{-3} mol m^{-3} yr^{-1}, and in marine sediments on the continental slope offshore of Oregon (Schulz et al., 2009), 1.0×10^{-4} to 1.0×10^{-2} mol m^{-3} yr^{-1}.

The 1 to 2.5 percent annual precipitation recharge rates and the CH_4 production rates applied did not cause ebullition in either of the two cross-sections. There are no data supporting ebullitive processes in the glacial sediments overlying the Mahomet Aquifer. Therefore, recharge rates where ebullition does not occur provide the best representation of the infiltration of groundwater through the aquitard.

Table 10. Recharge rates, CH_4 production rates, CO_2 production rates, and hydraulic conductivities of the diamicton used for the successful generation of drift gas pockets.

	Recharge (m/s)	CH_4 prod. (mol m^{-3} yr^{-1})	CO_2 prod. (mol m^{-3} yr^{-1})	Diamicton K (m/s)
X-sect A				
1% annual prec.	3.31×10^{-10}	2.14×10^{-3}	3.37×10^{-3}	6.65×10^{-10}
2.5% annual prec.	8.26×10^{-10}	4.90×10^{-3}	8.44×10^{-3}	1.73×10^{-9}
5% annual prec.	1.65×10^{-9}	1.00×10^{-2}	1.69×10^{-3}	3.67×10^{-9}
10% annual prec.	3.31×10^{-9}	2.10×10^{-2}	3.37×10^{-2}	7.82×10^{-9}
15% annual prec.	4.96×10^{-9}	3.20×10^{-2}	5.06×10^{-2}	1.20×10^{-8}
X-sect B				
1% annual prec.	3.31×10^{-10}	1.61×10^{-3}	3.37×10^{-3}	4.03×10^{-10}
2.5% annual prec.	8.26×10^{-10}	2.42×10^{-3}	8.44×10^{-3}	1.01×10^{-9}
5% annual prec.	1.65×10^{-9}	4.83×10^{-3}	1.69×10^{-3}	2.03×10^{-9}
10% annual prec.	3.31×10^{-9}	9.67×10^{-3}	3.37×10^{-2}	4.10×10^{-9}
15% annual prec.	4.96×10^{-9}	1.45×10^{-2}	5.06×10^{-2}	6.18×10^{-9}

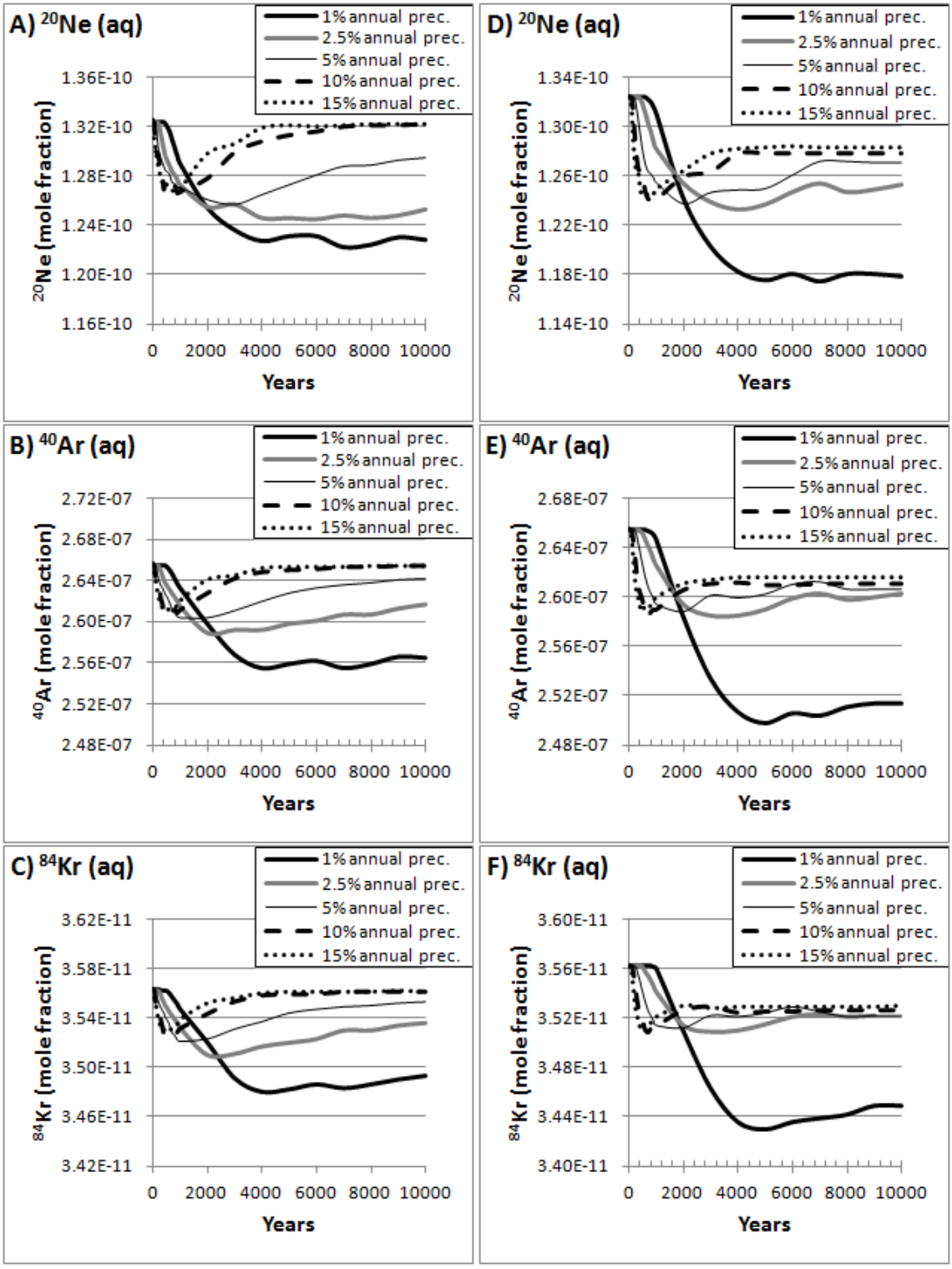

Figure 25. Dissolved noble gas concentrations exiting the model through the output cell. A, B, and C show noble gas concentrations for cross-section A and D, E, and F show noble gas concentrations for cross-section B over time.

Conclusions

The goal of this study was to constrain the recharge rate through the glacial till that confines the Mahomet aquifer by simulating the generation of drift gas pockets found throughout central Illinois. A 2D multiphase flow model successfully simulated the generation of drift gas pockets in two of the cross-sections through Piatt County. The models produced dissolved noble gas concentrations and drift gas compositions similar to what has been observed in the field.

Recharge rates greater than 2.5 percent annual precipitation produced some conditions that have not been observed in the field. The enrichment of noble gases and ebullition seen in the higher recharge rates could be occurring where drift gas has formed, but there are no data that support these processes. So, it appears recharge rates from 5 to 15 percent annual precipitation are not plausible.

It was originally hypothesized that a greater amount of groundwater was recharging through the glacial till units southwest of the main recharge area of the Mahomet Aquifer than previously reported. It was suspected that the progressively depleted noble gas concentrations seen with distance southwest from the main recharge area was indicative of significant amount groundwater recharging through the confining glacial tills. The results of this study suggest otherwise, that slower recharge rates actually contribute more groundwater depleted of dissolved noble gases. A recharge rate between 1 to 2.5 percent annual precipitation (3.31×10^{-10} to 8.26×10^{-10} m/s) through the aquitards gives the best representation of the dissolved noble gas ratios observed in the Glasford Formation and Mahomet Aquifer.

The dissolved noble gas ratios observed in the Glasford were successfully produced, but the models failed to replicate the extent of the depleted groundwater that is

transported to the Mahomet Aquifer. Much more depleted noble gas concentrations have been observed in the Mahomet Aquifer than what the models produced. The stripped groundwater is attenuated by mixing with non-degassed groundwater and water from the Mahomet Aquifer, resulting in less depleted groundwater exiting the model.

The failure of the model to produce the more depleted noble gas concentrations observed in the Mahomet Aquifer could be due to the small size of the drift gas pockets simulated. Groundwater interaction with a larger drift gas pocket would contribute more of the stripped groundwater signature to the Mahomet Aquifer. Another scenario may be that the groundwater in the aquifer already has depleted noble gas concentrations from groundwater that has recharged and interacted with drift gas upgradient. Successive areas with drift gas pockets downgradient could progressively deplete noble gas concentrations in the Mahomet Aquifer as more stripped groundwater is recharged.

It should also be noted that the models presented only simulate the very top of the Mahomet Aquifer, and do not realistically model the entire aquifer from which the groundwater samples were taken. Furthermore, the range of dissolved noble gas depletion observed in the Mahomet Aquifer may not have been simulated correctly due to the inability of the models to capture the 3D mixing occurring in reality.

The CH_4 production rates applied in the 1 to 2.5 percent annual precipitation recharge rates were the most plausible to be occurring in the Robein Formation. The CH_4 production rates used in these simulations are very similar to the reported rates observed in a Wisconsinan loess (Simpkins and Parkin, 1993). Although the CH_4 production rates reported by Simpkins and Parkin (1993) are from a nearly identical geologic feature as the Robein, the lab conditions in which these results were acquired may have produced

higher production rates than found in situ. The 1 percent annual precipitation recharge rate simulation for both cross-section A and B required CH_4 production rates less than the range reported by Simpkins and Parkin (1993).

References

Aeschbach-Hertig, W., El-Gamal, H., Wieser, M. and Palcsu, L. 2008. Modeling excess air and degassing in groundwater by equilibrium portioning with a gas phase. Water Resources Research, 44, W08449, doi:10.1029/2007WR006454.

Amos, R.T., Mayer, K.U., Bekins, B.A., Delin, G.N. and Williams R.L. 2005. Use of dissolved and vapor-phase gases to investigate methanogenic degradation of petroleum hydrocarbon contamination in the subsurface. Water Resources Research, 41, W02001, doi:10.1029/2004WR003433.

Amos, R.T. and Mayer, K.U. 2006. Investigating ebullition in a sand column using dissolved gas analysis and reactive transport modeling. Environmental Science and Technology, 40, 5361-5367.

Amos, R.T. and Mayer, K.U. 2006. Investigating the role of gas bubble formation and entrapment in contaminated aquifers: Reactive transport modeling. Journal of Contaminant Hydrology, 87, 123-154.

Anliker, M.A. and Sanderson, E.W. 1995. Reconnaissance study of ground-water levels and withdrawals in the vicinity of Dewitt and Piatt counties, Contract Report 589. Illinois State Water Survey.

Blicher-Mathiesen, G., McCarty, G.W. and Nielsen, L.P. 1998. Denitrification and degassing in groundwater estimated from dissolved dinitrogen and argon. Journal of Hydrology, 208, 16-24.

Brennwald, M.S., Hofer, M., Peeters, F., Aeschbach-Hertig, W., Strassmann, K., Kipfer, R., and Imboden, D.M. 2003. Analysis of dissolved noble gases in the porewater of lacustrine sediments. Limnology and Oceanography: Methods, 1, 51-62.

Coleman, D.D., 1979. The origin of drift-gas deposits as determined by radiocarbon dating of methane. In: R. Berger and H.E. Suess (Editors), Radiocarbon Dating, Proceedings of the Ninth International Conference. University of California Press, Los Angeles, Calif., pp. 365-387.

Coleman, D.D., Liu, C.L. and Riley, K.M., 1988. Microbial methane in the shallow Paleozoic sediments and glacial deposits of Illinois, U.S.A. In: M. Schoell (Guest Editor), Origins of Methane in the Earth. Chem. Geol., 71: 23-40.

Fetter, C.W. 2001. Contaminant Hydrogeology Second Edition. Prentice-Hall, Inc., Upper Saddle River, NJ 07458, 1999.

Fortuin, N.P.M. and Willemsen, A. 2005. Exsolution of nitrogen and argon by methanogenesis in Dutch ground water. Journal of Hydrology, 301, 1-13.

Gerber, R.E. and Howard, K. 2000. Recharge through a regional till aquitard: three-dimensional flow model water balance approach. Ground Water, 38, 410-422.

Glessner, J.J.G. and Roy W.R. 2009. Paleosols in central Illinois as potential sources of ammonium in groundwater. Ground Water Monitoring & Remediation, 29 (4), 56-64.

Hackley, K.C., Panno, S.V. and Anderson, T.F. 2010. Chemical and isotopic indicators of groundwater evolution in the basal sands of a buried bedrock valley in the Midwestern United States: Implications for recharge, rock-water interactions, and mixing. GSA Bulletin, 122 (7/8), 1047-1066, doi:10.1130/B26574.1.

Hansen, L.K., Jakobsen, R., and Postma, D. 2001. Methanogenesis in a shallow sandy aquifer, Romo, Denmark. Geochimica et Cosmochimica Acta, 65 (17), 2925-2935.

Ho, C.K. and Webb, S.W. 2006. Gas Transport in Porous Media. Springer, Berlin.

Holzner, C.P., McGinnis, D.F., Schubert, C.J., Kipfer, R. and Imboden, D.M. 2008. Noble gas anomalies related to high-intensity methane gas seeps in the Black Sea. Earth and Planetary Letters, 265, 396-409.

Jarsjo, J. and Destouni, G. 2000. Degassing of deep groundwater in fractured rock around boreholes and drifts. Water Resources Research, 36 (9), 2477-2492.

Jones, E.J.P., Voytek, M.A., Warwick, P.D., Corum, M.D., Cohn, A., Bunnell, J.E., Clark, A.C., and Orem, W.H. 2008. Bioassay for estimating the biogenic methane-generating potential of coal samples. International Journal of Coal Geology, 76, 138-150.

Kellner, E., Baird, A.J., Oosterwoud, M., Harrison, K., and Waddington, J.M. Effect of temperature and atmospheric pressure on methane. 2006. (CH_4) ebullition form near-surface peats. Geophysical Research Letters, 33, L18405, doi:10.1029/2006GL027509.

Kempton, J.P., Johnson, W.H., Heigold, P.C. and Cartwright, K. 1991. Mahomet Bedrock Valley in east-central Illinois: Topography, glacial drift stratigraphy, and hydrogeology. Geology and Hydrogeology of the Teays-Mahomet Bedrock Valley System, Special Paper Geological Society of America, 258: 91-124.

Kipfer, R., Aeschbach-Hertig, W., Peeters, F., and Stute, M. 2002. Noble gases in lakes and ground waters. Reviews in mineralogy and geochemistry, 47 (1), 615-700, doi:10.2138/rmg.2002.47.14.

Laing, C.G., Shreeve, T.G., and Pearce, D.M.E. Methane bubbles in surface peat cores: in situ measurements. 2008. Global Change Biology, 14, 916-924, doi:10.1111/j.1365-2486.2007.01534.x

Luca Technologies. Active biogenesis of methane in Wyoming's powder river basin. Luca Technologies, 1625 Broadway Street, Denver, CO 80202.

Ludvigsen, L., Albrechtsen, H.J., Heron, G., Bjerg, P.L., and Christensen, T.H. 1998. Anaerobic microbial redox processes in a landfill leachate contaminated aquifer (Grindsted, Denmark). Journal of Contaminant Hydrology, 33, 273-291.

Neuzil, C.E. 1986. Groundwater flow in Low-Permeability Environments. Water Resources Research, 22 (8), 1163-1195.

Nitao, J.J. 2000. User's manual for the USNT module of the NUFT code, version 3.0 (NP-phase, NC-component, thermal). Earth and Environmental Sciences, Lawrence Livermore National Laboratory.

Panno, S.V., Hackley, K.C., Cartwright, K. and Liu, C.L. 1994. Hydrochemistry of the Mahomet Bedrock Valley Aquifer, east-central Illinois: Indicators of recharge and ground-water flow. Ground Water, 32, 591-604.

Schaap, M.G. 1999. Rosetta Version 1.0. U.S. Salinity Laboratory, U.S. Department of Agriculture, Riverside, CA.

Schulz, H.M., Berk, W.V., Bechtel, A., Struck, U., and Faber, E. 2009. Marine and Petroleum Geology, 26, 1163-1179.

Simpkins, W.W. and Parkin, T.B. 1993. Hydrogeology and redox geochemistry of CH_4 in a late Wisconsinan till and loess sequence in central Iowa. Water Resources Research, 29 (11), 3643-3657.

Solomon, D.K., Poreda, R.J., Schiff, S.L. and Cherry, J.A. 1992. Tritium and helium 3 as groundwater age tracers in the Borden Aquifer. Water Resources Research, 28, 741-755.

Solomon, D.K., Cook, P.G., and Sanford, W.E. 1998. Dissolved gases in subsurface hydrology. In: Kendall, c., McDonnell, J. (Eds.), Isotope Tracers in Catchment Hydrology. Elsevier, Amsterdam, 291-318.

U.S. Geological Survey (USGS), 1999, Ground-water studies in Illinois, http://il.water.usgs.gov/proj/gwstudies/ (November 2010).

Van der Hoven, S.J., Wright, R.E., and Carstens, D.A. 2005. Radiogenic ^{4}He as a conservative tracer in buried-valley aquifers. Water Resources Research, 41, W11414, doi:10.1029/2004WR003857.

Visser, A., Broers, H.P. and Bierkens, M.F.P. 2007. Dating degassed groundwater with ^{3}H/^{3}He. Water Resources Research, 43, W10434, doi:10.1029/2006WR005847.

Wilhelm, E., Battino, R., and Wilcock, R.J. 1977. Low-pressure solubility of gases in liquid water. Chemical Reviews, 77, 219-262.

Willman, H.B. and Frye, J.C. 1975. Quaternary System. Illinois State Geological Survey Bulletin 95, 211-239.

Wilson, S.D., Roadcap, G.S., Herzog, B.L., Larson, D.R. and Winstanley, D. 1998. Hydrogeology and ground-water availability in southwest McLean and southeast Tazwell counties, part 2: Aquifer modeling and final report, Coop. Ground Water Rep. 19, III. State Water Survey, Champaign.

Yager R.M. and Fountain J.C. 2001. Effect of natural gas exsolution on specific storage in a confined aquifer undergoing water level decline. Ground Water, 39, 517-525.

Yavitt, J.B., Downey, D.M., Lancaster, E., and Lang, G.E. 1990. Methane consumption in decomposing sphagnum-derived peat. Soil Biology and Biochemistry, 22 (4), 441-447.

Zhou, Z., Ballentine, C.J., Kipfer, R., Schoell, M. and Thibodeaux, S. 2005. Noble gas tracing of groundwater/coalbed methane interaction in the San Juan Basin, USA. Geochimica et Cosmochimica Acta, 69 (23), 5413-5428.

CHAPTER III

DISCUSSION AND IMPLICATIONS OF RESEARCH

The occurrence of drift gas is a fairly common phenomenon in the glaciated Midwest (Meents, 1960, Coleman, 1979, Coleman et al., 1988). CH_4 is produced in the glacial sediments as organic material decomposes under anoxic conditions. The low permeability of the glacial deposits traps gas from escaping to the surface. The occurrence of drift gas can have significant chemical and physical effects on groundwater systems. The frequent occurrence of drift gas pockets can make them valuable tools for assessing hydrogeological processes in the glacial deposits throughout the Midwest. By simulating the generation of drift gas pockets, poorly understood processes may be able to be constrained.

Quantifying In Situ CH_4 Production Rates

As shown earlier biogenic CH_4 production is quite variable. Most often biogenic CH_4 production rates are measured in a laboratory setting. CH_4 productions under these ideal conditions are not always an accurate representation of what is occurring in the field. Quantifying in situ biogenic CH_4 production has proven to be a difficult task due to the physical and chemical heterogeneity of the subsurface. In situ CH_4 production rates have been determined from concentration gradients and groundwater transport rate estimates (Jakobsen and Postma, 1999) and by isotopic analysis of dissolved inorganic carbon (DIC) in the associated groundwater (Hansen et al., 2001, Sivan et al., 2007). Both of these approaches are indirect measures of CH_4 production and instead involve analysis of the groundwater composition. Groundwater mixing and upgradient sources of CH_4 and DIC provide uncertainty and complexity to either of these methods.

Where gas pockets occur, such as drift gas, simulating the generation of these features may be an alternative approach to constrain CH_4 production rates. The models in this study were very sensitive to CH_4 production. Production rate was well constrained in order to reproduce the dissolved gas concentrations observed. Where groundwater data is available multiphase geochemical flow models appear to be a plausible and cost effective way to assess in situ CH_4 production.

Assessing usage for natural gas

In Illinois drift gas mainly occurs in the northeast fourth of the state where thicker glacial deposits exist. Meents (1960) reported there are about 460 gas producing wells in 27 counties and 200 gas wells that were abandoned before 1946. Many of the wells were drilled before 1900 (Meents, 1960). Meents (1960) collected samples from 216 wells throughout Illinois and reported gas volumes ranged from a few cubic meters per day up to 48,000, with an average of ~2,000 cubic meters per day. It has been estimated that several billion cubic feet per day of drift gas has been consumed by residential homes in Illinois since 1900. Mostly drift gas is used in low-volume gas units such as, cooking stoves and water heaters (Meents, 1960). A common question of landowners with rights to this natural gas is how long the supply will last.

Modeling the generation of the drift gas pocket could be a viable method to answering this question. As discussed earlier the models in this study are capable of constraining the CH_4 production rate of the decomposing organic material. Also, the models have shown that the amount of degassing is directly correlated to the fractionation of noble gases. More degassing causes greater fractionation of the lighter noble gases, e.g. Ne, from the heavier noble gases, e.g. Ar and Kr. By successfully modeling the

amount of degassing, the volume of the drift gas pocket in question could be constrained. With constraints on a starting drift gas volume and CH_4 production rate, a predictive model could be constructed to assess how long the gas supply would last. A model with an extraction well, with varying consumption rates could predict how long and at what rate gas could be consumed before the drift gas pocket is exhausted.

Quantifying biodegradation rates

Biodegradation of an organic contaminant plume can be an advantageous remediation strategy. This in situ, naturally occurring process can be more cost effective then other ex situ remediation strategies, as excavation or pump and treat operations are not required. The ability to assess the extent of biodegradation occurring in the subsurface thus becomes important for site assessment and cost management. The assessment of biodegradation processes of specific contaminants at field sites is very demanding and sometimes impossible. The commonly used methods to assess the occurrence of biodegradation such as; monitoring decreasing downgradient contaminant concentrations, depletion of terminal electron acceptors, presence of metabolites, and production of CO_2, can be complicated with the heterogeneity of field conditions and possible co-contaminants. Physical processes such as dilution and adsorption can cause a decrease in contaminant concentration, but do not permanently remove the contaminant from the system. So, it is important to have a direct way to assess the occurrence of biodegradation.

Biogenic gas production, such as CH_4 and N_2, rate is often used to calculate biodegradation rate of organic material under anoxic conditions. If degassing occurs biodegradation will be underestimated if the gas lost to degassing is not accounted for.

Degassing is commonly observed as a result of N_2 production by denitrification from agricultural pollution (Blicher-Mathiesen et al., 1998; Visser et al., 2007) and as a result of CH_4 production under landfills (Solomon et al., 1992), and biodegradation of petroleum hydrocarbons (Amos et al, 2005; Amos and Mayer, 2006b). Where degassing occurs, and noble gases are depleted, models similar to this study are a cost effective way to quantitatively assess biodegradation rates.

Evaluating Hydrogeologic Properties of Aquitards

Evaluating hydrogeologic properties of aquitards has proven to be a difficult task and is poorly understood (Gerber and Howard, 2000, Neuzil, 1986). Response of large scale tests of flow through aquitards takes too long to observe and is severely limited by constraints of time. Thus, the best estimates for flow through aquitards are normally obtained by integrating values obtained from a wide range of tests small in scale relative to the volume of interest (Neuzil, 1986). The uncertainty involved with these small scale tests is further amplified with heterogeneity of aquitards containing features such as sand lenses, as the case of the glacial tills confining the Mahomet Aquifer (Gerber and Howard, 2000). It has also been shown that the occurrence of gas bubbles can greatly influence hydraulic conductivity, further complicating flow through glacial tills confining the Mahomet Aquifer.

In many cases, as with the Mahomet Aquifer, aquitards are confining major freshwater resources. So, it becomes imperative to understand the hydrogeologic properties of theses aquitards in order to assess groundwater management and potential contamination pathways. This study shows that geochemical flow models provide another approach to assess hydrogeologic properties of aquitards. When dissolved gas

data is available geochemical modeling can be a practical method to verify physical flow model results.

Conclusions

This study has shown the capability of 2D multiphase geochemical flow model to constrain recharge rate through an aquitard. The models have successfully simulated the generation of drift gas pockets and the subsequent depletion of dissolve noble gases. Flow through aquitards has historically been difficult to constrain. The goal of this study was to offer another approach to analyze recharge through an aquitard through analysis of the dissolved gas composition of the groundwater.

It was originally hypothesized that a greater amount of groundwater was recharging through the glacial till units southwest of the main recharge area of the Mahomet Aquifer than previously reported. It was suspected that the progressively depleted noble gas concentrations seen with distance southwest from the main recharge area was indicative of significant amount groundwater recharging through the confining glacial tills. The results of this study suggest otherwise, that slower recharge rates actually contribute more groundwater depleted of dissolved noble gases. A recharge rate between 1 to 2.5 percent annual precipitation (3.31×10^{-10} to 8.26×10^{-10} m/s) through the aquitards gives the best representation of the dissolved noble gas ratios observed in the Glasford Formation and Mahomet Aquifer.

The CH_4 production rates applied in the 1 to 2.5 percent annual precipitation recharge rates were the most plausible to be occurring in the Robein Formation. The CH_4 production rates used in these simulations are very similar to the reported rates observed in a Wisconsinan loess (Simpkins and Parkin, 1993). Although the CH_4 production rates

reported by Simpkins and Parkin (1993) are from a nearly identical geologic feature as the Robein, the lab conditions in which these results were acquired may have produced higher production rates than found in situ. The 1 percent annual precipitation recharge rate simulation for both cross-section A and B required CH_4 production rates less than the range reported by Simpkins and Parkin (1993).

Flow through heterogeneous aquitards such as the glacial tills confining the Mahomet Aquifer is poorly understood. Hydrogeological complexities are even further amplified with the presence of drift gas pockets. Gas bubbles have been shown to greatly influence hydraulic conductivity, groundwater flow, and groundwater composition. Further studies in the area of groundwater processes in aquitards are needed to gain a better understanding of hydrogeologic implications of these features.

REFERENCES

Aeschbach-Hertig, W., El-Gamal, H., Wieser, M. and Palcsu, L. 2008. Modeling excess air and degassing in groundwater by equilibrium portioning with a gas phase. Water Resources Research, 44, W08449, doi:10.1029/2007WR006454.

Amos, R.T., Mayer, K.U., Bekins, B.A., Delin, G.N. and Williams R.L. 2005. Use of dissolved and vapor-phase gases to investigate methanogenic degradation of petroleum hydrocarbon contamination in the subsurface. Water Resources Research, 41, W02001, doi:10.1029/2004WR003433.

Amos, R.T. and Mayer, K.U. 2006. Investigating ebullition in a sand column using dissolved gas analysis and reactive transport modeling. Environmental Science and Technology, 40, 5361-5367.

Amos, R.T. and Mayer, K.U. 2006. Investigating the role of gas bubble formation and entrapment in contaminated aquifers: Reactive transport modeling. Journal of Contaminant Hydrology, 87, 123-154.

Anliker, M.A. and Sanderson, E.W. 1995. Reconnaissance study of ground-water levels and withdrawals in the vicinity of Dewitt and Piatt counties, Contract Report 589. Illinois State Water Survey.

Blicher-Mathiesen, G., McCarty, G.W. and Nielsen, L.P. 1998. Denitrification and degassing in groundwater estimated from dissolved dinitrogen and argon. Journal of Hydrology, 208, 16-24.

Brennwald, M.S., Hofer, M., Peeters, F., Aeschbach-Hertig, W., Strassmann, K., Kipfer, R., and Imboden, D.M. 2003. Analysis of dissolved noble gases in the porewater of lacustrine sediments. Limnology and Oceanography: Methods, 1, 51-62.

Coleman, D.D., 1979. The origin of drift-gas deposits as determined by radiocarbon dating of methane. In: R. Berger and H.E. Suess (Editors), Radiocarbon Dating, Proceedings of the Ninth International Conference. University of California Press, Los Angeles, Calif., pp. 365-387.

Coleman, D.D., Liu, C.L. and Riley, K.M., 1988. Microbial methane in the shallow Paleozoic sediments and glacial deposits of Illinois, U.S.A. In: M. Schoell (Guest Editor), Origins of Methane in the Earth. Chem. Geol., 71: 23-40.

Fetter, C.W. 2001. Contaminant Hydrogeology Second Edition. Prentice-Hall, Inc., Upper Saddle River, NJ 07458, 1999.

Fortuin, N.P.M. and Willemsen, A. 2005. Exsolution of nitrogen and argon by methanogenesis in Dutch ground water. Journal of Hydrology, 301, 1-13.

Gerber, R.E. and Howard, K. 2000. Recharge through a regional till aquitard: three-dimensional flow model water balance approach. Ground Water, 38, 410-422.

Glessner, J.J.G. and Roy W.R. 2009. Paleosols in central Illinois as potential sources of ammonium in groundwater. Ground Water Monitoring & Remediation, 29 (4), 56-64.

Hackley, K.C., Panno, S.V. and Anderson, T.F. 2010. Chemical and isotopic indicators of groundwater evolution in the basal sands of a buried bedrock valley in the Midwestern United States: Implications for recharge, rock-water interactions, and mixing. GSA Bulletin, 122 (7/8), 1047-1066, doi:10.1130/B26574.1.

Hansen, L.K., Jakobsen, R., and Postma, D. 2001. Methanogenesis in a shallow sandy aquifer, Romo, Denmark. Geochimica et Cosmochimica Acta, 65 (17), 2925-2935.

Ho, C.K. and Webb, S.W. 2006. Gas Transport in Porous Media. Springer, Berlin.

Holzner, C.P., McGinnis, D.F., Schubert, C.J., Kipfer, R. and Imboden, D.M. 2008. Noble gas anomalies related to high-intensity methane gas seeps in the Black Sea. Earth and Planetary Letters, 265, 396-409.

Jakobsen, R. and Postma, D. 1999. Redox zoning, rates of sulfate reduction and interactions with Fe-reducing and methanogenesi in a shallow sandy aquifer, Romo, Denmark. Geochimica et Cosmochimica Acta, 63, 137-151.

Jarsjo, J. and Destouni, G. 2000. Degassing of deep groundwater in fractured rock around boreholes and drifts. Water Resources Research, 36 (9), 2477-2492.

Jones, E.J.P., Voytek, M.A., Warwick, P.D., Corum, M.D., Cohn, A., Bunnell, J.E., Clark, A.C., and Orem, W.H. 2008. Bioassay for estimating the biogenic methane-generating potential of coal samples. International Journal of Coal Geology, 76, 138-150.

Kehew, A.E., 2000. Applied Chemical Hydrogeology: Prentice-Hall, Upper Saddle River, N.J. p. 236.

Kellner, E., Baird, A.J., Oosterwoud, M., Harrison, K., and Waddington, J.M. Effect of temperature and atmospheric pressure on methane. 2006. (CH4) ebullition form near-surface peats. Geophysical Research Letters, 33, L18405, doi:10.1029/2006GL027509.

Kempton, J.P., Johnson, W.H., Heigold, P.C. and Cartwright, K. 1991. Mahomet Bedrock Valley in east-central Illinois: Topography, glacial drift stratigraphy, and hydrogeology. Geology and Hydrogeology of the Teays-Mahomet Bedrock Valley System, Special Paper Geological Society of America, 258: 91-124.

Kipfer, R., Aeschbach-Hertig, W., Peeters, F., and Stute, M. 2002. Noble gases in lakes and ground waters. Reviews in mineralogy and geochemistry, 47 (1), 615-700, doi:10.2138/rmg.2002.47.14.

Laing, C.G., Shreeve, T.G., and Pearce, D.M.E. Methane bubbles in surface peat cores: in situ measurements. 2008. Global Change Biology, 14, 916-924, doi:10.1111/j.1365-2486.2007.01534.x

Luca Technologies. Active biogenesis of methane in Wyoming's powder river basin. Luca Technologies, 1625 Broadway Street, Denver, CO 80202.

Ludvigsen, L., Albrechtsen, H.J., Heron, G., Bjerg, P.L., and Christensen, T.H. 1998. Anaerobic microbial redox processes in a landfill leachate contaminated aquifer (Grindsted, Denmark). Journal of Contaminant Hydrology, 33, 273-291.

Meents, W.F. 1960. Glacial-drift gas in Illinois. Illinois State Geological Survey: Circular 292, 58 p.

Neuzil, C.E. 1986. Groundwater flow in Low-Permeability Environments. Water Resources Research, 22 (8), 1163-1195.

Nitao, J.J. 2000. User's manual for the USNT module of the NUFT code, version 3.0 (NP-phase, NC-component, thermal). Earth and Environmental Sciences, Lawrence Livermore National Laboratory.

Panno, S.V., Hackley, K.C., Cartwright, K. and Liu, C.L. 1994. Hydrochemistry of the Mahomet Bedrock Valley Aquifer, east-central Illinois: Indicators of recharge and ground-water flow. Ground Water, 32, 591-604.

Schaap, M.G. 1999. Rosetta Version 1.0. U.S. Salinity Laboratory, U.S. Department of Agriculture, Riverside, CA.

Schulz, H.M., Berk, W.V., Bechtel, A., Struck, U., and Faber, E. 2009. Marine and Petroleum Geology, 26, 1163-1179.

Simpkins, W.W. and Parkin, T.B. 1993. Hydrogeology and redox geochemistry of CH4 in a late Wisconsinan till and loess sequence in central Iowa. Water Resources Research, 29 (11), 3643-3657.

Sivan, O., Schrag, D.P. and Murray, R.W., 2007. Rates of methanogenesis and methanotrophy in deep-sea sediments. Geobiology, 5, 141-151.

Solomon, D.K., Poreda, R.J., Schiff, S.L. and Cherry, J.A. 1992. Tritium and helium 3 as groundwater age tracers in the Borden Aquifer. Water Resources Research, 28, 741-755.

Solomon, D.K., Cook, P.G., and Sanford, W.E. 1998. Dissolved gases in subsurface hydrology. In: Kendall, c., McDonnell, J. (Eds.), Isotope Tracers in Catchment Hydrology. Elsevier, Amsterdam, 291-318.

U.S. Geological Survey (USGS), 1999, Ground-water studies in Illinois, http://il.water.usgs.gov/proj/gwstudies/ (November 2010).

Van der Hoven, S.J., Wright, R.E., and Carstens, D.A. 2005. Radiogenic 4He as a conservative tracer in buried-valley aquifers. Water Resources Research, 41, W11414, doi:10.1029/2004WR003857.

Visser, A., Broers, H.P. and Bierkens, M.F.P. 2007. Dating degassed groundwater with 3H/3He. Water Resources Research, 43, W10434, doi:10.1029/2006WR005847.

Visser, A., Schaap, J.D., Broers, H.P., and Bierkens, M.F.P. 2009. Degassing of 3H/3He, CFCs and SF6 by denitrification: Measurements and two phase transport simulations. Journal of Contaminant Hydrology, 103, 206-218, doi:10.1016/j.jconhyd.2008.10.013.

Whiticar, M.J., Faber, E. and Schoell, M. 1986. Biogenic methane formation in marine and freshwater environments: CO2 reduction vs. acetate fermentation-isotope evidence. Geochimica et Cosmochimica Acta, 50, 693-709.

Wilhelm, E., Battino, R., and Wilcock, R.J. 1977. Low-pressure solubility of gases in liquid water. Chemical Reviews, 77, 219-262.

Willman, H.B. and Frye, J.C. 1975. Quaternary System. Illinois State Geological Survey Bulletin 95, 211-239.

Wilson, S.D., Roadcap, G.S., Herzog, B.L., Larson, D.R. and Winstanley, D. 1998. Hydrogeology and ground-water availability in southwest McLean and southeast Tazwell counties, part 2: Aquifer modeling and final report, Coop. Ground Water Rep. 19, III. State Water Survey, Champaign.

Yager R.M. and Fountain J.C. 2001. Effect of natural gas exsolution on specific storage in a confined aquifer undergoing water level decline. Ground Water, 39, 517-525.

Yavitt, J.B., Downey, D.M., Lancaster, E., and Lang, G.E. 1990. Methane consumption in decomposing sphagnum-derived peat. Soil Biology and Biochemistry, 22 (4), 441-447.

Zhou, Z., Ballentine, C.J., Kipfer, R., Schoell, M. and Thibodeaux, S. 2005. Noble gas tracing of groundwater/coalbed methane interaction in the San Juan Basin, USA. Geochimica et Cosmochimica Acta, 69 (23), 5413-5428.